Nanowires and Neural interfaces. Biocompatibility in the brain

Gällentoft, Lina

2016

Link to publication

Total number of authors:
1

Nanowires and Neural interfaces

Biocompatibility in the brain

LINA GÄLLENTOFT
DEPARTMENT OF EXPERIMENTAL MEDICAL SCIENCE | LUND UNIVERSITY 2016

Nanowires and Neural interfaces

Nanowires and Neural interfaces

Biocompatibility in the brain

Lina Gällentoft

DOCTORAL DISSERTATION
by due permission of the Faculty of Medicine, Lund University, Sweden.
To be defended at Segerfalksalen. The 30th of September, at 13.00.

Faculty opponent
Dr. Andrew Jackson

Organization LUND UNIVERSITY Faculty of Medicine Department of Experimental Medical Science	Document name DOCTORAL DISSERTATION	
Neuronano Research Center	Date of issue 30th of September, 2016	
Author Lina Gällentoft	Sponsoring organization	
Title and subtitle Nanowires and Neural interfaces – biocompatibility in the brain		

Abstract

Chronic neural interfaces able to record or stimulate neurons in the CNS are valuable instruments in use today and they hold great promise for the future both within neuroscience research and in the clinic. However, a major obstacle is that they show a decline in performance over time. Many different approaches to improve the interface designs are gradually evaluated in hope of overcoming this obstacle. One approach is to enhance the biomaterials ability to integrate with the surrounding tissue by manipulating the surface structure. One way of doing this is to construct a nanostructured electrode surface. A nanostructured electrode surface, in this case nanowires, has the potential to improve the electrical properties of the neural interface a well as to improve the interface biocompatibility and tissue integration. However, before nanowires can be used as an electrode surface structure it is crucial to investigate the safety aspects of exposing the brain tissue to nanowires. Nanowires share morphological features with asbestos fibers and if some of the nanowires were to break off from the electrode surface a possible asbestosis-like pathology might develop. To address this issue we assessed the inflammatory tissue response and neuronal survival following injection of biostable nanowires of different lengths (paper I). Furthermore, we also evaluated the tissue response following injection of short degradable nanowires (paper II). We found that short biodegradable or biostable nanowires did not cause a significant tissue response or neuronal loss. However, we found that debris from degradable nanowires as well as intact biostable nanowires remained in the brain one year post injection. Suggesting that nanoparticle clearance from the brain is a very slow process.

A neural interface with a nanostructured surface needs to be protected from damage during the implantation procedure. In paper III, we showed that embedding the nanowire substrate in a temporary protective and stiffening matrix, consisting of gelatin and glycerol, preserved the majority of the nanowires during implantation into agar.

In paper IV, we showed that implanting multiple wire bundles in the brain does not result in an increased glial response to each individual implant. This implies that it is feasible to interface and interact with several brain structures in parallel without the confounding factor of an over all cumulatively increased glial response.

In summary, this thesis has provided key knowledge about how to design and implant a nanowire structured neural interface. The development of a seamlessly integrating neural interface would have immense implications in neuroscience research as well as in clinical settings.

Key words: neural interface, BMI, nanowires, tissue responses, rat, biocompatibility, astrocytes, microglia, neurons		
Classification system and/or index terms (if any)		
Supplementary bibliographical information		Language: English
ISSN and key title: 1652-8220		ISBN: 978-91-7619-319-8
Recipient's notes	Number of pages	Price
	Security classification	

Signature _(signature)_   Date 2016-08-31

Nanowires and Neural interfaces

Biocompatibility in the brain

Lina Gällentoft

LUND
UNIVERSITY

Cover: The cover shows nanowires in the brain tissue. The nanowires in white can be seen engulfed by microglia. Astrocytes are shown in red and cell nuclei in blue.

Artwork: Linda Carlsson, Jerker Eriksson and Lina Gällentoft.

Table of contents

Abbreviations

CNS	Central Nervous System
CNT	Carbon nanotubes
DAPI	4-, 6-diamidino-2-phenylindole, staining cell nuclei
ED1	Antibody staining microglial cells
GaP	Gallium Phosphide
GFAP	Glial fibrillary acidic protein
HBSS	Hank's balanced salt solution
HfOx	Hafnium oxide
NeuN	Neuronal Nuclei
PBS	Phosphate buffered saline
SiOx	Silicon oxide

Original Papers included in this Thesis

Paper I:

Size-dependent long-term tissue response to biostable nanowires in the brain.

Lina Gällentoft, Lina M.E. Pettersson, Nils Danielsen, Jens Schouenborg, Christelle N. Prinz, Cecilia Eriksson Linsmeier. Biomaterials, 2015. 42:172-183.

Paper II:

Impact of degradable nanowires on long-term brain tissue responses.

Lina Gällentoft, Lina M.E. Pettersson, Nils Danielsen, Jens Schouenborg, Christelle N. Prinz, Cecilia Eriksson Linsmeier. Journal of Nanobiotechnology. 2016;14(1):1-11.

Paper III:

Gelatin/glycerol coating to preserve mechanically compliant nanowire electrodes from damage during brain implantation.

Jolanda A. Witteveen, Dmitry B. Suyatin, **Lina Gällentoft**, Jens Schouenborg, Nils Danielsen, Christelle N. Prinz. Journal of Vacuum Science & Technology B. 2010. 28(6):C6K13-C6K16.

Paper IV:

Multiple implants do not aggravate the tissue reaction in the rat brain.

Gustav Lind, **Lina Gällentoft**, Nils Danielsen, Jens Schouenborg, Lina M. E. Pettersson. PLoS One. 2012. 7(10):e47509.

Populärvetenskaplig Sammanfattning

Det är sannolikt att implanterbar elektrodteknik för direkt kommunikation med nervceller i hjärnan kommer att revolutionera vår förståelse av hur hjärnan fungerar och möjliggöra helt nya och mycket effektiva behandlingsmetoder för svåra neurologiska sjukdomar. Elektroder som används för att registrera eller stimulera nervceller i hjärnan, kallas för "neurala interface" och används redan idag inom forskning och klinik. Ett exempel är "Deep Brain Stimulation" som mycket framgångsrikt används idag vid behandling av Parkinsons sjukdom. Ett annat exempel är elektrodimplantat som hjälper förlamade patienter att styra robotarmar. Tyvärr fungerar de neurala interface som används idag inte helt optimalt vilket till stor del beror på de vävnadsreaktioner som uppkommer efter implantation. Dessa vävnadsreaktioner beror förmodligen till största del på att reaktiva celler i hjärnan, såsom astrocyter, kapslar in elektroderna i en slags ärrvävnad. Denna inkapsling kallas för ett glia-ärr och det verkar som en isolering runtom elektroden. En annan celltyp i hjärnan som spelar en viktig roll i dess inflammatoriska försvar är mikrogliaceller. Mikrogliaceller aktiveras vid skada och städar upp rester från bl.a. döda celler. Mikrogliaceller frisätter även neurotoxiska ämnen som kan döda nervceller i dess omgivning. Sammantaget leder dessa akuta och kroniska inflammatoriska reaktioner i hjärnvävnaden till att en del nervceller dör direkt vid elektrodimplantationen, en del dör till följd av den toxiska inflammatoriska miljön och en del nervceller trycks även bort eller isoleras från elektroden på grund av det glia-ärr som har uppstått.

För att optimera funktionen hos neurala interface är det viktigt att designa dem så att de minimerar dessa inflammatoriska reaktioner, både i det akuta skedet och i det långa loppet. Det är idag känt att den framkallade inflammatoriska reaktionen kan påverkas dels av elektrodens storlek, styvhet och ytstruktur, samt av fixeringsläge och implantationsmetod. Ett sätt att försöka minska vävnadsreaktionen är att modifiera ytan på elektroderna, till exempel genom att tillverka nanostrukturerade elektroder. Vid tillverkning av nanostrukturerade elektroder finns det möjlighet designa dem till att efterlikna miljön i hjärnvävnaden, eftersom cellerna i hjärnan och den extracellulära miljön är strukturerad i mikro- och nanoskala. Nanostrukturerade elektroder har därmed möjlighet att kamoufleras bättre i vävnaden än en elektrod med slät yta. Nanostrukturen kan även fungera som ett slags ankare i vävnaden som håller elektroden på plats och upprätthåller en stabil kontakt med enskilda nervceller. En möjlig form av nanostruktur som kan användas till att täcka elektrodytan är så kallade nanopinnar, dessa nanopinnar är ungefär 1000 gånger tunnare än ett hårstrå. Det har visat sig att nervceller, som odlas utanför kroppen, kan växa på ytor täckta med nanopinnar, till och med när cellerna genomborras av dessa nanopinnar. Detta innebär att elektroder med en nanopinnstrukturerad yta har

möjlighet att bidra till en ökad *biokompatibilitet*, det vill säga de skulle kunna göra elektroden mer *vävnadsvänlig*. Detta öppnar upp för tillverkning av en ny typ av neuralt interface med möjlighet att registrera signaler från enskilda nervceller, eftersom cell-elektrodavståndet kan göras mycket litet med hjälp av dessa nanopinnar.

Denna avhandling handlar om hur hjärnans olika celler reagerar på implantationer av olika nanostrukturer och elektrod-komponenter. Innan nanostrukturerade elektroders funktion och biokompatibilitet kan testas är det emellertid viktigt att ta reda på hur hjärnvävnaden och dess celler reagerar på implantation av fria nanopinnar, då dessa nanopinnar liknar asbestfiber till morfologin. Det är känt att asbestfiber kan orsaka kronisk inflammation i lungvävnad som eskalerar med tiden. Vid en implantation av en elektrod med nanopinnar på är det sannolikt att en del av nanopinnarna går av vid själva implantationsproceduren. Det är också möjligt att en del nanopinnar går av med tiden på grund av slitage eftersom hjärnan konstant rör sig inne i skallen, vid till exempel andning och hjärtslag. Av dessa anledningar var det av yttersta vikt att genomföra en säkerhetsstudie där vi undersöker hjärnans kroniska svar på fria nanopinnar.

I arbete I och II utvärderar vi hur hjärnan reagerar på injektion av fria nanopinnar av olika längd och material; ett material som bryts ned med tiden och ett material som är stabilt i vävnaden. Dessa två arbeten utvärderar vävnadsreaktionen i råtthjärna vid två kroniska tidpunkter, 12 veckor respektive ett år efter injektion. Ett år motsvarar ungefär en råttas halva livslängd och är en sann kronisk tidpunkt som sällan utvärderas histologiskt. För att kunna injicera de fria nanopinnarna är de uppslammade i en vävnadsvänlig saltlösning. I dessa två arbeten har vi utvärderat en stor mängd insamlat material (I, II) och vi kommer här fram till en längd på nanopinnarna (2 μm) som framkallar ett ytterst litet vävnadssvar, motsvarande vad en injektion av endast saltlösning (utan nanopinnar i) framkallar. Vi visar även injicerade degraderbara nanopinnar av samma längd (2 μm) ger ett liknande, minimalt inflammatoriskt svar som de biostabila nanopinnarna. Vi såg ingen eskalering av det inflammatoriska svaret i någon av grupperna, vilket tyder på att det ur säkerhetsaspekt är fullt möjligt att använda nanopinnar som ytstruktur på neurala interface.

I arbete III utvärderar vi hur olika vävnadsvänliga gel-inbäddningar av elektroderna kan bidra till att så få nanopinnar som möjligt bryts av vid själva implantationsproceduren. Denna gel-inbäddning är relativt hård vid inbäddning men löser sedan upp sig efter implantation och möjliggör därmed implantation av flexibla elektroder med nanostrukturerade ytor.

I arbete IV analyserar vi hur hjärnan och dess celler påverkas av antalet elektroder som implanteras i hjärnan. Detta gör vi genom att implantera flera gel-inbäddade elektroder i mikroskala i olika områden i hjärnbarken, dock maximalt fem per

hjärnhalva i denna studie. Att kunna implantera flera elektroder utan att det sker något kumulativt ökat svar möjliggör för oss att kunna registrera eller stimulera flera olika områden i hjärnan samtidigt och därmed kan vi till exempel se hur dessa områden interagerar med varandra.

Sammanfattningsvis har arbetena i denna avhandling klargjort vilka typer av nanopinnar som kan användas vid tillverkning av nanopinnestrukturerade elektroder och löst problemet hur dessa elektroder kan implanteras med hjälp av en skyddande gel.

Vi har även kommit fram till att det inte sker något kumulativt ökat vävnadssvar till de enskilda implantationerna när ett ökat antal implantat sätts in i hjärnan. Vi har med dessa arbeten tagit oss några få men viktiga steg närmre mot att kunna designa ett mer vävnadsvänligt nanostrukturerat neuralt interface.

Abstract

Chronic neural interfaces that are able to record or stimulate neurons in the CNS are valuable instruments in use today and they hold great promise for the future both within neuroscience research and in the clinic. However, a major obstacle is that they show a decline in performance over time. Many different approaches to improve the interface designs are gradually evaluated in hope of overcoming this obstacle. One approach is to enhance the biomaterials ability to integrate with the surrounding tissue by manipulating the surface structure. One way of doing this is to construct a nanostructured electrode surface. A nanostructured electrode surface, in this case nanowires, has the potential to improve the electrical properties of the neural interface a well as to improve the interface biocompatibility and tissue integration. However, before nanowires can be used as an electrode surface structure it is crucial to investigate the safety aspects of exposing the brain tissue to nanowires. Nanowires share morphological features with asbestos fibers and if some of the nanowires were to break off from the electrode surface a possible asbestosis-like pathology might develop. To address this issue we assessed the inflammatory tissue response and neuronal survival following injection of biostable nanowires of different lengths (paper I). Furthermore, we also evaluated the tissue response following injection of short degradable nanowires (paper II). We found that short biodegradable or biostable nanowires did not cause a significant tissue response or neuronal loss. However, we found that debris from degradable nanowires as well as intact biostable nanowires remained in the brain one year post injection. Suggesting that nanoparticle clearance from the brain is a very slow process.

A neural interface with a nanostructured surface needs to be protected from damage during the implantation procedure. In paper III, we showed that embedding the nanowire substrate in a temporary protective and stiffening matrix, consisting of gelatin and glycerol, preserved the majority of the nanowires during implantation into agar.

In paper IV, we showed that implanting multiple wire bundles in the brain does not result in an increased glial response to each individual implant. This implies that it is feasible to interface and interact with several brain structures in parallel without the confounding factor of an over all cumulatively increased glial response.

In summary, this thesis has provided key knowledge about how to design and implant a nanowire structured neural interface. The development of a seamlessly integrating neural interface would have immense implications in neuroscience research as well as in clinical settings.

Introduction

Neural interfaces – *background, potential & limitations*

Neural interfaces chronically implanted for stimulation or recording within the central nervous system (CNS) holds great promise in the field of neuroscience, both as research tools and for clinical applications [1-6]. Indeed, successful recordings have been obtained in awake, freely moving animals [7-10]. Hence, attaining such recordings opens up for elucidating neural mechanisms underlying for example movement and cognition in real time and also to clarify mechanisms underlying different neurological conditions. Moreover, it has been shown that tetraplegic human patients can learn to control a prosthetic hand or a cursor on a computer screen with microelectrode arrays implanted in motor cortex [4, 11]. Implanted electrodes can also be used for stimulation. Treatment of symptoms in levodopa resistant Parkinson's disease using Deep Brain Stimulation (DBS) has been quite successful and has since the 80's, when the use of DBS in Parkinsonian patients started [12], provided almost 100 000 patients with symptom relief [13]. There are many other possible applications for neural interfaces, such as for treatment of depression, bladder control and epilepsy [2, 14, 15]. However, a major challenge in the field of neural interfaces is that the function of the neural interfaces used today often deteriorates over time [16-20]. This deterioration is in part due to the brain tissue response that arises and forms an insulating layer between the interface and the neurons, but may also be due to a loss of neurons. As a result, the neural circuits to be studied or interacted with becomes reorganized and/or damaged. Finding ways to reduce the tissue responses is thus fundamental in order to establish stable long-term communication with the brain.

Brain tissue responses

An inflammatory brain tissue response is an immunological reaction that serves to heal or protect the brain from damage caused by for example bacterial infections, from damage caused by a traumatic brain injury or an implantation of a neural interface. In the case of an implantation, the chronic inflammatory process serves

to isolate the indwelling foreign body from the surrounding tissue. This ongoing process leads to loss or displacement of neurons in the vicinity of the neural interface and could thus lead to device failure.

As a neural interface enters the brain parenchyma the blood vessels and cells are more or less damaged and the tissue is displaced [21]. The initial vascular damage caused by an implantation contributes greatly to the inflammatory tissue response as the blood brain barrier (BBB) is breached and blood-borne macrophages and neutrophil granulocytes can infiltrate the insertion site along with for example plasma proteins [22]. The initial tissue trauma will also activate resident phagocytizing microglial cells in the brain tissue (Fig. 1). Activated microglia and macrophages are both recognized by the same marker, ED1, although they have different origins [23]. ED1 is widely used as a measure of inflammatory tissue response in the brain [18, 24]. When the microglia and macrophages fail to engulf and break down the inorganic foreign material they encounter, these cells might become frustrated and fuse to form multinucleated giant cells. These highly activated giant cells can produce large amounts of neurotoxic substances, such as reactive oxygen species and proteolytical enzymes [25, 26].

Astrocytes are another type of glial cell in the brain that plays a major part in the brain tissue response. In a normal healthy state, astrocytes are very important when it comes to for example energy provision to cells, regulating blood flow and clearing metabolic products [27, 28]. However, when a CNS insult occurs, as for example when implanting a neural interface, the astrocytes will become reactive, a process also known as astrogliosis. The reactive astrocytes form a glial scar that encloses the foreign body from the surrounding brain tissue (Fig. 1). This scar formation has been described as a continuation of the glia limitans and it serves to separate damaged tissue or a foreign body from healthy tissue in the brain [29, 30]. To evaluate astrogliosis in the brain tissue we have in our histological evaluations stained the tissue with the commonly used astrocyte-specific cytoskeletal protein called glial fibrillary acidic protein (GFAP) [19, 31, 32].

Other cells are involved in wound healing and scar formation, such as pericytes and fibroblast. Pericytes have been suggested to play a role in controlling the rate at which inflammatory cells leave the blood stream and they have also been suggested to play a role in the scar formation in the wound healing process [33]. Furthermore, meningeal cells can also migrate from the injury at the meningeal surface and along with astrocytes take part in the re-formation of the glia limitans [30]. However, today, markers for these cells are not commonly used to evaluate the brain tissue response following implantation of foreign materials. To assess a possible increase in cells that are involved in the inflammatory brain tissue response, other than astrocytes and microglia/macrophages specifically, we have

also quantified the overall cell nuclei density using the cell nuclei staining DAPI (4-, 6-diamidino-2-phenylindole).

For the use of neural interfaces, the most important cell type is of course neurons. In order to record from neurons with good signal-to-noise ratio they need to be close to the interface, depending on neuron type approximately within 50 µm of the electrode tip [34, 35]. Previously, several papers have reported evidence of a so-called "kill zone" surrounding implants, this is a region defined by a significantly low or non-existent neuronal density with a high density of inflammatory cells, up to as far as 100 µm away from the electrode [16] (Fig. 1). This is not only a problem for recordings but also for stimulation purposes. In order to stimulate the neurons outside of the "kill zone" and the glial scar, current electrodes need to be relatively large resulting in poor specificity.
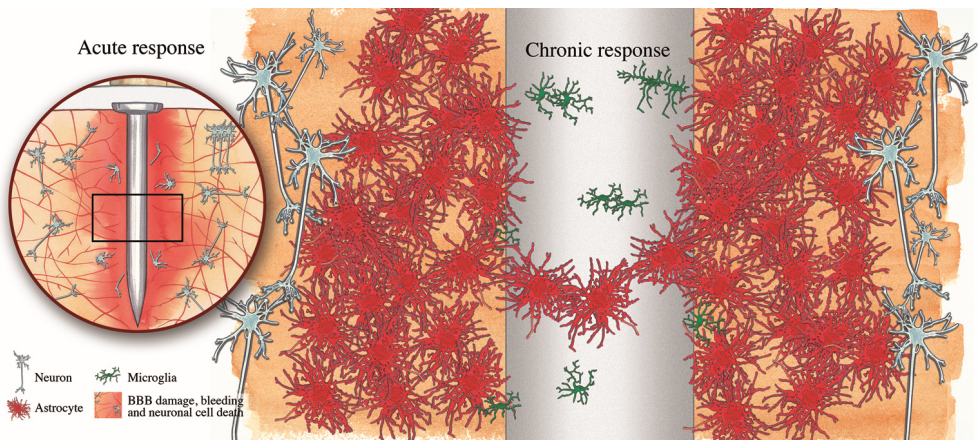
Figure 1. Illustration of the inflammatory response in the brain following implantation of a neural interface.
Following an implantation of a neural interface of today, the acute trauma will damage blood vessels and cause local cell death. The cell death is a consequence of the implantation trauma itself and is also caused by toxic substances that are released from damaged cells and that are leaking into the tissue from the damaged blood vessels. This will activate resident microglia and blood-borne macrophages. The activated microglia and macrophages will phagocytize cell debris as well as release inflammatory factors, which in turn will activate astrocytes in the tissue. The reactive astrocytes will encapsulate the interface and form a glial scar to protect the surrounding tissue from further damage and infection. Over time the number of activated microglia/macrophages will diminish, while the glial scar will stabilize and remain in the tissue chronically. The glial scar both acts as insulation around the electrode and it pushes the surrounding tissue away from the interface. These events result in a loss of neurons at the electrode interface and are thus major contributors to device failure. Hence, finding ways to reduce the acute and chronic tissue responses is fundamental in order to establish stable long-term communication with the brain.

Thus, when re-designing neural interfaces one of the most important objective is to minimize the inflammatory tissue response and try to eliminate the "kill zone", this would reduce the gap between the interface and the neurons. To evaluate neuronal survival in the papers in this thesis we have assessed the neuronal density by staining for neuronal nuclei using the antibody NeuN.

Definition of biocompatibility

The term biocompatibility is widely used in many different scientific disciplines and it is applicable to a plethora of devices intended to interact with the body, ranging from for example orthopedic devices to neural interfaces. The term has been around for decades, it surfaced in peer-review journals in the 1970's [36, 37]. The materials used in these medical devices are typically defined as biomaterials and have been described as "non-viable materials used in medical devices, intended to interact with a biological system" [38]. The concept of biocompatibility have since then started to move from a biomaterial that is not directly toxic or harmful to a biomaterial that does "good", for example encouraging wound healing and tissue integration [39]. The ability to control and understand the host inflammatory response and the healing that follows an implantation of a medical device have advanced significantly since the 1970's. Thus, one might say that the criteria for a biomaterial to be called biocompatible have evolved and this calls for a new consensual view of what biocompatibility truly is. Ratner 2011, have proposed an apt new definition of biocompatibility that reflects the increased knowledge we now have of the mechanisms underlying biological responses and the ability we now have to manipulate these responses [40]:

> "BIOCOMPATIBILITY: the ability of a material to locally trigger and guide non-fibrotic wound healing, reconstruction and tissue integration"

In the field of neural interfaces this new definition of biocompatibility would translate to a neural interface causing a minimal inflammatory tissue response and minimal alterations to the neural circuits. A truly biocompatible neural interface would thus not lead to glial scarring and the interface would not be insulated from the surrounding neurons, this would enable the neural interface to record and stimulate neural tissues over long periods of time.

Towards nanostructured neural interfaces

The brain tissue response that arises when a neural interface is implanted is influenced by many factors, such as implant size [41, 42], flexibility [31, 43-45], density [46, 47], material [47, 48], surface structure [47] and fixation mode [19, 42]. Moreover, in order to study the interaction of different areas in the brain, at the same time, multiple neural interfaces need to be implanted. Whether or not multiple implants could result in an increased brain tissue response to each individual implant is not known.

One way of minimizing the inflammatory brain tissue response could be to develop state-of-the-art neural interfaces with a nanostructured surface. With a nanostructured surface the interface has the possibility to mimic brain tissue, since the cells and the extra-cellular matrix are structured in nano-scale, and the interface thereby has the potential to go 'under the radar' of the inflammatory tissue response. Indeed, nanostructured (and microstructured) electrode surfaces have been shown to improve recording properties and lower the evoked inflammatory tissue response [49-51]. Nanostructured surfaces have the potential to mimic the extra cellular matrix, which is composed of nanoscale proteins, in a way flat surfaces cannot, this could enhance the biocompatibility of the implant and thus lessen the brain tissue response [52]. A nanostructured electrode surface would also increase the surface to volume ratio, which would improve the electrode properties. Furthermore, using nanoparticles, such as nanowires, as electrode tips opens up the possibility to record and interact with the smallest parts of neurons, e.g. dendrites and synapses.

Micro-motions between the brain, which exhibits constant movement due to for example breathing and blood flow, and the typically poorly compliant neural interfaces is also thought to play an important role in exacerbating the inflammatory brain tissue response [19, 53]. Flexible nanomaterials, such as nanowires or carbon nanotubes (CNTs), on the surface of a neural interface could improve the local mechanical compliance of the interface and would thereby allow the interface to move better with the brains micro-motions.

Studies done *in vitro* have shown that cells can grow on and interact with arrays of nanowires or nanopillars [54-58] and neurite outgrowth, guidance of optic nerves and reduced glial cell spreading have been demonstrated on gallium phosphide (GaP) nanowire substrates [59-62]. Indeed, acute *in vivo* recordings in rat cortex have been obtained using a GaP nanowire-based electrode [63]. However, using nanowires as a surface structure on neural interfaces might result in nanowires detaching from the surface during or after implantation. These high-aspect-ratio nanoparticles have similar morphological features as asbestos fibers. It has been shown *in vivo* that nanotubes and nanowires of lengths comparable to immune cells can induce frustrated phagocytosis in pleural and abdominal cavity resulting in a chronic inflammation that escalates over time, which is also seen in asbestosis [64-66]. Thus, there is a need to investigate the long-term brain tissue response to nanowires of different material and lengths in order to find out which parameters that could be used when designing a nanowire-structured neural interface. It is also of importance to detect if there is a possible nanowire clearance from the brain and if that could lead to injury or inflammation in other tissues. The nanowire length and material chosen for the neural interface design should evoke minimal inflammatory tissue response if they were to detach from the electrode.

There is also a need to develop an implantation method that would preserve the majority of the nanowires on the surface of the interface. This implantation method should provide mechanical support to the implant during implantation and compliance once implanted. One possible way of doing this is by using gelatin as an embedding material. Gelatin can be made stiff in room temperature, providing mechanical support to the implant, and dissolve once the interface is implanted. Gelatin has been shown to reduce tissue reactions towards implants, possibly due to the hemostatic properties of collagen, which is a main component of gelatin, and possibly also due to the fact that the gelatin surface becomes slippery when it starts to dissolve during the implantation [67]. Furthermore, it is well known that neurons can thrive on gelatin-based surfaces in cultures [68, 69]. However, the internal forces of the gelatin solution would need to be reduced so the nanowires does not break during the drying process. This can be achieved by adding a biocompatible plasticizer to the gelatin solution. Glycerol is a commonly used plasticizer that could increase the water content and the flexibility of the embedding solution [70, 71].

Hence, in order to design a state-of-the-art biocompatible neural interface there are many key properties that need to be considered and evaluated. In this thesis work the main focus have been on identifying a nanowire length suitable as an interface topography, on developing an implantation method that could preserve the nanowires on the electrode surface as well as evaluating whether multiple implants results in an increased brain tissue response to each individual implant.

Aims

The overall aim of this thesis was to clarify safety aspects of implanted nanostructures and neural interfaces, as well as to develop a technique that allows implantation of nanostructured surfaces into the brain tissue.

The specific goals were:

I. To investigate the long-term brain tissue response to biostable nanowires of different lengths in rat after 12 weeks and 12 months of implantation.

II. To investigate the long-term brain tissue response to short biodegradable nanowires in the rat brain after one year of implantation.

III. To develop a method enabling implantation of flexible nanowire-structured electrodes, providing mechanical support during implantation and compliance once implanted.

IV. To evaluate the effect multiple neural implants have on the ensuing tissue response.

General Methods and Protocols

In this section, key methods and protocols used during this thesis work are presented. All procedures described involving animals were approved in advance by the Lund/Malmö local ethical committee on animal experiments.

Nanowire growth and coating (I, II, III)

Gallium phosphide (GaP) nanowires were grown from gold (Au) aerosol particles ($\varnothing$ 40 nm) using metal organic vapour phase epitaxy (Aix 200/4, Aixtron, Germany), as previously described [59, 72, 73]. The gold aerosol particles were randomly distributed on a (111)B GaP substrate (Girmet Ltd, Moscow, Russia) at an average density of $1/\mu m^2$.

For paper I, the nanowire growth duration was adjusted to make nanowire lengths of 2 μm (± 0.2 μm), 5 μm (± 0.2 μm) or 10 μm (± 0.5 μm). In order to obtain a stable and inert nanowire surface chemistry, hafnium oxide (HfOx) was used as a surface coating. Hafnium belongs to the same group (IVB) as titanium (Ti) in the periodic table of elements and has been shown to present similar biocompatible traits as titanium [74, 75]. Furthermore, HfOx has been shown to be biocompatible in a nano-configuration [76]. Thus, the GaP nanowires were coated with a 20 nm layer of HfOx using atomic layer deposition (Savannah-100 system, Cambridge NanoTech Inc., USA). For paper II, the nanowire growth time was adjusted to obtain a nanowire length of 2 μm and the GaP nanowires were coated with a 20 nm layer of silicon oxide (SiOx) or HfOx using atomic layer deposition (Fiji, Cambridge NanoTech Inc., USA).

The final diameter and length of the nanowires were characterized using a scanning electron microscope (SEM) (Fig. 2); the final nanowire diameter was 80 μm ± 5 nm for the 2 and 5 μm long nanowires and 80 μm ± 10 nm for the 10 μm long nanowires.
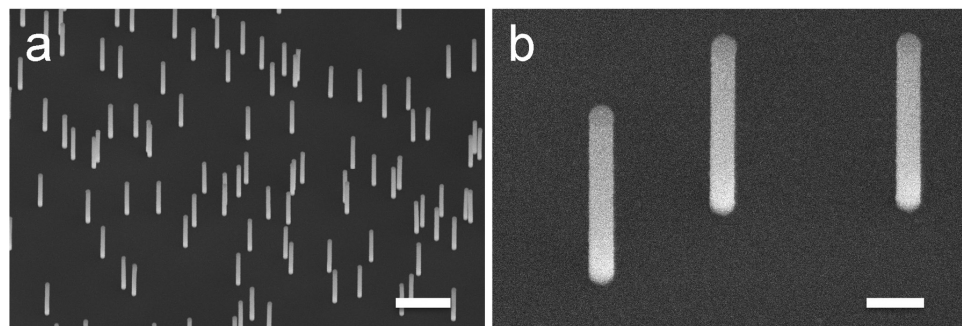
Figure 2. SEM images of nanowires.
Representative SEM images of 2 µm long HfOx-coated GaP nanowires. Scale bars: 1 µm (a), and 200 nm (b).

The substrates with the coated GaP nanowires were cleaned with an oxygen plasma chamber (Plasma Preen, Plasmatic Systems Inc., USA). To break the nanowires off from the substrate, the substrates were ultrasonicated and the nanowires were dispersed in Hank's balanced salt solution (HBSS) as vehicle solution. The final nanowire concentration in the solution was 70 000 nanowires/µL.

For paper III, the growth time was adjusted to obtain 4–5 µm long nanowires with a diameter of approximately 60–80 nm. After the nanowire growth, the substrates were coated with a 50 nm layer of HfOx using atomic layer deposition. The nanowires were subsequently coated with 15 nm of Ti and 75 nm Au in a magnetron sputtering system (Orion 5, AJA International, USA), which resulted in additional layers of 3–5 nm Ti and 20–25 nm Au. The final nanowire diameter was estimated to be approximately 200-240 nm.

Multiple implants (IV)

The gelatin embedded wire bundles used in this study were produced as described in a previous study from our laboratory [67]. In short, each implant consisted of 32 tungsten wires (∅ 7.5 µm) with an insulation layer of 3 µm polyimide. The wire bundles were molded into a gelatin needle (gelatin type B, VWR Inc., Sweden) with a final diameter of 300 µm. The gelatin embedding gives stability to the highly flexible wires while penetrating the meninges and brain tissue. The gelatin dissolves after implantation leaving only the wire bundle (∅ ~180 µm) in place in the cortex.

Animals (I, II, IV)

Female Sprague-Dawley (SD) rats (Taconic, Denmark) were used. All rats received food and water ad libitum and were kept in a 12-h day-night cycle. At the beginning of the experiments the rats weighed approximately 225 g and they followed a normal weight curve after the surgeries.

In paper I and II a total of 126 SD rats were used. The different experimental groups for the two time points, 12 weeks and 1 year, are summarized in Table 1.

The 12 week time point had seven different experimental groups (I). One group was kept naïve (no surgical procedures). One group received bilateral control vehicle-injections of Hank's balanced salt solution (HBSS injection only). Three animal groups received bilateral injections of 2, 5 or 10 µm long HfOx-coated GaP nanowires in HBSS. One group of animals received stab wounds (SW) in one hemisphere and control-injections of HBSS (HBSS injection only) in the contralateral hemisphere. Stab wounds vs. control injection comparisons were performed to ensure that the control solution, HBSS, did not have an adverse effect on the tissue.

For the one year time point (I, II), six experimental groups were used. One group was kept naïve (no surgical procedures). One group received bilateral control-injections (HBSS injection only). Three groups received bilateral injections of 2, 5 or 10 µm long HfOx-coated GaP nanowires in HBSS. One group received striatal bilateral injections of 2 µm long SiOx-coated nanowires suspended in HBSS.

In the one year animal groups we found spontaneous tumors in ten out of the 60 animals. At this point the rats were approximately 425 days old. Upon tumor detection, these animals were immediately euthanized and excluded from the study. The prevalence of tumors was distributed over all groups, including the naïve group (no surgical procedures). The prevalence of tumors in both the naïve and the control rats (HBSS injection only) and the well-documented occurrence of spontaneous age-related tumors in old SD rats [77-80], led us to conclude that the tumors were not linked to our experimental procedures. Furthermore, at both time points, animals were excluded for not meeting our histological inclusion criteria (for example poor tissue fixation or unsuccessful injection).

Table 1.
Experimental setup for paper I and II. The table show total number in each experimental group (n = one unilateral implantation).

	Naïve	SW	SW-control HBSS	Control HBSS	2 µm SiOx	2 µm HfOx	5 µm HfOx	10 µm HfOx
Groups at 12 w	**18**	**8**	**8**	**24**	**-**	**26**	**24**	**24**
12 w included	18	8	8	20	-	20	18	16
12 w excluded	0	0	0	4	-	6	6	8
Groups at 1 y	**20**	**-**	**-**	**20**	**20**	**20**	**20**	**20**
1 y included	18	-	-	16	14	11	15	15
1 y excluded	2	-	-	4	6	9	5	5

In paper IV a total of 23 female SD rats were used. The animals were kept for one or six weeks and were divided into four experimental groups (Fig. 3). The four groups: 1) one week, implanted with five wire bundles in the left hemisphere with 1 mm spacing between each bundle, and one wire bundle implanted in the right hemisphere (n = 6); 2) one week, implanted with only one wire bundle in the left hemisphere (n = 6); 3) six weeks, implanted with five wire bundles in the left hemisphere, with 1 mm spacing between each bundle, and one wire bundle implanted in the right hemisphere (n = 6); 4) six weeks, implanted with only one wire bundle in the left hemisphere (n = 5).
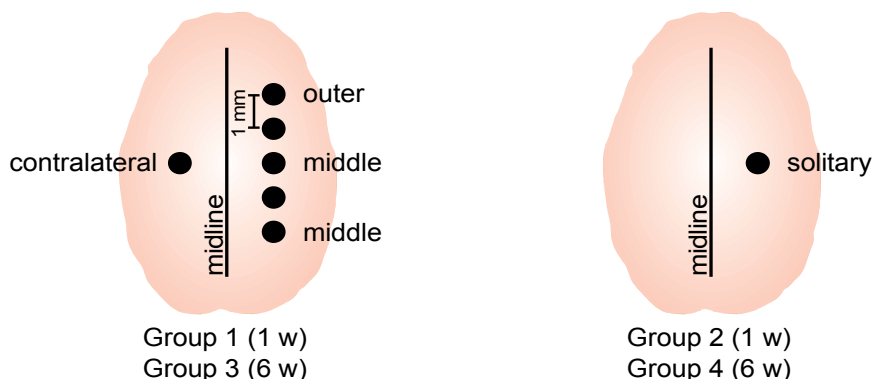
Figure 3. Schematic overview of wire bundle locations in the four different experimental groups.
Dorsal view of cortex with wire bundle locations indicated. The wire bundles in the left hemisphere of Group 1 & 3 are referred to as the contralateral implants and the wire bundles in the right hemisphere in group 1 & 3 are referred to as middle and outer implants. The wire bundles in the right hemisphere of group 2 & 4 are referred to as the solitary implants. Unnamed wire bundles in the right hemisphere of Group 1 &3 were not analyzed in this study.

Surgery (I, II, IV)

The anesthetic procedures have been described in detail elsewhere [81]. In short, the animals were anesthetized by intraperitoneal (i.p.) injections of Fentanyl (0.3 mg/kg body weight (BW)) and Domitor vet (metedetomidin hydrochloride, 0.3 mg/kg BW). The surgical area was shaved and the anesthetized animals were attached to a stereotactic frame (KOPF instruments, USA) prior to surgical procedures. The scalp was disinfected with 70% ethanol. After surgery, the skin was closed with surgical clips. The animals received subcutaneous injections (s.i.) of Temgesic (buprenorphine, 50 µg/kg body weight) to reduce postoperative pain, and Antisedan as an antidote to the anesthesia (atipamezole hydrochloride, 0.5 mg/kg body weight), and were awakened under supervision.

The surgical procedures for paper I and II have been described in detail previously [82]. In short, local anesthetic was administered (0.25% Marcaine, bupivacaine, 0.33 mg/kg BW). To expose the skull a 2 cm midline incision was made and bilateral craniotomies were drilled at 1 mm anterior and 2.5 mm lateral to bregma ($\varnothing$ 1 mm^2). The dura mater was incised and deflected with fine forceps. Manual stereotactic injections were made using a 2 µL Hamilton syringe with a glass microcapillary (tip $\varnothing \sim 130$ µm) attached. The HBSS suspension (with or without nanowires) was injected into striatum at two depths; i) 5 mm (1 µL) and ii) 4 mm (1 µL); in total 2 µL/hemisphere over a total time of 2 x 2 min. Stab wounds were performed in an identical manner with a Hamilton syringe with a glass microcapillary (tip $\varnothing \sim 130$ µm) attached, without injection of HBSS. Before and after each session of nanowire injections a drop of the nanowire suspension was ejected from the syringe onto a microscope slide and the presence of individually suspended nanowires was confirmed using a Nikon eclipse 80i microscope (Nikon, Japan).

For paper IV, a midline incision was made to expose the skull and craniotomies ($\varnothing$ 1 mm^2) were drilled at the single bundle implantation sites and one craniotomy (6 x 1 mm) was made at the five bundle implantation site. The dura mater was incised and deflected. The implants were attached to a hydraulic micromanipulator (KOPF instruments, USA) using a small clip holding on to the top of the wire bundle. This top part of the gelatin embedded bundle contained only gelatin and no wires. Implantations were made to a depth of 2 mm at a speed of 10 µm/s. The gelatin attaching the bundle to the micromanipulator was flushed with room temperature (RT) saline solution until the gelatin dissolved and thereby released the implant. This insertion method enables implantation and release of implants without moving them while inside the brain. The implants were left untethered in the tissue, i.e. they had no attachment to the skull or each other.

Histology (I, II, IV)

The animals were killed by an i.p. overdose of pentobarbital at 1 or 6 weeks (IV) or after 12 weeks or one year (I, II) post implantation/injection. The animals were transcardially perfused with 200 mL of ice-cold saline solution (sodium chloride 0.9% in distilled water) followed by 125 mL of ice-cold 4% paraformaldehyde (PFA) in 0.1 M phosphate buffer (pH 7.4). The brains were dissected and post-fixed in 4% PFA overnight (4 °C). In addition, cervical lymph nodes (I, II), liver (I), heart (I) and vessels (I) from all experimental groups were dissected and post-fixed in 4% PFA overnight (4 °C). Following post-fixation in PFA, the tissues were cryoprotected in 25% sucrose solution until equilibrated (4 °C).

For paper I and II, the brains or tissues were snap frozen with dry ice and attached to a sectioning block using Tissue Tek optimal cutting temperature (O.C.T.) compound (Sakura Finetek, USA). Consecutive coronal sections of the brains were cut serially (6 series) in increments of 10 μm onto Super Frost® plus slides (Menzel-Gläser, Germany) using a cryostat (Microm, Germany).

For paper IV, the wire bundles were carefully removed and the brains were snap frozen and horizontally cryosectioned serially (4 series) in increments of 10 μm onto Super Frost® plus slides.

The primary antibodies used to visualize activated microglia or macrophages (CD68/ED1), astrocytes (glial fibrillary acidic protein (GFAP)), and neurons (neuronal nuclei (NeuN)) are listed in Table 2. All stained sections were also counterstained with 4′,6-diamidino-2-phenylindole (DAPI), an all cell nuclei marker. Tissue sections were hydrated and rinsed with phosphate buffered saline (PBS) three times. Following rinsing, the sections were incubated with blocking solution to prevent unspecific binding (5% normal goat serum and 0.25% Triton X-100 in PBS, 1 hr, at room temperature (RT)). Incubation with the primary antibodies (in blocking solution) was made at RT overnight. The following day, sections were rinsed in PBS followed by incubation (light sealed chambers, RT, 2 hrs) with DAPI and the secondary antibodies: goat anti-rabbit IgG Alexa 594 and goat anti-mouse IgG Alexa 488 (in blocking solution) (Table 2). Sections were rinsed in PBS three times and coverslipped using PVA/DABCO (Fluka/Sigma-Aldrich, Switzerland).

For paper I and II, the tissues were from older animals (~ 5 and 14 months) and thus, when staining with the NeuN antibody, an antigen retrieval method was also performed. In short, after hydration and rinsing the sections, they were immersed in a 10 mM sodium citrate buffer (0.05% Tween 20, pH 6) and subsequently microwaved for 3 x 5 min at 500 W. PBS was omitted from the staining protocol and a Tris-buffer (Sigma-Aldrich, Germany) was used instead and Triton X-100

was excluded from the blocking solution, otherwise all steps were made according to the staining protocol above.

The lymph nodes, liver, heart and vessels were sectioned in increments of 10 µm and labeled with ED1 and DAPI, in the same manner as mentioned above. The sections were screened for presence of nanowires using a Nikon eclipse 80i microscope and a laser scanning confocal microscope (Zeiss LSM 510). Nanowires can be visualized using the laser reflection mode, since they scatter confocal laser light.

Table 2.
List of primary antibodies, secondary antibodies and nucleic acid stain used in paper I, II and IV.

Name	Characteristics	Host	Working dilution	Source
CD68/ED1	Activated microglia/macrophages	Mouse	1:250	Cat. Nr. MCA341R, AbD Serotec, UK
GFAP	Glial fibrillary acidic protein, activated astrocyte marker	Rabbit	1:5000	Cat. Nr. Z0334, Dako, Denmark
NeuN	Neuronal nuclei, an neuronal marker	Mouse	1:100	Cat. Nr. MAB377, Millipore, USA
DAPI	Nucleic acid stain (4',6-diamidino-2-phenylindole), all cell nuclei marker	-	1:1000	Cat. Nr. D3571, Invitrogen, USA
Alexa Fluor 594	Goat anti-rabbit IgG (H + L), secondary antibody	Goat	1:500	Cat. Nr. A11005, Invitrogen, USA
Alexa Fluor 488	Goat anti-mouse IgG (H + L), secondary antibody	Goat	1:500	Cat. Nr. A11001, Invitrogen, USA

Image acquisition and analysis

Image acquisition was done with a DS-2MV digital camera (Nikon, Japan) mounted on a Nikon eclipse 80i microscope (Nikon, Japan) with a 10x objective (I, II, IV).

For paper I and II, the quantification analysis was carried out according to a previously described method [82]. In order to quantify the density of neurons and activated glial cells in defined regions of interest (ROIs), we quantified selected cell markers in the tissue (Table 2). The scar in the tissue was located using ED1- and GFAP-positive area. A photograph was taken of the fluorescence of the ED1- and GFAP-positive cells and cell nuclei (DAPI), where the injection scar was seen at its maximum. The images were used to quantify ED1, GFAP and DAPI. The adjacent sections (from the second series) were stained with NeuN, GFAP and DAPI and photographs of the scar were taken. These images were used to quantify neuronal density in the scar area.

A rectangular shaped ROI (ROI; total ROI area 300 x 800 µm) was centered on the scar to evaluate the inflammatory response (ED1, GFAP), all cell (DAPI) and neuronal density (NeuN). The rectangle was divided into an inner and an outer ROI (100 x 800 µm and 200 x 800 µm, respectively) (Fig. 4). The inner ROI quantifies the area 0-50 µm from the injection tract, this area was chosen since neuronal activity can be recorded up to ~50 µm from an electrode and thus it is crucial that there are viable neurons in this area [83]. The outer ROI quantifies the area 50-150 µm from the injection tract and this ROI was chosen in order to detect a possible widespread inflammatory tissue response or neuronal death in the tissue.
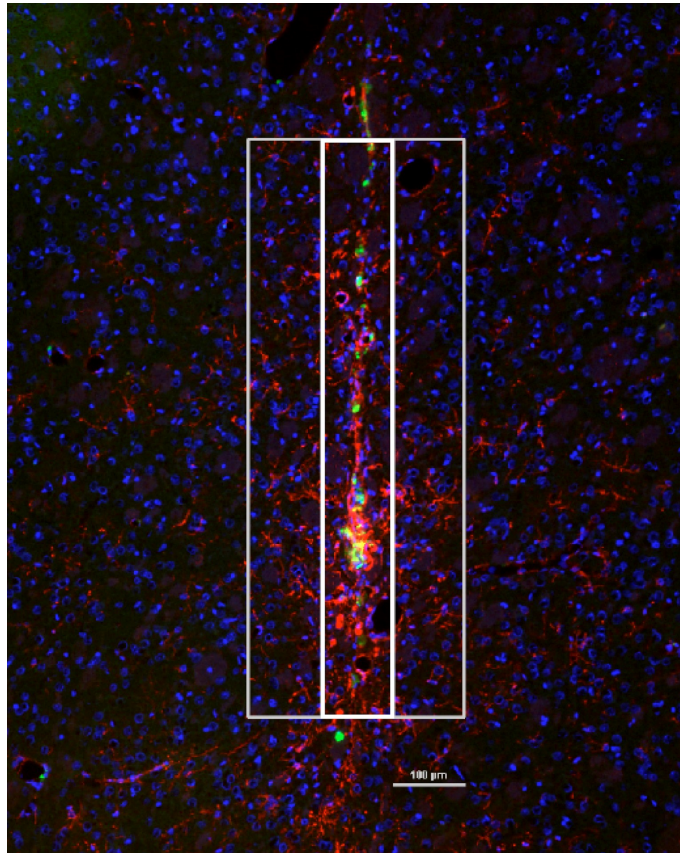

Figure 4.Quantification method (I, II).
Representative image of the two regions of interest (ROIs). The inner ROI (100 x 800 µm) is depicted here in white and the outer ROI (200 x 800 µm) in grey. This image shows the scar after injection of 10 µm long nanowires after 12 weeks. ED1-positive cells (green), GFAP-positive cells (red), and cell nuclei (blue). Scale bar: 100 µm.

The quantifications of the different markers were carried out by measuring the proportion of immunoreactive area (ED1, GFAP) or by counting the number of cells (NeuN, DAPI) within the total screened area, i.e. inner or outer ROI. In order to ensure that nonspecific staining was not included in the area assigned as ED1 or GFAP-positive, thresholds were set for each image at a fixed ratio of the mean background intensity. Thus, only the fraction of area in the ROI with intensity above this set threshold was quantified. Intensity thresholds for the signal to background ratio were set at 5.5 times the background intensity for ED1 immunofluorescence and at 4.5 times for GFAP immunofluorescence. Neuronal nuclei were quantified manually by counting NeuN-positive cells with a co-stained DAPI-positive nucleus within the ROIs. Cell nuclei were quantified by counting DAPI-positive nuclei (nuclei above $\varnothing$ 3 µm, to avoid counting debris/artefacts) within the ROIs.

To visualize nanowires in the tissue, we used confocal imaging. Confocal images were obtained with a laser scanning confocal microscope (Zeiss LSM 510, Germany) with a 63x oil-immersion objective (N.A. 1.4) and Zen software (Zeiss, Germany). The nanowires can be seen in the tissue using the laser-reflection mode. Image J was used for processing of all confocal images.

For paper IV, images from the middle of the shaft of each bundle track, at an approximate depth of 1 mm below brain surface, were captured. The ROIs were set at 0–50 µm and 50–200 µm distance from the rim of the scar left by the wire bundles. The histological quantification method has previously been described in detail [42, 67]. Intensity thresholds for quantification of astrocytes and microglia were used as in paper I and II. The intensity thresholds were set at 6 times the background intensity for GFAP and at 5 times for ED1 immunofluorescence. Due to variability in the markers and the different marker batches antigen-specificity, the thresholds were set at individual levels for each marker and each study. The larger the contrast between the unspecific background and the positively labeled cells, the higher the threshold was set.

Nanowire substrate embedment (III)

Porcine skin type A gelatin (~300 Bloom) (Sigma Aldrich, Switzerland) was dissolved in de-ionized water at 50 mg/ml (5%) or 100 mg/ml (10%). The gelatin solutions were subsequently heated up to 70 °C and cooled down to 50 °C. To increase the gels flexibility, glycerol was added to the 100 mg/ml gelatin solution at a concentration of 100/40 gelatin/glycerol (w/w) or 100/60 gelatin/glycerol (w/w) (20 min, 50 °C). The substrates were dip-coated in the gelatin or gelatin/glycerol solutions and were left to dry horizontally at RT overnight. To

remove the embedding matrixes the substrates were soaked in de-ionized water at 50 °C (90 min).

Brain model insertion (III)

A brain tissue model for substrate implantations was made by mixing 1% agar in de-ionized water. The solution was heated up to 80–90 °C (15 min). The nanowire substrates with different embedding were inserted into the agar gel and immediately retracted using a micromanipulator (Kopf Instruments) at 25 µm/s.

Statistical analyses

To compare the experimental groups the Kruskal Wallis with Dunn's multiple comparison test was used (I). For comparison of two paired groups (SW vs. SW-control (HBSS injection only)) Wilcoxon matched-pairs signed rank test was used (I). Mann-Whitney test was used to compare the SiOx-coated nanowire group to the HfOx-coated nanowire group (II).

Kruskal-Wallis and the Dunn's post hoc test were used for comparison of selected pairs (IV). The comparisons made were as follows: i) middle implant and the mean of the two outer implants; ii) middle implant and the contralateral implant; and iii) the contralateral implant and the solitary implant (see Fig. 3 for schematic). All values in graphs are presented as median values with indication of the 25 and 75 percentiles and p-values of <0.05 (*) were considered significant (I, II and IV). Analyses in the study were performed using the GraphPad Prism software (GraphPad Software Inc., USA) (I, II, IV).

For paper III, analysis was done using scanning electron microscopy (SEM) (microscope JSM 6400F, SEM Leo 1560, or FEI Nova NanoLab 600) with stage tilted at 20° unless otherwise indicated. Percentage of broken or bent nanowires was quantified by counting the number of nanowires with a horizontal projection of 1.5 µm or more on SEM images taken with no stage tilt. On a non-tilted stage, nanowires not affected by the embedding or insertion process remain vertical and remain point-like in the images, while a 1.5 µm length corresponds to approximately a bending of the wires by 20°. A total area of 6645 μm^2 was imaged in the middle of the substrates and the broken or bent nanowires were counted using a cell counter plugin in Image J software.

Results and comments

Brain tissue response to free nanowires (I, II)

Nanowire-structured neural interfaces hold promise for enhanced biocompatibility and improved electrode properties, as well as the possibility to record and interact with individual spines and neurons. However, stress put on the nanowires, for example during the implantation procedure and later by wear and tear, a portion of the nanowires might detach from the surface. These high-aspect-ratio nanowires share similar morphological features as asbestos fibers and could in a worst-case scenario give rise to an escalating inflammatory response, as seen in asbestosis. Hence, there was a need to clarify the risks involved in exposing brain tissue to free nanowires. Here, in a long-term nanosafety study we aim to identify a nanowire length suitable for use as a surface structure on a neural interface. Thus 2, 5 and 10 µm long biostable high-aspect ratio nanowires were injected into striatum (I). Furthermore, we compared the long-term brain tissue response to two different surface coatings, SiOx (degradable) vs. HfOx (biostable), of 2 µm long nanowires (II). The animals were killed 12 weeks or 1 year after nanowire injection. It should be noted that one year correspond to approximately half the lifetime of a rat. We chose to evaluate the tissue response at this time point in order to ensure that any possible escalation in inflammatory response or neurotoxicity that might occur over longer time periods could be detected. The different cell markers used were quantified in two ROIs (inner and outer ROI) centered on the injection tract. To assess the tissue response, activated microglia (ED1) and astrocytes (GFAP) were quantified as well as the neuronal survival (NeuN) and cell nuclei density (DAPI). Confocal microscopy was used to detect nanowires or nanowire debris present in the dissected tissues (brain, cervical lymph nodes, liver and heart).

Evaluating the control solution

In order to ensure that the control solution, HBSS, did not have an adverse effect on the tissue, the tissue response following an HBSS injection alone was compared to that of a stab wound in a 12 week study. Bilateral surgery was performed on

eight animals, with stab wound in one hemisphere and a HBSS injection in the contralateral hemisphere. No significant difference in the outer ROI for any of the markers was found and there was no significant difference in the inner ROI in ED1-positive area, neuronal density or cell nuclei density. For the GFAP-positive area we found, in fact, a small but significant increase for the stab wound group in the inner ROI, mean 17.4% ± 2.3% compared to 10.9% ± 1.3% for the control injection. This finding suggests that HBSS might actually have a beneficial effect on the tissue response that follows the injection trauma. One plausible explanation for this could be that the injection of the solution results in a dilution of pro-inflammatory factors in the injection tract, factors such as interleukins, nuclear transcription factor-κB or transforming growth factor-β, that are known to be involved in the recruitment of astrocytes [84]. This could possibly result in a lowered level of astrocytic reactivity and thus in a decrease in GFAP-positive area. The finding is interesting but further investigations are needed in order to elucidate mechanisms responsible. However, we concluded that the control solution did not have an adverse effect on the brain tissue and could safely be used as vehicle solution.

Microglia/macrophage activity (ED1) (I)

Figure 5 and 6 show representative fluorescence microscopy images of the inflammatory tissue response 12 weeks and one year, respectively, after injections of control solution (HBSS injection only) or biostable nanowires of different lengths (2, 5 and 10 μm). The figures show microglia (green) localized to the center of the scar and astrocytes (red) in a more widespread area surrounding the injection tract.

Figure 5. Tissue response 12 weeks after nanowire injection.
Representative fluorescent images of the brain tissue response 12 weeks after injection of a) control solution, b) 2, c) 5 and d) 10 µm long HfOx-coated nanowires. ED1-positive cells (green), GFAP-positive cells (red), cell nuclei (blue) and merge. Scale bars: 100 µm.
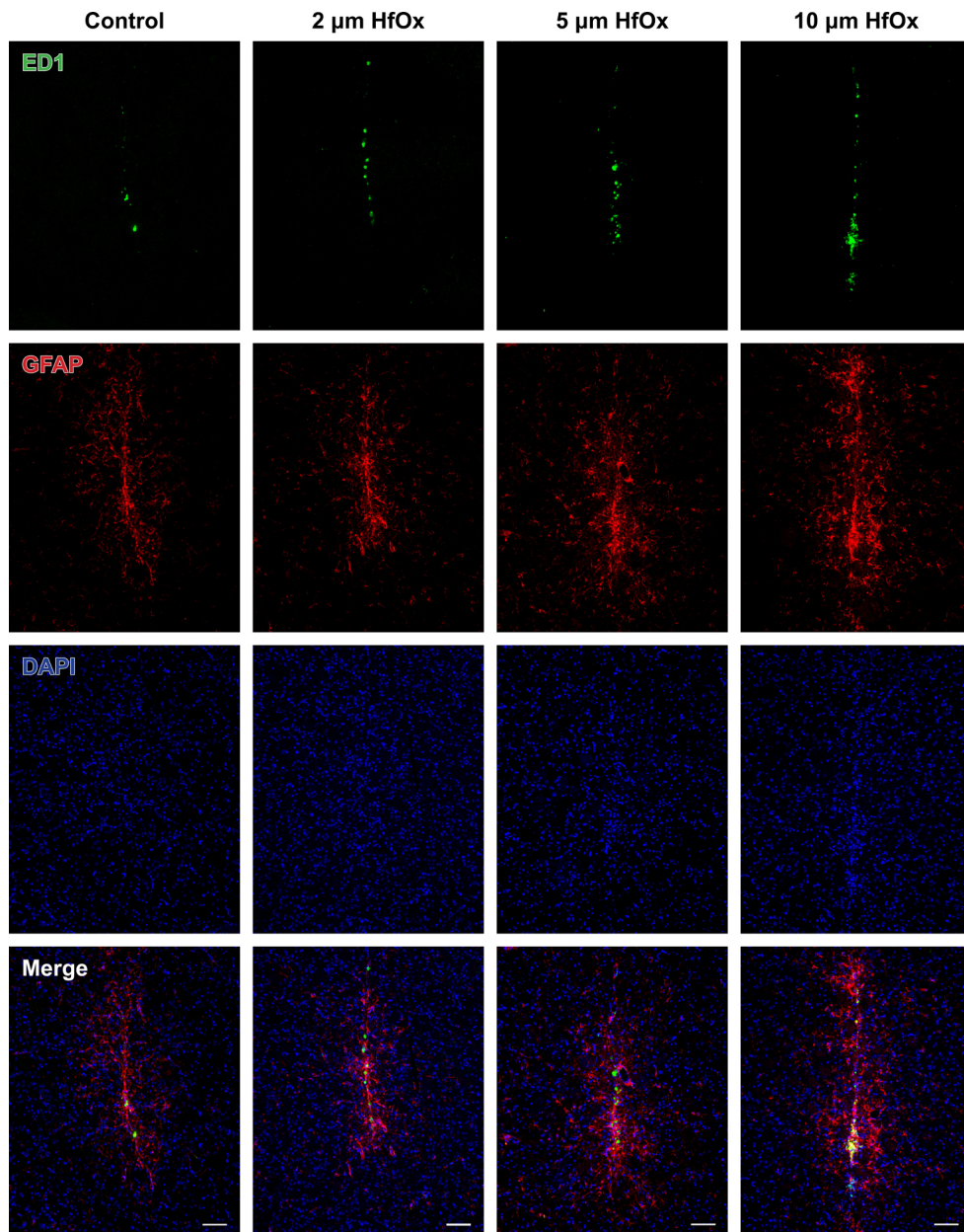
Figure 6. Tissue response 1 year after nanowire injection.
Representative fluorescent images of the brain tissue response 1 year after injection of a) control solution, b) 2, c) 5 and d) 10 μm long HfOx-coated nanowires. ED1-positive cells (green), GFAP-positive cells (red), cell nuclei (blue) and merge. Scale bars: 100μm.
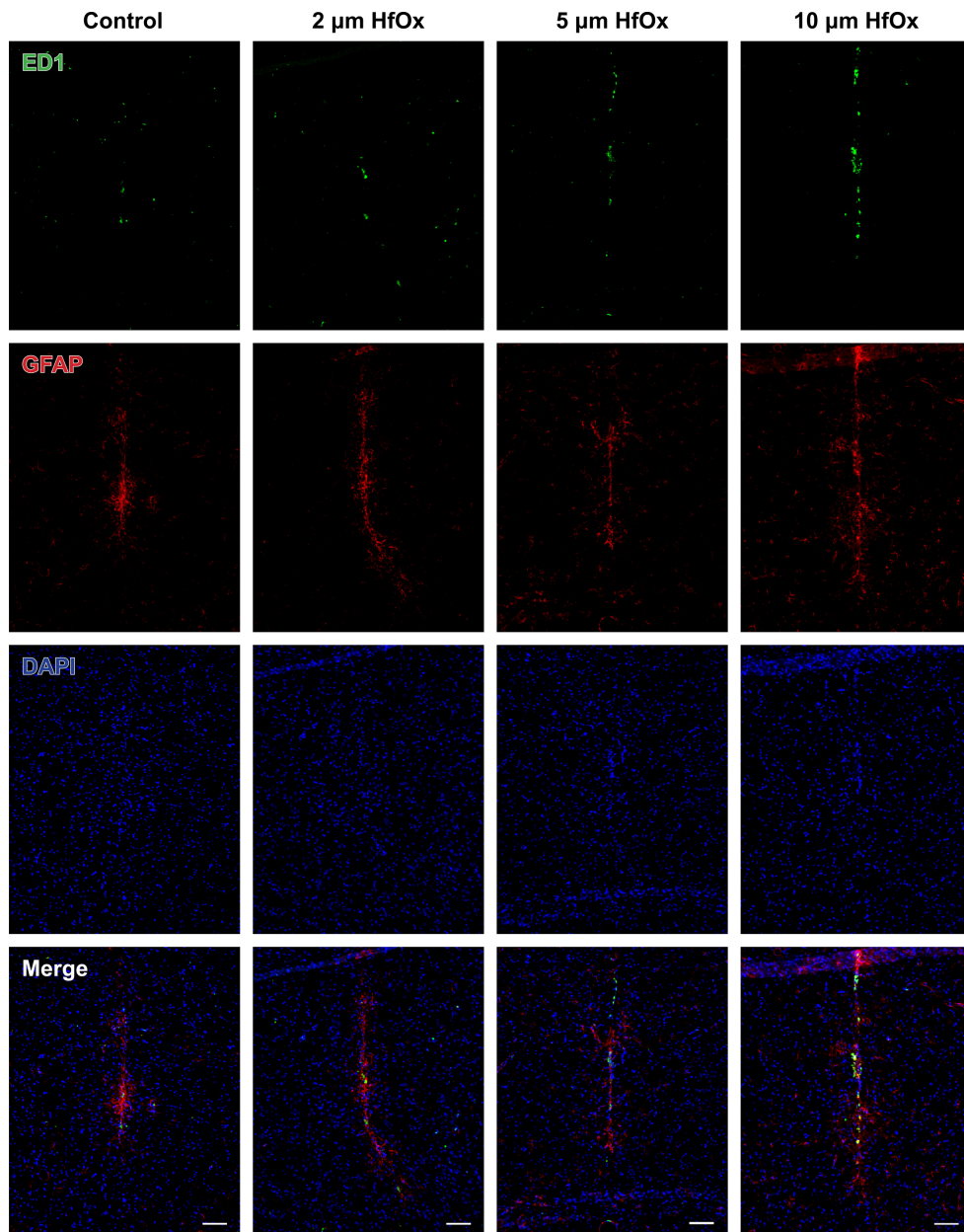
In the inner ROI after 12 weeks there was a significant increase in ED1-positive area when comparing the 10 µm long nanowire group to both the control group (HBSS injection only) and to the group receiving 2 µm long nanowires (Fig. 7). At one year post injection there was a significant increase in ED1-positive area in the inner ROI comparing the groups receiving 10 and 5 µm long nanowires to the control group (HBSS injection only) (Fig. 8). The increased ED1 immunoreactivity seen for the longer nanowire groups might reflect a length dependent limit of the phagocytic capacity of the microglia. Indeed, when the nanowire lengths are approximately equal to the diameter of the phagocytizing cell (~ 5-10 µm), difficulty in engulfing the nanowires would be expected. This could possibly lead to the cells becoming frustrated, triggering a continuous release of toxic agents. However, no sign of escalation over time in the ED1 response was detected. In the outer ROI, there was no significant difference in ED1-positive area comparing the groups at any of the two time points. The overall immunoreactive area for ED1 in the outer ROI was close to zero after one year in all groups, thus, the microglial and macrophage activity is essentially limited to the inner ROI.

Astrocytic reactivity (GFAP) (I)

In the inner ROI at 12 weeks post injection, the group receiving 10 µm long nanowires exhibited a significant increase in GFAP-positive area compared to the control group (HBSS injection only) (Fig. 7). No significant difference was found in the inner ROI after one year. In the outer ROI, there was a significant increase in GFAP-positive area for the 5 µm nanowire group compared to the control group (HBSS injection only) (Fig. 7) and after one year a significant increase in GFAP-positive area was found comparing the 10 µm long nanowire group to the 5 µm long nanowire group (Fig. 8).

The increase in astrocytic activity found for the 10 µm long nanowires at 12 weeks in the inner ROI did not persist at one year. However, the GFAP immunoreactivity appears to be slightly more widespread in the tissue after one year in the 10 µm nanowire group (see outer ROI, Fig. 8). However, no obvious escalation in astrocytic activity was observed for any of the groups.
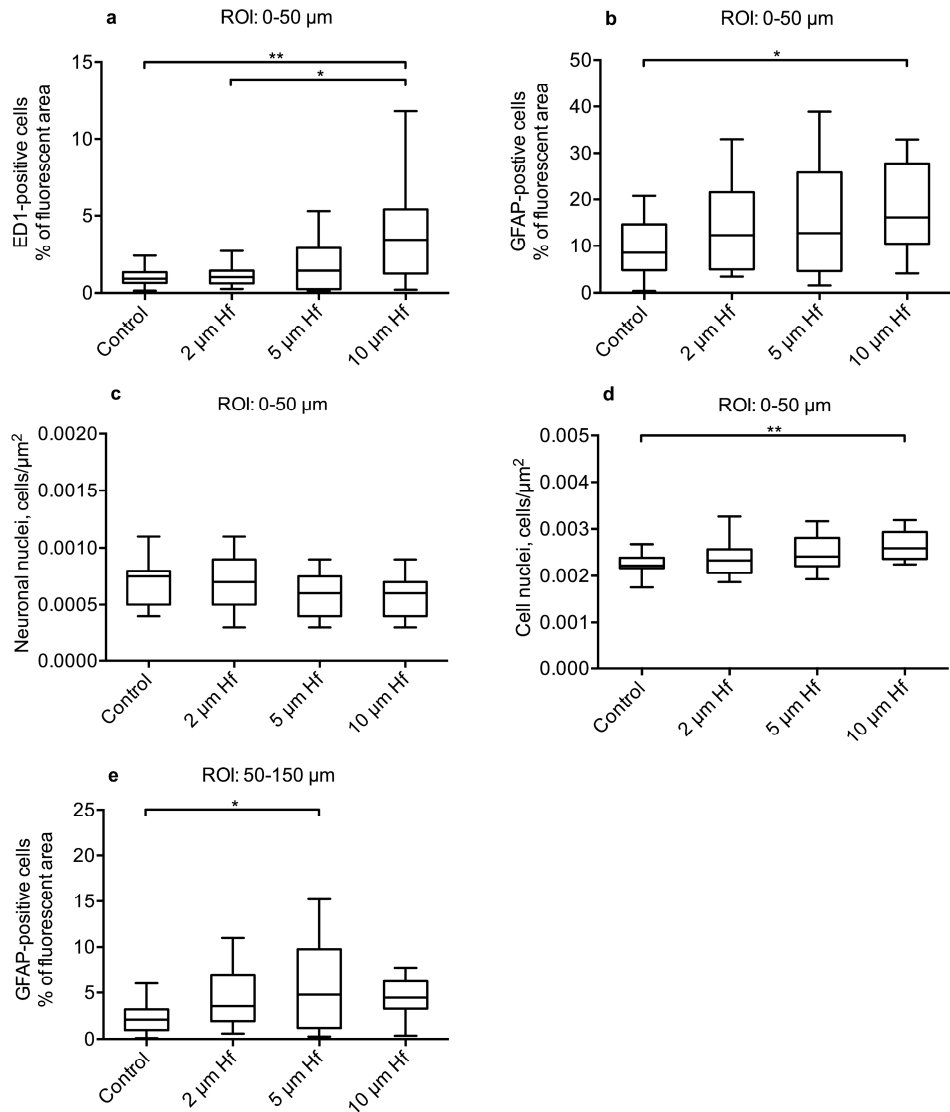
Figure 7. Inflammatory tissue response, neuronal and cell density 12 weeks post nanowire injection.
Boxplots showing the quantification in the inner ROI (0-50 µm) of a) ED1-positive area, b) GFAP-positive area, c) NeuN density and d) cell density at 12 weeks post nanowire and control injection (HBSS only). Quantification in the outer ROI (50-150 µm) of e) GFAP-positive area at 12 weeks post nanowire and control injection (HBSS only).

38
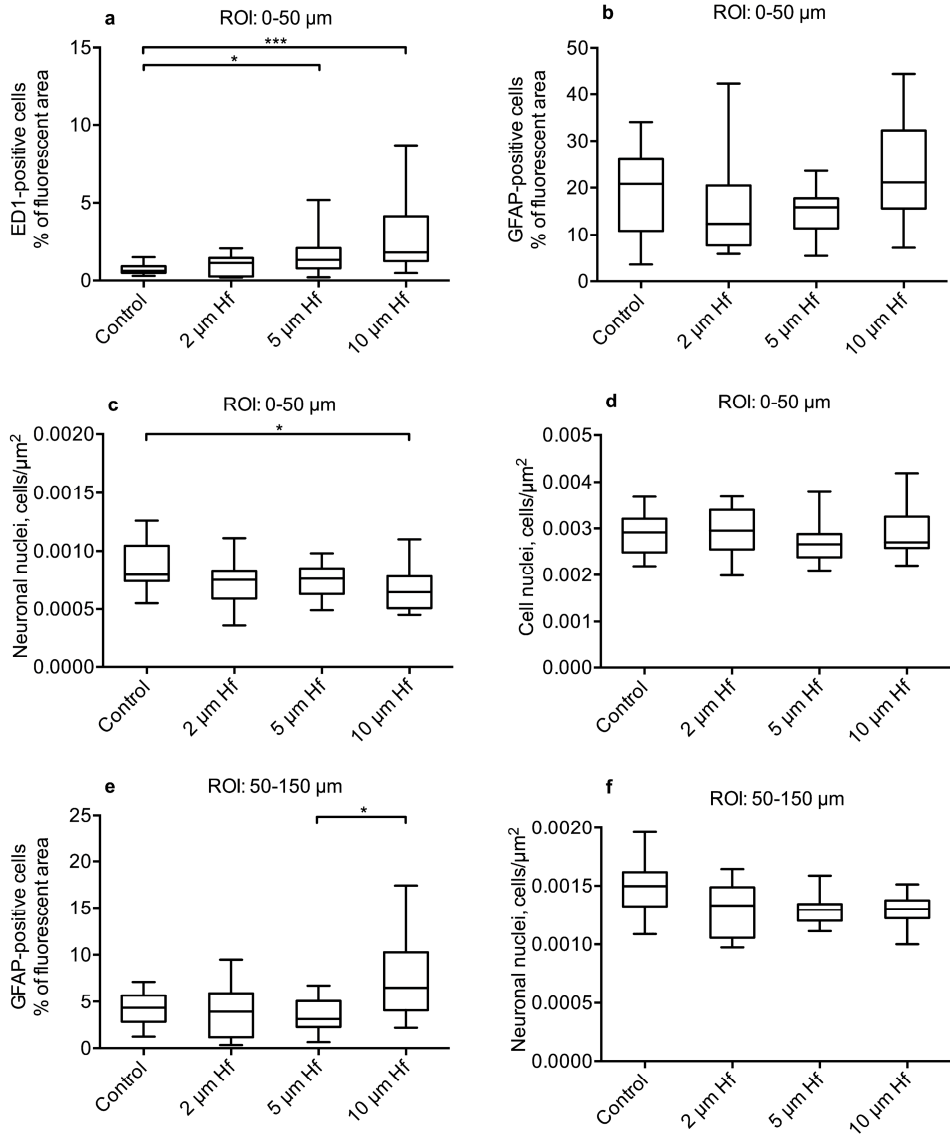
Figure 8. Inflammatory tissue response, neuronal and cell density one year post nanowire injection.
Boxplots showing the quantification in the inner ROI (0-50 μm) of a) ED1-positive area, b) GFAP-positive area, c) NeuN density and d) cell density at one year post nanowire and control injection (HBSS only). Quantification in the outer ROI (50-150 μm) of e) GFAP-positive area and f) NeuN density at one year post nanowire and control injection (HBSS only).

Neurons (NeuN) (I)

No significant difference was found in neuronal density, in the inner (Fig. 7) or outer ROI at 12 weeks post injection, indicating that no nanowire-induced neurotoxicity had developed. However, at the one year time point, in the inner ROI, there was a significant decrease in neuronal density in the group receiving 10 μm long nanowires compared to the control group (HBSS injection only) (Fig. 8). The decrease observed corresponds to approximately a 24% loss of neurons in the 10 μm nanowire group compared to the control group (HBSS injection only). In the outer ROI, no significant difference in neuronal density was found when comparing the different groups, hence, indicating that the loss of neurons in the 10 μm group in the inner ROI, was likely not caused by a displacement of neurons from the inner to the outer ROI.

Cell nuclei (DAPI) (I)

In the inner ROI we found a significant increase in the number of cell nuclei (DAPI) in the 10 μm long nanowire group compared to the control group (HBSS injection only) after 12 weeks. This corresponds to a cell nuclei increase of approximately 17% in the 10 μm nanowire group compared to the control group (HBSS injection only). The increase could be explained by the increase in the markers for activated microglia (ED1) and astrocytes (GFAP) noted in the group at this time point. Nevertheless, we can not exclude that other un-labeled cells that are involved in the inflammatory response and wound healing, e.g. pericytes or fibroblast, contribute to this increased cell density. There was no significant difference in cell nuclei density when comparing the groups at one year post injection (Fig. 8).

Degradable vs biostable nanowires (II)

Figure 9 and 10 show representative fluorescence microscopy images and quantification of the inflammatory tissue response one year post injections of 2 μm long biostable or degradable GaP nanowires. When comparing the ED1-positive area, GFAP-positive area, neuronal density and the cell nuclei density for the two groups no significant difference was seen in the inner or outer ROI (Fig. 9, 10). The injection of 2 μm long biostable nanowires results in a tissue response and neuronal density not significantly different from a control injection (HBSS injection only) (I). Hence, the degradable nanowires evaluated here show no obvious neurotoxicity or biosafety issues.
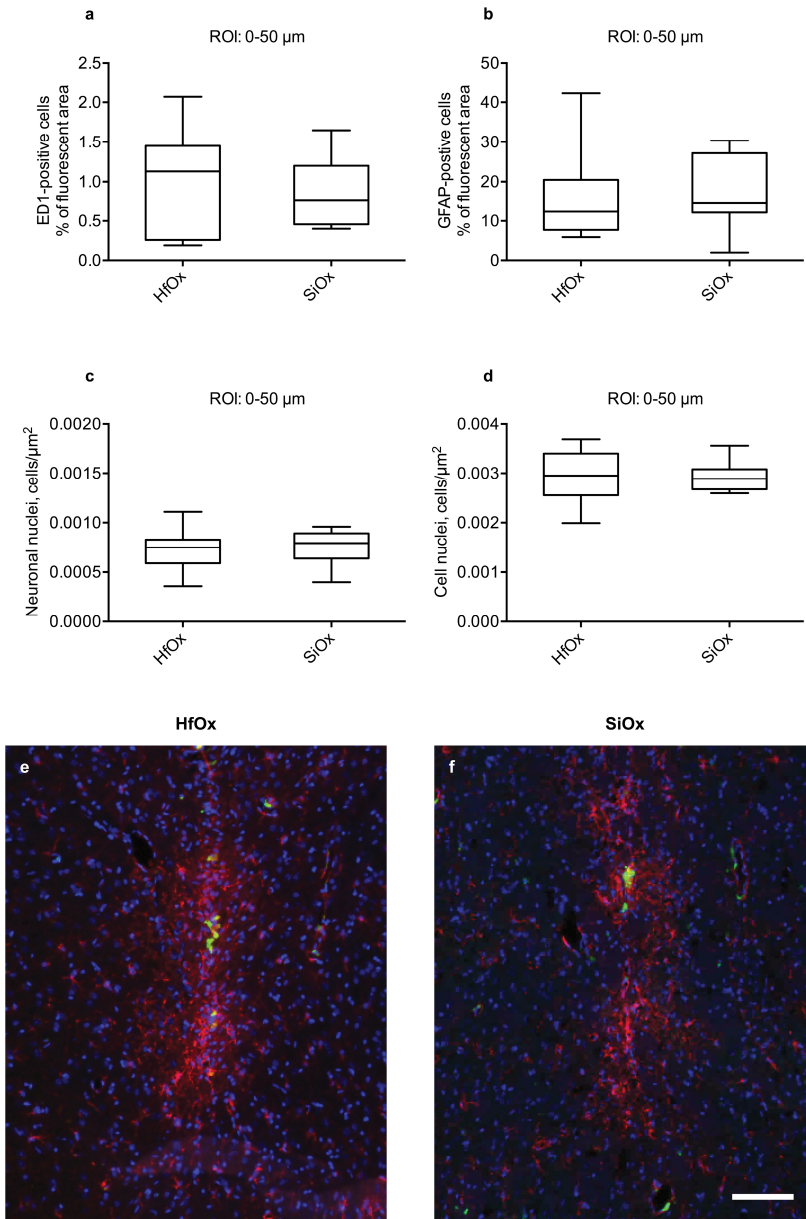
Figure 9. Quantification (inner ROI) and representative fluorescent images of GaP nanowires with biostable (HfOx) vs. degradable (SiOx) coating.
Quantification in the inner ROI (0-50 µm) of ED1-positive area (a), GFAP-positive area (b), neuronal density (c), and cell nuclei density (d) for 2 µm long HfOx-coated GaP nanowires and 2 µm long SiOx-coated GaP nanowires one year post injection. Representative fluorescent images one year post injection of (e) 2 µm long HfOx-coated GaP nanowires and (f) 2 µm long SiOx-coated GaP nanowires. ED1-positive cells (green), GFAP-positive cells (red), and cell nuclei (blue). Scale bar: 100 µm.

41

Figure 10. Quantification (inner ROI) and representative fluorescent images of GaP nanowires with biostable (HfOx) vs. degradable (SiOx) coating.
Quantification in the inner ROI (50-150 μm) of ED1-positive area (a), GFAP-positive area (b), neuronal density (c), and cell nuclei density (d) for 2 μm long HfOx-coated GaP nanowires and 2 μm long SiOx-coated GaP nanowires one year post injection. Representative fluorescent images one year post injection of (e) 2 μm long HfOx-coated GaP nanowires and (f) 2 μm long SiOx-coated GaP nanowires. Neuronal nuclei (green), GFAP-positive cells (red), and cell nuclei (blue). Scale bar: 100 μm.

Confocal analysis (I, II)

At both time points, confocal examination of the experimental groups receiving biostable nanowires of different lengths showed that microglia or macrophages had engulfed most of the 2 μm long nanowires. Whereas, for the groups receiving 5 μm and 10 μm long nanowires, some nan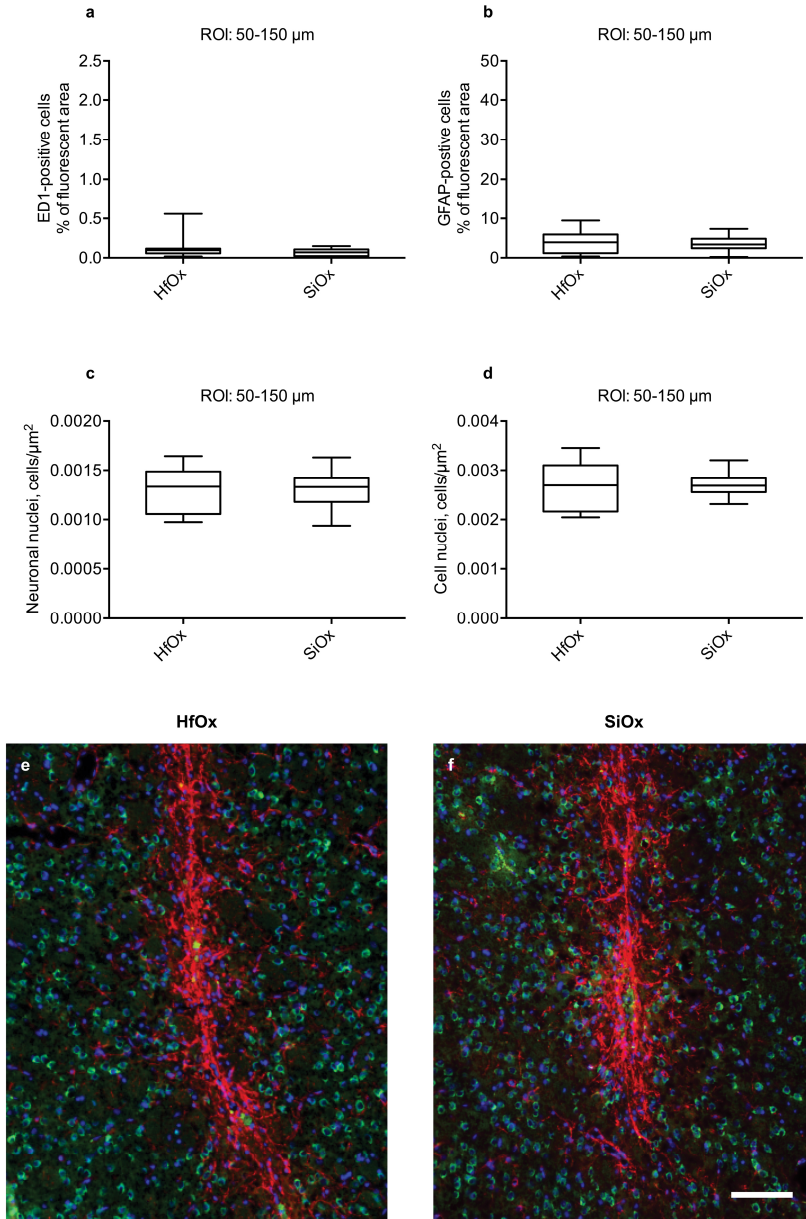owires were not engulfed and was seen free in the tissue. Furthermore, in the injection scar, small aggregations of co-localized ED1 and GFAP staining was observed. These aggregates, possibly cell debris or aggregations of cells, most often contained nanowires, see Figure 11. The double positive (ED1 and GFAP) aggregates were frequently lacking DAPI-positive nuclei, indicating that the aggregates may not have contained viable cells. Furthermore, the aggregates were mostly seen in the groups with the longer nanowires (5 and 10 μm) at one year post injection and they were rarely seen at the early time point, i.e. at 12 weeks.
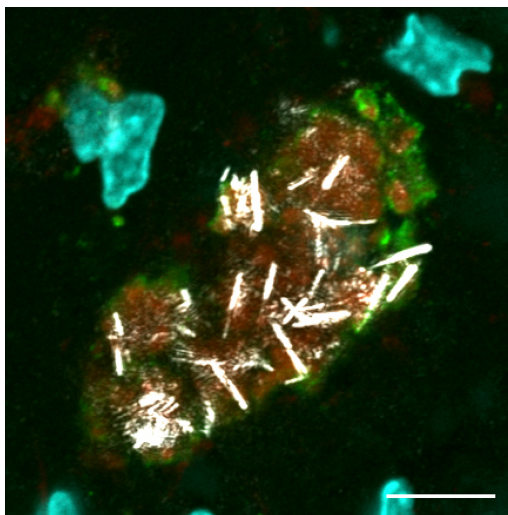
Figure 11. Confocal image of aggregate one year after injection of biostable nanowires into the brain
Laser scanning confocal microscopy image of the scar area after injection of 5 μm long HfOx-coated GaP nanowires one year post injection. The image shows an aggregate of cells or cell debris with internalized nanowires. The aggregate lacks DAPI-positive nuclei. ED1-positive cells (green), GFAP-positive cells (red), cell nuclei (blue), and nanowires (white). Scale bar: 10 μm.

For the two different nanowire coatings, we found ED1-positive cells with both engulfed degraded nanowire residue (SiOx-coated) and intact biostable nanowires (HfOx-coated) (Fig. 12). The intact HfOx-coated biostable nanowires were found both in larger cells and in cell aggregates, as well as in smaller ED1-positive cells. For the degradable SiOx-coated nanowires residues were primarily seen in large ED1-positive cells or in ED1-positive cell aggregates. It is possible that the aggregates seen in the tissue were macrophages/microglial cells that had fused to

form multinucleated giant cells. In a few instances intact SiOx-coated nanowires were present in the tissue, primarily in single, small ED1-positive cells. This might be expected since the degradation process is probably much slower in the single, small ED1-positive cells compared to the giant cells. The giant cells are assumed to be highly activated cells that can produce large amounts of free radicals and proteolytical enzymes, this would likely speed up the breakdown of the degradable nanowires [25]. Confocal examination of the ED1-positive cells also suggest that more nanowire material remain at or in the vicinity of the injection site for the HfOx-coated nanowire group compared to the degradable SiOx-coated nanowire group. This could result from that the nanowires are broken down into very small fragments that might not be visualized using confocal microscope, since the smaller the fragments the less they scatter the laser light. However, this could also be a result of clearance from the brain.
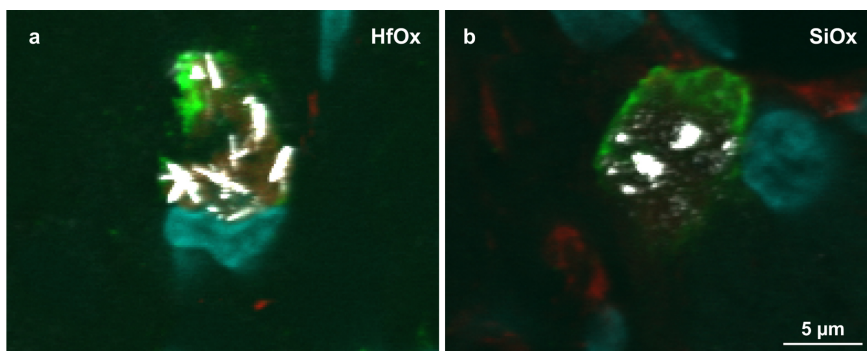
Figure 12. Close-up confocal images one year post injection of biostable and degradable GaP nanowires.
Laser scanning confocal microscopy images showing ED1-positive cells with engulfed nanowires or nanowire debris. a) 2 μm long HfOx-coated nanowires injected into striatum and b) 2 μm long SiOx-coated GaP nanowires one year post injection into rat striatum. ED1-positive cells (green), GFAP-positive cells (red), cell nuclei (blue) and nanowires (white, scattered laser light). Scale bar 5 μm.

For both paper I and II, we scanned external tissue (cervical lymph nodes, liver, blood vessels, and heart) for presence of nanowires or nanowire debris. The cervical lymph nodes are a known target for monocytes emigrating from the brain [85]. However, we found no nanowires or nanowire debris, free or engulfed, in any group at any of the two time points. This suggests, that there is a very slow or non-existent nanowire clearance from the brain. This hypothesis agrees with reports showing that nanoparticles introduced orally, can pass the BBB, accumulate in the brain and remain in the brain tissue months after delivery [86, 87].

Developing a technique for implantation of nanostructured neural interfaces (III)

In order to implant a thin and flexible nanostructured neural interface into the brain we needed to develop a method that enabled implantation without destroying the nanostructure. To do this we evaluated nanowire preservation after embedding nanowire substrates with an embedding matrix with different concentrations of gelatin/glycerol, where glycerol acts as a plasticizer.

Embedding in gelatin solution

Figure 13 shows a nanowire substrate embedded in 5% gelatin (A) before and (B) after gelatin removal, i.e. after soaking the substrate in de-ionized water (50 °C, 90 min). The nanowires on the substrates were bent, broken, or agglomerated with the same pattern that was seen in the gelatin layer. This was probably due to internal forces during the drying process, caused by stress in the cross-links. As a control step, a nanowire substrate was washed according to the gelatin removal process and the nanowires on the substrate remained vertical. Thus, the gelatin embedding was responsible for the nanowire damage and not the gelatin removal step.
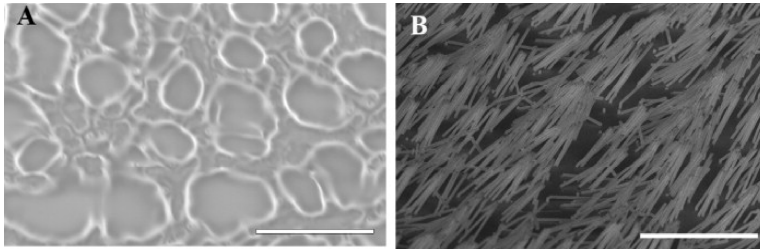
Figure 13. SEM images of a nanowire substrate before and after gelatin removal.
Nanowire substrate embedded in 5% gelatin solution (A) before and (B) after gelatin removal step. Nanowires on the substrate are bent, broken, or agglomerated due to the forces caused by the gelatin drying step. Scale bars: 10µm.

Embedding in gelatin/glycerol solution

The internal forces of the gelatin embedding needed to be reduced in order to preserve the nanowires on the substrate surface. Hence, the plasticizer glycerol was added to the embedding matrix in different concentrations. Figure 14 shows SEM images of nanowire substrates after removal of the embedding matrix: (A) control (removal step only), (B) nanowire substrate embedded in 100/40 gelatin/glycerol, (C) nanowire substrate embedded in 100/60 gelatin/glycerol, and

(D) nanowire substrate embedded in 100/60 gelatin/glycerol and inserted into agar. Embedding the nanowire electrodes in a 100/40 gelatin/glycerol (w/w) solution resulted in 18% of the nanowires bent or broken. Control surfaces showed 5% of broken or bent nanowires. Increasing the amount of glycerol to 100/60 gelatin/glycerol led to only 8.5% of the nanowire being broken or bent. A 100/60 gelatin/glycerol embedded nanowire substrate was also dipped in agar to mimic a brain insertion. The agar insertion step resulted in 13% of the nanowires being broken or bent after the gelatin/glycerol removal step. Thus, the 100/60 gelatin/glycerol solution could be appropriate for brain insertion, since the embedding process preserved 96% of the nanowires and 95% of the remaining nanowires were protected during the implantation in agar. Hence, the gelatin/glycerol solution is flexible enough to preserve the majority of the nanowires during the drying process and at the same time strong enough to preserve most of them during the implantation step.

Figure 14. SEM images of nanowires after gelatin/glycerol removal.
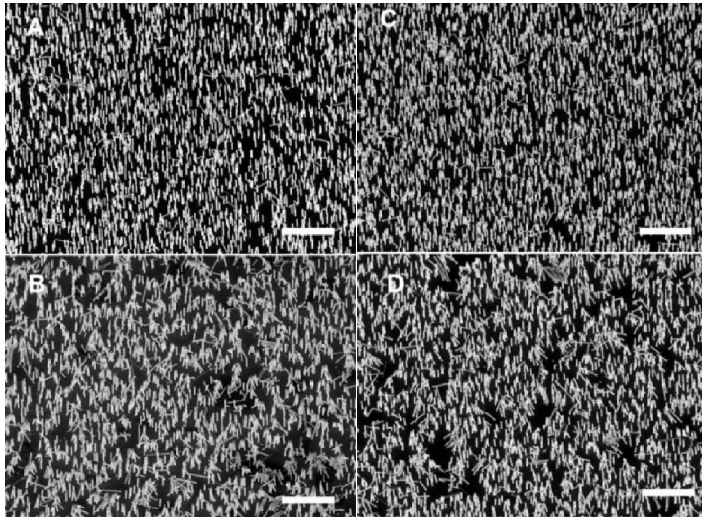(A) Control (removal step only) (B) nanowire substrate after removal of embedding of a 100/40 gelatin/glycerol (w/w) gel, (C) nanowire substrate after removal of embedding in 100/60 gelatin/glycerol, and (D) nanowire substrate that have been embedded in 100/60 gelatin/glycerol and inserted into 1% agar prior to removal of embedding. Scale bars: 10 µm.

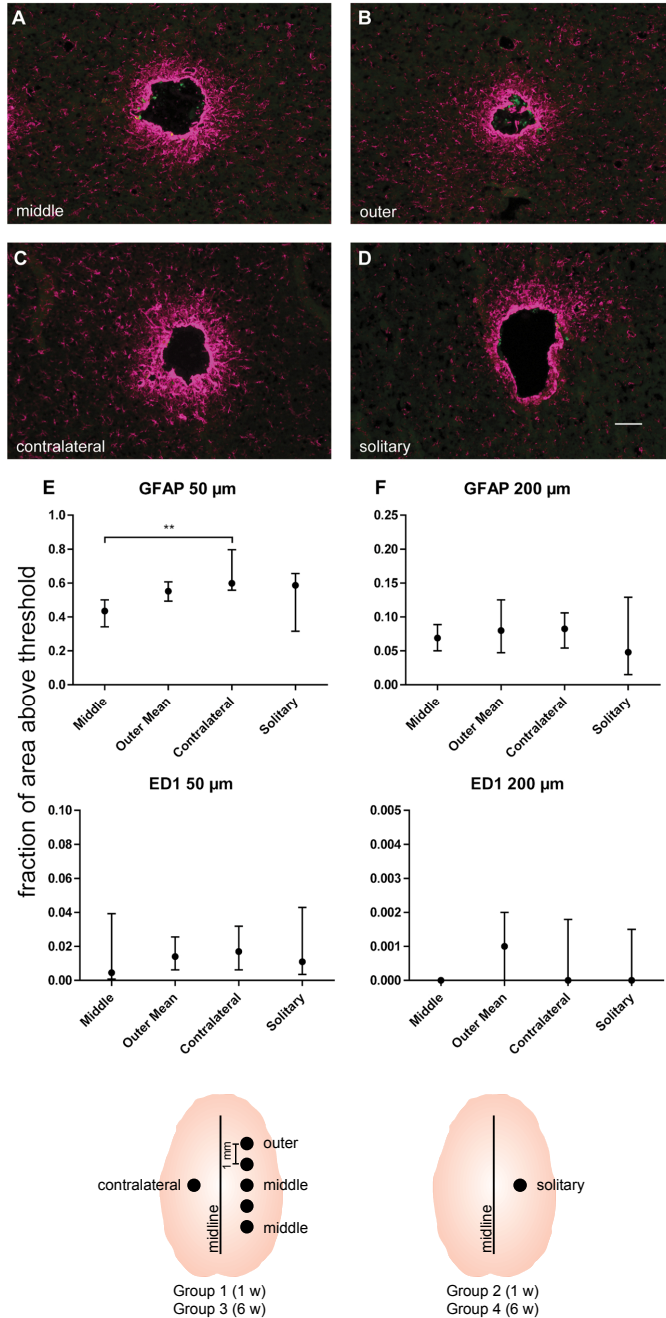# The brain tissue response to multiple implants (IV)

In order to study the activity in neural circuits or interaction of different areas in the brain, at the same time, multiple neural interfaces need to be implanted in different structures in the brain. However, it is not known whether or not multiple implants could result in an increased brain tissue response to each individual implant. In paper IV we wanted to assess whether multiple implants in one hemisphere would lead to cumulatively larger immune responses to individual implants in the same hemisphere and/or in the contralateral hemisphere (see experimental group overview in Figure 15).

Intrahemispheric interactions

We found significantly smaller GFAP-positive areas around the middle implants in the inner ROI (0–50 µm) six weeks post implantation when compared to the contralateral implant (Fig. 15). This effect was quite small, however, it could be explained by a possible competitive recruitment from a limited local pool of astrocytes. When the implants are placed in close vicinity of each other, the middle implant would thus have to compete with the surrounding implants for the local pool of astrocytes. Furthermore, the middle scar tended to have less GFAP-positive areas than both the contralateral scar and the outer scars in all animals (inner ROI, six weeks), although the difference was not statistically significant. A similar trend was observed one week post implantation, where the contralateral scar and the outer implants tended to have larger GFAP-positive areas than the middle implant in the inner ROI. However, these differences were not statistically significant. We found no differences or even tendencies to differences when quantifying ED1-positive areas (Fig. 15). Indicating that multiple implants in one hemisphere did not aggravate the tissue response to each implant.

Interhemispheric interactions

Potential interactions between hemispheres were examined by comparing the inflammatory tissue response to the contralateral implant vs. the solitary implant (Fig. 15). No statistically significant differences were found between these groups at one or six weeks, neither for astrocytic nor microglial reactions (Fig. 15). Indicating that the multiple implants in one hemisphere did not have an adverse effect on the tissue response toward the contralateral implant. These results taken together indicate that it is feasible to implant multiple neural interfaces in various neural structures without causing a cumulatively larger inflammatory response.

Figure 15. Inflammatory response surrounding implant scars six weeks post implantation.
Representative images of GFAP (magenta) and ED1 (green) staining from a) middle, b) outer, c) contralateral and d) solitary implant scars after six weeks. Scale bar 100 μm. Quantifications of GFAP and ED1-positive areas after six weeks in e) inner ROI (0–50 μm) and f) outer ROI (50–200 μm).
A schematic overview of implant locations in the experimental groups.

General discussion

The main aim of this thesis was to clarify safety aspects of implanted nanostructures and multiple neural interfaces, as well as to develop a technique that allows implantation of nanostructured interfaces into the brain tissue. The studies presented in this thesis give key information of the nanowire dimension that would be safe to use when designing a nanowire-structured neural interface. Moreover, a method for implanting a thin substrate with a mechanically compliant nanowire-structured surface was developed. This opens up for the development and use of a nanowire-structured neural interface that have the potential to interface the nervous tissue optimally so that the electrodes may interact with neurons on a sub cellular level with minimal side effects.

Furthermore, another key finding was that implanting multiple wire bundles in the brain is feasible without aggravating the inflammatory response to each individual implant. This allows for studying larger neural circuits and interactions between different structures in the brain in parallel, without risking a cumulatively larger inflammatory response.

Nanowire biocompatibility

Neural interfaces with nanostructured topography have great potential for improving both the biocompatibility of the interface as well as the recording properties [49, 50, 54, 59, 61].

Patterning an electrode surface with nanowires has the potential to guide cell attachment. For example, guidance of axons has been demonstrated *in vitro* using rows of GaP nanowires [62]. Here, they found that focal adhesions had formed at the nanowires, thus establishing possible sites of interaction between the electrode surface and the neurons. Furthermore, substrates with vertical nanowires intercalated by flat regions were capable of separating neurons from glial cells [61]. Hence, in contrast to conventional neural interfaces of today, nanowire-structured electrodes show potential for enabling recordings from sub-cellular structures or compartments, such as spines, synapses or even organelles. However, the findings demonstrated *in vitro* remains to be tested and verified *in vivo*. A step

in this direction was taken by Suyatin et al. 2013, where they achieved the first *in vivo* "proof of principle" using a nanowire-based electrode by performing acute recordings in rat cortex [63].

Nanowires also show potential within the upcoming field of neurophotonics. Nanowires have been proposed to be used as membrane-based nanosensors for biological applications [88] as well as for light-induced and electrical stimulation of biological cells, such as neurons or retinal cells [89]. Khraiche et al. 2011 have presented novel technology applicable for restoring retina function, were they used nanowires as photodetectors and the obtained signal transduction performances approached those of the rods and cones in the mammalian retina [90].

However, caution is warranted when it comes to using high-aspect-ratio nanoparticles, such as nanowires, as a surface structure on a chronically implanted neural interface, since biostable high-aspect-ratio nanowires share morphological features with asbestos fibers and it has been known for decades that retention of asbestos fibers in lung tissue can lead to chronic inflammation and scarring [91, 92]. The fiber pathogenicity paradigm for asbestosis predicts that long, thin and biostable fibers lead to frustrated phagocytosis and would thus elicit a chronic inflammatory response in the tissue. Consequently, finding out what would happen in the brain tissue over time, if some nanowires would to detach from an implanted neural interface, was of utmost importance. A chronic and escalating inflammatory response in the vicinity of the neural interface could possibly generate a detrimental neurotoxic milieu. In order to detect a possible escalation of the inflammatory response over time, as is observed in asbestosis, a truly chronic end point was needed. Hence, we kept the rats for approximately half their expected lifetime in our nanowire safety studies.

In paper I, after one year, we found that the neuronal survival in the 10 µm long nanowire group was significantly lower compared to the control group, indicating a possible neurotoxic effect developing over time. The neuronal loss might have been caused by a continuous release of neurotoxic factors from activated microglia/macrophages present in the scar area [93, 94]. This loss of neurons would not have been detected had we not included a one year end point. However, the inflammatory tissue response observed, was over all very limited at this point and not alarming regarding the possible similarities with asbestosis.

Notably, the glial response and neuronal survival following injection of biostable 2 µm long nanowires did not differ significantly at any point from the tissue response observed following the injection of the control solution alone. Furthermore, we did not observe any significant difference in glial response or neuronal survival following injection of 2 µm long degradable nanowires compared to the injection of 2 µm long biostable nanowires. Thus, we found that the trauma caused by the implantation procedure alone gives rise to a long-lasting

albeit very small chronic inflammatory response. It is a risk that the possible tissue response caused by the short nanowires might be hidden by the reaction to the injection trauma. The implantation procedure used in our studies (I, II), i.e. using a Hamilton syringe with a glass capillary attached, is a widely used technique, for example during cell transplantation. The finding that the control injection gives rise to a long-lasting tissue response in the injection tract calls for a refinement of the implantation procedure. In our studies, one way of circumventing the implantation trauma could be to incorporate the nanowires in a gelatin needle. This needle could be implanted with minimal tissue trauma, as has been demonstrated by Lind et al. 2010 [67], and the possible chronic tissue response would then be caused by the nanowires alone.

Nanowire clearance from the brain

A surprising finding in this thesis was that the residue from the degradable nanowires was not cleared from the brain, even after one year. Debris from the broken down or fragmented nanowires was clearly visualized inside microglia/macrophages in the injection tract. This hints to a very slow elimination of nanoparticles from the brain. This in turn begs the question: Are the nanowires or the microglia/macrophages with engulfed nanowires/nanowire debris not able to leave the CNS?

The CNS has long been considered an immune privileged site that lacks conventional lymphatic drainage. However, studies have now revealed a functional meningeal lymphatic system that drains cerebrospinal to deep cervical lymph nodes [95, 96]. Furthermore, monocytes have also been shown capable of migrating from CNS to cervical lymph nodes [85]. However, considering nanowires and nanowire debris were observed in the injection tract inside microglia/macrophages one year post injection and that no nanowires or nanowire debris were found in the cervical lymph nodes scanned in our studies (I, II), the elimination process of nanoparticles from the CNS appear to be a very slow process. In line with this, several studies have shown that nanoparticles tend to accumulate in the brain; this was shown both following oral [86, 87] as well as intravenous administration [97]. Notably, in the studies where the nanoparticles were administered orally a retention of nanoparticles was found in the brain several months post administration. Furthermore, concern might be raised that it is the amount of nano debris in the brain that is the main player in the chronic tissue reactions. However, as we show in paper IV, when implanting multiple wire bundles in the brain we found no overall increased brain tissue response, which might indicate that the accumulation of nano debris in the brain does not result in

an expanded toxic reaction. Indeed, the shorter nanowires, degradable or biostable, showed no sign of giving rise to a neurotoxic environment or an escalating inflammatory response in the tissue, not even after one year.

These findings indicate that it is indeed feasible to implant a nanowire-structured neural interface, intended for long-term communication with the neural tissue, without risking an asbestosis-like pathology if part of the nanostructure, i.e. in this case nanowires, were to detach from the surface. However, the goal is to keep the nanostructure intact for biocompatibility purposes as well as for recording/stimulation purposes, thus, an implantation method that preserves the majority of the nanowires during implantation was needed.

Implantation method for nanostructured neural interfaces

We have showed that implanting a nanowire-structured substrate embedded in a protective layer of gelatin/glycerol is feasible and would leave the majority of the nanowires intact. This method would apply to other mechanically compliant nanostructured substrates. Furthermore, Lind et al. 2010 showed that pure gelatin needles evoked a significantly smaller chronic scar than stab wounds [67], indicating that embedding implants in gelatin ameliorates the damage caused by the implantation. This could be due to the gradual dissolution of the gelatin during the insertion, which provides a slippery surface coating and thus inflicts minimal stress on the tissue during insertion. Hence, we used this method as a starting point for embedding our nanostructured substrates. However, gelatin alone caused the nanowires to break during the drying process. In order to increase the water content of the gelatin solution we added the biocompatible and commonly used plasticizer glycerol. We found a combination of gelatin and glycerol that preserved the majority of the nanowire-structured surface during the implantation procedure. This role of the embedding gel is crucial in order to maintain the enhanced electrical properties of the electrode as well as the biocompatibility of the interface, which was the purpose of the nanostructure to begin with.

The gelatin embedding method also allows for incorporating drugs in the gelatin solution. This could be used for promoting an anti-inflammatory environment. Incorporating neurotropic factors, such as nerve growth factor, in the embedding solution could also have a local direct positive effect on the neurons and their processes [98].

Thus, previous results as well as findings in this thesis work show that the gelatin embedding method allows for implanting nanostructured highly flexible neural interfaces. The flexibility of an implanted interface has been shown to be a vital

for minimize the evoked inflammatory tissue response [31, 44]. Thus, the possibility to combine a flexible neural interface with a flexible nanostructured surface would be a promising step towards achieving a long-term communication with the brain.

Cells at the neural interface

It is known that macrophages/microglia are among the first cells to respond to CNS injury. Thus, quantifying ED1, a marker of activated microglia and macrophages is a good measure of the inflammatory process. Furthermore, Köhler et al. 2015, showed a correlation between neuronal survival and a small ED1 immunoreactivity [44]. However, recently it has become known that there are subsets of microglia and that they are capable of promoting both injury and repair. "Classically activated" M1 microglia are the pro-inflammatory subset and the "alternatively activated" M2 microglia are the anti-inflammatory subset that has been shown to promote neurite outgrowth and length [99]. The cells differentiation into the M1 or M2 subset depends on signals in the injured tissue. Thus, when implanting a neural interface one could incorporating factors in the embedding gel, such as interleukin-4 and substance P, that have been shown to promote microglia and macrophages to differentiation into the M2 subset [100]. This might help promote restitution of the neural circuits after the injury caused by the implantation trauma.

To further elucidate what happens in tissue following an implantation it might be necessary to look beyond the astrocytic and the microglial response. For example, a leaky BBB have been associated with a reduction in recording performances [22], thus adding IgG to our histological investigations could help to estimate the expected performance of the neural interface. Furthermore, since it is now known that there are subsets of microglia involved in the tissue repair, it would be of interest in future studies to look at the different markers of microglia subsets. The aim might no longer be to minimize the microglial activation at all, rather to guide the activated microglia cells into an anti-inflammatory state that promote wound healing and tissue repair.

In our studies, we look at neuronal nuclei density as a measure of neuronal survival; however, it does not necessarily mean that the stained neurons are functioning normally or that the neuronal processes are intact. Looking further into the viability of the neurons and staining with for example a neurofilament marker, to assess possible axon degeneration in the tissue would be of interest for future studies. This would provide a better insight as to whether the neural circuits are intact at the interface. For future studies this would enable correlations to be made

between for example recording quality and the amount of intact dendrites/axons at the interface. However, as a general estimation of neuronal survival as a first assessment of biocompatibility or safety of a material, neuronal nuclei density is a useful and common measure to use.

It is known that astrocytes and microglia constitutes the main part of a glial scar, hence, they are widely used as a measure of the glial response and those are the inflammatory cells that we have focused on in our studies. However, there are other types of cells that come in to play following an implantation, such as pericytes and meningeal cells. Unpublished results from our laboratory have shown that there are a number of unidentified cells residing in between the *glial limitans* and an implanted probe. Some of these cells do not stain positive for ED1 but showed expression of the markers fibronectin, nestin, vimentin and PDGFR-beta. The origin of these cells are not clear, however, they could possibly descend from pericytes coming from nearby blood vessels or meningeal fibroblasts that have been displaced during the implantation procedure or that have possibly migrated down along the implantation track. Further studies are needed in order to clarify what types of cells are and what role they play in the scar formation and wound healing.

Towards a biocompatible nanostructured neural interface

The design of a neural interface should aim to minimize the harmful inflammatory response that produces and maintains a compact glial scar, which in turn isolates the electrode from the brain. To this end, this thesis provides evidence that it is vital to minimize the acute tissue trauma caused by the implantation procedure, since it strongly influences the ensuing chronic tissue response. Furthermore, in line with the new proposed definition of biocompatibility, we should aim to guide the tissue response towards a non-fibrotic wound healing, with optimal tissue integration [40]. If these requirements are met we might be able to circumvent the development of an insulating glial scar.

This thesis has provided key information when it comes to constructing and implanting a chronically biocompatible nanostructured neural interface. There still remain a number of hurdles to overcome before an optimal neural interface becomes a reality, the brain is a complex milieu and there is a need to elucidate the possible anti- and pro-inflammatory roles different cell types play at the abiotic-biotic interface. However, the implications of constructing a perfectly integrating neural interface, which may no longer be a far-fetched idea, would be immense, both in the neuroscience research field as well as in the clinic.

Acknowledgements

Over the years as a PhD-student at Neuronano Research Center (NRC), I have many people to thank for making this thesis a reality and for making the work exciting.

Firstly, I would like to thank my supervisors.

Cecilia Eriksson Linsmeier, my main supervisor. We first met when I did my bachelor thesis back in 2008. Since then you have always been a source of encouragement and inspiration. You have given me great support and feedback over the years. Our personality types might be as different as night and day, but we have developed a great symbiotic way of communicating and working together, perhaps due to our differences. Thank you for being such a nice person and for being a great supervisor!

Jens Schouenborg, I admire your ability to keep details of so many different projects in your mind at once. You also have a way of finding time for us PhD-students in your busy schedule when there is need for it. Thank you for your support and for your valuable critique that has pushed me to perform better! Pun intended or not, this encouraging quote from you, got stuck in my mind:

"Lina, you need to understand the big thing about nano!"

Nils Danielsen, for numerous helpful discussions and for generously sharing your knowledge. Thank you for your support over the years.

Christelle Prinz, for the help with the confocal microscopy and for all the nanowires I have received over the years, as well as for your valuable feedback on manuscripts.

Thank you to the persons at or around the lab for the help they have provided and for making it a nice place to work at: Lina Petersson, Jonas Thelin, Martin Garwicz, Pär Halje, Ulrike Richter, Per Petersson, Andrea Nord, Linda Eliasson, Lucas Kumosa, Petter Pettersson, Agneta SanMartin, Palmi Thor Thorbergsson, Peter Paulander, Ali Ghasemi Azar, Mengliang Zhang, Niclas Lindqvist, Marcus Granmo and Dan-Anders Jirenhed.

References

[1] Birbaumer N, Murguialday AR, Cohen L. Brain-computer interface in paralysis. Current Opinion in Neurology 2008;21:634-8.

[2] Awan NR, Lozano A, Hamani C. Deep brain stimulation: current and future perspectives. Neurosurgical Focus 2009;27.

[3] Daly JJ, Wolpaw JR. Brain-computer interfaces in neurological rehabilitation. Lancet Neurology 2008;7:1032-43.

[4] Hochberg LR, Serruya MD, Friehs GM, Mukand JA, Saleh M, Caplan AH, et al. Neuronal ensemble control of prosthetic devices by a human with tetraplegia. Nature 2006;442:164-71.

[5] Kipke DR, Shain W, Buzsaki G, Fetz E, Henderson JM, Hetke JF, et al. Advanced Neurotechnologies for Chronic Neural Interfaces: New Horizons and Clinical Opportunities. Journal of Neuroscience 2008;28:11830-8.

[6] Silva GA. Neuroscience nanotechnology: progress, opportunities and challenges. Nature reviews Neuroscience 2006;7:65-74.

[7] Nicolelis MAL, Dimitrov D, Carmena JM, Crist R, Lehew G, Kralik JD, et al. Chronic, multisite, multielectrode recordings in macaque monkeys. Proceedings of the National Academy of Sciences of the United States of America 2003;100:11041-6.

[8] Ivica N, Tamte M, Ahmed M, Richter U, Petersson P. Design of a high-density multi-channel electrode for multi-structure parallel recordings in rodents. Conference proceedings : Annual International Conference of the IEEE Engineering in Medicine and Biology Society IEEE Engineering in Medicine and Biology Society Annual Conference 2014;2014:393-6.

[9] Agorelius J, Tsanakalis F, Friberg A, Thorbergsson PT, Pettersson LME, Schouenborg J. An array of highly flexible electrodes with a tailored configuration locked by gelatin during implantation – initial evaluation in cortex cerebri of awake rats. Frontiers in Neuroscience 2015;9.

[10] Michon F, Aarts A, Holzhammer T, Ruther P, Borghs G, McNaughton B, et al. Integration of silicon-based neural probes and micro-drive arrays for chronic recording of large populations of neurons in behaving animals. J Neural Eng 2016;13:046018.

[11] Simeral JD, Kim SP, Black MJ, Donoghue JP, Hochberg LR. Neural control of cursor trajectory and click by a human with tetraplegia 1000 days after implant of an intracortical microelectrode array. J Neural Eng 2011;8:025027.

[12] Limousin P, Pollak P, Benazzouz A, Hoffmann D, Le Bas JF, Broussolle E, et al. Effect of parkinsonian signs and symptoms of bilateral subthalamic nucleus stimulation. Lancet (London, England) 1995;345:91-5.

[13] Benabid AL, Chabardes S, Mitrofanis J, Pollak P. Deep brain stimulation of the subthalamic nucleus for the treatment of Parkinson's disease. The Lancet Neurology 2009;8:67-81.

[14] Benabid AL. What the future holds for deep brain stimulation. Expert Review of Medical Devices 2007;4:895-903.

[15] Gaunt RA, Prochazka A. Control of urinary bladder function with devices: successes and failures. Progress in brain research 2006;152:163-94.

[16] Polikov VS, Tresco PA, Reichert WM. Response of brain tissue to chronically implanted neural electrodes. Journal of Neuroscience Methods 2005;148:1-18.

[17] Williams JC, Rennaker RL, Kipke DR. Long-term neural recording characteristics of wire microelectrode arrays implanted in cerebral cortex. Brain Research Protocols 1999;4:303-13.

[18] Biran R, Martin DC, Tresco PA. Neuronal cell loss accompanies the brain tissue response to chronically implanted silicon microelectrode arrays. Experimental Neurology 2005;195:115-26.

[19] Biran R, Martin DC, Tresco PA. The brain tissue response to implanted silicon microelectrode arrays is increased when the device is tethered to the skull. Journal of Biomedical Materials Research Part A 2007;82A:169-78.

[20] Barrese JC, Rao N, Paroo K, Triebwasser C, Vargas-Irwin C, Franquemont L, et al. Failure mode analysis of silicon-based intracortical microelectrode arrays in non-human primates. Journal of Neural Engineering 2013;10.

[21] Bjornsson CS, Oh SJ, Al-Kofahi YA, Lim YJ, Smith KL, Turner JN, et al. Effects of insertion conditions on tissue strain and vascular damage during neuroprosthetic device insertion. Journal of Neural Engineering 2006;3:196-207.

[22] Nolta NF, Christensen MB, Crane PD, Skousen JL, Tresco PA. BBB leakage, astrogliosis, and tissue loss correlate with silicon microelectrode array recording performance. Biomaterials 2015;53:753-62.

[23] Tay TL, Hagemeyer N, Prinz M. The force awakens: insights into the origin and formation of microglia. Current Opinion in Neurobiology 2016;39:30-7.

[24] Szarowski DH, Andersen MD, Retterer S, Spence AJ, Isaacson M, Craighead HG, et al. Brain responses to micro-machined silicon devices. Brain Research 2003;983:23-35.

[25] Tambuyzer BR, Ponsaerts P, Nouwen EJ. Microglia: gatekeepers of central nervous system immunology. Journal of Leukocyte Biology 2009;85:352-70.

[26] Gehrmann J, Matsumoto Y, Kreutzberg GW. Microglia: Intrinsic immuneffector cell of the brain. Brain Research Reviews 1995;20:269-87.

[27] Gordon GRJ, Mulligan SJ, MacVicar BA. Astrocyte control of the cerebrovasculature. Glia 2007;55:1214-21.

[28] Sofroniew MV. Molecular dissection of reactive astrogliosis and glial scar formation. Trends in Neurosciences 2009;32:638-47.

[29] Mathewson AJ, Berry M. Observations on the astrocyte response to a cerebral stab wound in adult rats. Brain Research 1985;327:61-9.

[30] Fawcett JW, Asher RA. The glial scar and central nervous system repair. Brain Research Bulletin 1999;49:377-91.

[31] Sohal HS, Clowry GJ, Jackson A, O'Neill A, Baker SN. Mechanical flexibility reduces the foreign body response to long- term implanted microelectrodes in rabbit cortex. bioRxiv 2016.

[32] Kim YT, Hitchcock RW, Bridge MJ, Tresco PA. Chronic response of adult rat brain tissue to implants anchored to the skull. Biomaterials 2004;25:2229-37.

[33] Mills SJ, Cowin AJ, Kaur P. Pericytes, mesenchymal stem cells and the wound healing process. Cells 2013;2:621-34.

[34] Purcell EK, Thompson DE, Ludwig KA, Kipke DR. Flavopiridol reduces the impedance of neural prostheses in vivo without affecting recording quality. Journal of Neuroscience Methods 2009;183:149-57.

[35] Henze DA, Borhegyi Z, Csicsvari J, Mamiya A, Harris KD, Buzsaki G. Intracellular features predicted by extracellular recordings in the hippocampus in vivo. Journal of neurophysiology 2000;84:390-400.

[36] Homsy CA, Ansevin KD, O'Bannon W, Thompson SA, Hodge R, Estrella ME. Rapid In Vitro Screening of Polymers for Biocompatibility. Journal of Macromolecular Science: Part A - Chemistry 1970;4:615-34.

[37] Tetik RD, Galante JO, Rostoker W. A wear resistant material for total joint replacement--tissue biocompatibility of an ultra-high molecular weight (UHMW) polyethylene-graphite composite. Journal of biomedical materials research 1974;8:231-50.

[38] Donaruma LG. Definitions in biomaterials, D. F. Williams, Ed., Elsevier, Amsterdam, 1987, 72 pp. Journal of Polymer Science Part C: Polymer Letters 1988;26:414-.

[39] Helmus MN, Gibbons DF, Cebon D. Biocompatibility: meeting a key functional requirement of next-generation medical devices. Toxicologic pathology 2008;36:70-80.

[40] Ratner BD. The Biocompatibility Manifesto: Biocompatibility for the Twenty-first Century. Journal of Cardiovascular Translational Research 2011;4:523-7.

[41] Stice P, Gilletti A, Panitch A, Muthuswamy J. Thin microelectrodes reduce GFAP expression in the implant site in rodent somatosensory cortex. J Neural Eng 2007;4:42-53.

[42] Thelin J, Jorntell H, Psouni E, Garwicz M, Schouenborg J, Danielsen N, et al. Implant Size and Fixation Mode Strongly Influence Tissue Reactions in the CNS. Plos One 2011;6.

[43] Sohal HS, Jackson A, Jackson R, Clowry GJ, Vassilevski K, O'Neill A, et al. The sinusoidal probe: a new approach to improve electrode longevity. Front Neuroeng 2014;7:10.

[44] Kohler P, Wolff A, Ejserholm F, Wallman L, Schouenborg J, Linsmeier CE. Influence of probe flexibility and gelatin embedding on neuronal density and glial responses to brain implants. PLoS One 2015;10:e0119340.

[45] Nguyen JK, Park DJ, Skousen JL, Hess-Dunning AE, Tyler DJ, Rowan SJ, et al. Mechanically-compliant intracortical implants reduce the neuroinflammatory response. J Neural Eng 2014;11:056014.

[46] Lind G, Eriksson Linsmeier C, Schouenborg J. The density differences between tissue and neural probes is a key factor for glial scarring. Sci Rep 2013;3.

[47] Johansson F, Wallman L, Danielsen N, Schouenborg J, Kanje M. Porous silicon as a potential electrode material in a nerve repair setting: Tissue reactions. Acta Biomaterialia 2009;5:2230-7.

[48] Winslow BD, Christensen MB, Yang WK, Solzbacher F, Tresco PA. A comparison of the tissue response to chronically implanted Parylene-C-coated and uncoated planar silicon microelectrode arrays in rat cortex. Biomaterials 2010;31:9163-72.

[49] Cellot G, Cilia E, Cipollone S, Rancic V, Sucapane A, Giordani S, et al. Carbon nanotubes might improve neuronal performance by favouring electrical shortcuts. Nature Nanotechnology 2009;4:126-33.

[50] Keefer EW, Botterman BR, Romero MI, Rossi AF, Gross GW. Carbon nanotube coating improves neuronal recordings. Nature Nanotechnology 2008;3:434-9.

[51] Robinson JT, Jorgolli M, Shalek AK, Yoon M-H, Gertner RS, Park H. Vertical nanowire electrode arrays as a scalable platform for intracellular interfacing to neuronal circuits. Nat Nano 2012;7:180-4.

[52] McKenzie JL, Waid MC, Shi R, Webster TJ. Decreased functions of astrocytes on carbon nanofiber materials. Biomaterials 2004;25:1309-17.

[53] Gilletti A, Muthuswamy J. Brain micromotion around implants in the rodent somatosensory cortex. Journal of Neural Engineering 2006;3:189-95.

[54] Kim W, Ng JK, Kunitake ME, Conklin BR, Yang P. Interfacing silicon nanowires with mammalian cells. Journal of the American Chemical Society 2007;129:7228-9.

[55] Patolsky F, Timko BP, Yu G, Fang Y, Greytak AB, Zheng G, et al. Detection, stimulation, and inhibition of neuronal signals with high-density nanowire transistor arrays. Science 2006;313:1100-4.

[56] Prinz CN. Interactions between semiconductor nanowires and living cells. Journal of Physics: Condensed Matter 2015;27:233103.

[57] Xie C, Hanson L, Xie W, Lin Z, Cui B, Cui Y. Noninvasive neuron pinning with nanopillar arrays. Nano Lett 2010;10:4020-4.

[58] Xie C, Lin Z, Hanson L, Cui Y, Cui B. Intracellular recording of action potentials by nanopillar electroporation. Nat Nanotechnol 2012;7:185-90.

[59] Hallstrom W, Martensson T, Prinz C, Gustavsson P, Montelius L, Samuelson L, et al. Gallium phosphide nanowires as a substrate for cultured neurons. Nano Letters 2007;7:2960-5.

[60] Piret G, Perez M-T, Prinz CN. Neurite outgrowth and synaptophysin expression of postnatal CNS neurons on GaP nanowire arrays in long-term retinal cell culture. Biomaterials 2013;34:875-87.

[61] Piret G, Perez MT, Prinz CN. Support of Neuronal Growth Over Glial Growth and Guidance of Optic Nerve Axons by Vertical Nanowire Arrays. Acs Applied Materials & Interfaces 2015;7:18944-8.

[62] Prinz C, Hallstrom W, Martensson T, Samuelson L, Montelius L, Kanje M. Axonal guidance on patterned free-standing nanowire surfaces. Nanotechnology 2008;19:345101.

[63] Suyatin DB, Wallman L, Thelin J, Prinz CN, Jörntell H, Samuelson L, et al. Nanowire-Based Electrode for Acute In Vivo Neural Recordings in the Brain. PLoS ONE 2013;8:e56673.

[64] Donaldson K, Murphy F, Duffin R, Poland C. Asbestos, carbon nanotubes and the pleural mesothelium: a review of the hypothesis regarding the role of long fibre retention in the parietal pleura, inflammation and mesothelioma. Particle and Fibre Toxicology 2010;7:5.

[65] Poland C, Duffin R, Kinloch I, Maynard A, Wallace W, Seaton A. Carbon nanotubes introduced into the abdominal cavity of mice show asbestos-like pathogenicity in a pilot study. Nat Nanotechnol 2008;3:423 - 8.

[66] Schinwald A, Murphy FA, Prina-Mello A, Poland CA, Byrne F, Movia D, et al. The threshold length for fiber-induced acute pleural inflammation: shedding light on the early events in asbestos-induced mesothelioma. Toxicol Sci 2012;128:461-70.

[67] Lind G, Linsmeier CE, Thelin J, Schouenborg J. Gelatine-embedded electrodes-a novel biocompatible vehicle allowing implantation of highly flexible microelectrodes. Journal of Neural Engineering 2010;7.

[68] He W, Bellamkonda RV. Nanoscale neuro-integrative coatings for neural implants. Biomaterials 2005;26:2983-90.

[69] Garcia I, Kim C, Arenkiel BR. Revealing Neuronal Circuitry Using Stem Cell-Derived Neurons. Current Protocols in Stem Cell Biology: John Wiley & Sons, Inc.; 2007.

[70] Rivero S, Garcia MA, Pinotti A. Correlations between structural, barrier, thermal and mechanical properties of plasticized gelatin films. Innovative Food Science & Emerging Technologies 2010;11:369-75.

[71] Bergo P, Sobral PJA. Effects of plasticizer on physical properties of pigskin gelatin films. Food Hydrocolloids 2007;21:1285-9.

[72] Hallstrom W, Lexholm M, Suyatin DB, Hammarin G, Hessman D, Samuelson L, et al. Fifteen-piconewton force detection from neural growth cones using nanowire arrays. Nano Lett 2010;10:782-7.

[73] Suyatin DB, Hallstram W, Samuelson L, Montelius L, Prinz CN, Kanje M. Gallium phosphide nanowire arrays and their possible application in cellular force investigations. Journal of Vacuum Science & Technology B 2009;27:3092-4.

[74] Matsuno H, Yokoyama A, Watari F, Uo M, Kawasaki T. Biocompatibility and osteogenesis of refractory metal implants, titanium, hafnium, niobium, tantalum and rhenium. Biomaterials 2001;22:1253-62.

[75] Mohammadi S, Esposito M, Cucu M, Ericson LE, Thomsen P. Tissue response to hafnium. Journal of Materials Science: Materials in Medicine 2001;12:603-11.

[76] Maggiorella L, Barouch G, Devaux C, Pottier A, Deutsch E, Bourhis J, et al. Nanoscale radiotherapy with hafnium oxide nanoparticles. Future oncology (London, England) 2012;8:1167-81.

[77] Davis RK, Stevenson GT, Busch KA. Tumor Incidence in Normal Sprague-Dawley Female Rats. Cancer Research 1956;16:194-7.

[78] Nakazawa M, Tawaratani T, Uchimoto H, Kawaminami A, Ueda M, Ueda A, et al. Spontaneous neoplastic lesions in aged Sprague-Dawley rats. Experimental animals / Japanese Association for Laboratory Animal Science 2001;50:99-103.

[79] Prejean JD, Peckham JC, Casey AE, Griswold DP, Weisburger EK, Weisburger JH. Spontaneous Tumors in Sprague-Dawley Rats and Swiss Mice. Cancer Research 1973;33:2768-73.

[80] Thompson SW, Huseby RA, Fox MA, Davis CL, Hunt RD. Spontaneous Tumors in the Sprague-Dawley Rat. Journal of the National Cancer Institute 1961;27:1037-57.

[81] Linsmeier CE, Wallman L, Faxius L, Schouenborg J, Bjursten LM, Danielsen N. Soft tissue reactions evoked by implanted gallium phosphide. Biomaterials 2008;29:4598-604.

[82] Eriksson Linsmeier C, Prinz CN, Pettersson LME, Caroff P, Samuelson L, Schouenborg J, et al. Nanowire Biocompatibility in the Brain - Looking for a Needle in a 3D Stack. Nano Letters 2009;9:4184-90.

[83] Buzsaki G. Large-scale recording of neuronal ensembles. Nat Neurosci 2004;7:446-51.

[84] Kang W, Hébert JM. Signaling Pathways in Reactive Astrocytes, a Genetic Perspective. Mol Neurobiol 2011;43:147-54.

[85] Kaminski M, Bechmann I, Pohland M, Kiwit J, Nitsch R, Glumm J. Migration of monocytes after intracerebral injection at entorhinal cortex lesion site. Journal of Leukocyte Biology 2012;92:31-9.

[86] van der Zande M, Vandebriel RJ, Van Doren E, Kramer E, Rivera ZH, Serrano-Rojero CS, et al. Distribution, Elimination, and Toxicity of Silver Nanoparticles and Silver Ions in Rats after 28-Day Oral Exposure. Acs Nano 2012;6:7427-42.

[87] Lee JH, Kim YS, Song KS, Ryu HR, Sung JH, Park JD, et al. Biopersistence of silver nanoparticles in tissues from Sprague-Dawley rats. Particle and Fibre Toxicology 2013;10:14.

[88] Dabkowska AP, Piret G, Niman CS, Lard M, Linke H, Nylander T, et al. Surface nanostructures for fluorescence probing of supported lipid bilayers on reflective substrates. Nanoscale 2015;7:18020-4.

[89] Linke H, PRINZ C, PIRET G, Ohlsson J, PEREZ MT. Nanowire-based devices for light-induced and electrical stimulation of biological cells. Google Patents; 2013.

[90] Khraiche ML, Lo Y, Wang D, Cauwenberghs G, Freeman W, Silva GA. Ultra-high photosensitivity silicon nanophotonics for retinal prosthesis: electrical characteristics. Conference proceedings : Annual International Conference of the IEEE Engineering in Medicine and Biology Society IEEE Engineering in Medicine and Biology Society Annual Conference 2011;2011:2933-6.

[91] Sebastien P, Janson X, Gaudichet A, Hirsch A, Bignon J. Asbestos retention in human respiratory tissues: comparative measurements in lung parenchyma and in parietal pleura. 1980:237 - 46.

[92] Cugell D, Kamp D. Asbestos and the pleura: a review. Chest 2004;125:1103 - 17.

[93] Hanisch UK. Microglia as a source and target of cytokines. Glia 2002;40:140-55.

[94] Streit W, Mrak R, Griffin WS. Microglia and neuroinflammation: a pathological perspective. Journal of Neuroinflammation 2004;1:14.

[95] Louveau A, Harris TH, Kipnis J. Revisiting the Mechanisms of CNS Immune Privilege. Trends in Immunology;36:569-77.

[96] Weller R, Djuanda E, Yow H-Y, Carare R. Lymphatic drainage of the brain and the pathophysiology of neurological disease. Acta Neuropathol 2009;117:1-14.

[97] Kreyling WG, Abdelmonem AM, Ali Z, Alves F, Geiser M, Haberl N, et al. In vivo integrity of polymer-coated gold nanoparticles. Nat Nano 2015;10:619-23.

[98] Chang CJ. The effect of pulse-released nerve growth factor from genipin-crosslinked gelatin in schwann cell-seeded polycaprolactone conduits on large-gap peripheral nerve regeneration. Tissue engineering Part A 2009;15:547-57.

[99] Kigerl KA, Gensel JC, Ankeny DP, Alexander JK, Donnelly DJ, Popovich PG. Identification of two distinct macrophage subsets with divergent effects causing either neurotoxicity or regeneration in the injured mouse spinal cord. The Journal of neuroscience : the official journal of the Society for Neuroscience 2009;29:13435-44.

[100] Hu X, Leak RK, Shi Y, Suenaga J, Gao Y, Zheng P, et al. Microglial and macrophage polarization-new prospects for brain repair. Nature reviews Neurology 2015;11:56-64.

Paper I

Size-dependent long-term tissue response to biostable nanowires in the brain

Lina Gällentoft [a], Lina M.E. Pettersson [a], Nils Danielsen [a], Jens Schouenborg [a], Christelle N. Prinz [a, b, **], Cecilia Eriksson Linsmeier [a, *]

[a] Neuronano Research Center, Department of Experimental Medical Science, Medical Faculty, Lund University, BMCF10, Lund SE-221 84, Sweden
[b] Division of Solid State Physics, The Nanometer Structure Consortium, Lund University, Box 118, Lund SE-221 00, Sweden

ARTICLE INFO

ABSTRACT

Nanostructured neural interfaces, comprising nanotubes or nanowires, have the potential to overcome the present hurdles of achieving stable communication with neuronal networks for long periods of time. This would have a strong impact on brain research. However, little information is available on the brain response to implanted high-aspect-ratio nanoparticles, which share morphological similarities with asbestos fibres. Here, we investigated the glial response and neuronal loss in the rat brain after implantation of biostable and structurally controlled nanowires of different lengths for a period up to one year post-surgery. Our results show that, as for lung and abdominal tissue, the brain is subject to a sustained, local inflammation when biostable and high-aspect-ratio nanoparticles of 5 μm or longer are present in the brain tissue. In addition, a significant loss of neurons was observed adjacent to the 10 μm nanowires after one year. Notably, the inflammatory response was restricted to a narrow zone around the nanowires and did not escalate between 12 weeks and one year. Furthermore, 2 μm nanowires did not cause significant inflammatory response nor significant loss of neurons nearby. The present results provide key information for the design of future neural implants based on nanomaterials.

© 2014 The Authors. Published by Elsevier Ltd. This is an open access article under the CC BY-NC-SA license (http://creativecommons.org/licenses/by-nc-sa/3.0/).

1. Introduction

Achieving long-term monitoring and interaction with neuronal circuits of the central nervous system (CNS) in conscious individuals will have great impact in neuroscience, both for research and clinical applications [1—4]. However, current neural interfaces usually show a decline in performance over time and typically do not provide stable communication with individual neurons. It is commonly assumed that these shortcomings are due to an encapsulating inflammatory tissue response to the implant and consequent displacement/loss of neurons nearby [5—8]. Notably, this occurs despite using nontoxic materials. There is accumulating evidence indicating that microforces between the brain, which constantly exhibits movements, and neural interfaces, which

typically exhibit a poor mechanical compliance with the tissue, play an important part in fuelling the inflammatory tissue response and contribute to the instability of neural recordings [9—12].

A promising approach to locally improve the mechanical compliance of implants is to use flexible nanomaterials, such as nanorods or carbon nanotubes (CNTs), on the surface of the neural interfaces. Surfaces coated with CNTs have been reported to improve the electrical properties and lower the evoked inflammatory tissue response towards neural interfaces, both in vivo and in vitro [13,14]. Nanowire-modified substrates have been shown to promote neuronal growth and limit the proliferation of glial cells in vitro [15—17]. Furthermore, successful in vivo neural recordings have recently been achieved using nanowire-based electrodes [18].

In order to achieve long-term communication with the brain, these nanostructures need to be biostable. However, concerns have been raised about using biostable, long, and high-aspect-ratio nanoparticles (such as nanowires and CNTs) in the brain. In rodent abdominal tissue and lungs, it has been shown that biostable nanotubes, nanowires and nanorods of lengths comparable to the size of immune cells, can induce frustrated phagocytosis, resulting in a chronic inflammation which escalates over time, comparable to

* Corresponding author. BMCF10/F12, Lund SE-221 84, Sweden. Tel.: +46 (0)46 2224107.
** Corresponding author. Division of Solid State Physics, Lund University, Box 118, Lund SE-221 00, Sweden. Tel.: +46 (0)46 2224796.
E-mail addresses: Christelle.Prinz@ftf.lth.se (C.N. Prinz), Cecilia.Eriksson_Linsmeier@med.lu.se (C.E. Linsmeier).

asbestosis [19–21]. In the brain, the presence of biostable and high-aspect-ratio nanoparticles detached from implanted neural interfaces could pose a similar risk and give rise to an escalating inflammatory response as seen in asbestosis. At present, little is known concerning the brain tissue response after long-term exposure to biostable nanoparticles having morphological features similar to asbestos fibres.

To clarify the long-term risks involved in using nanostructured neural interfaces for stable communication with brain cells, we here examine the chronic brain tissue response to implantation of biostable nanorods of equal diameter but different lengths. Epitaxially grown nanowires were used as a model particle for high-aspect-ratio nanorods since their dimensions can be controlled precisely [22]. The glial response and neuronal survival after implantation of biostable nanowires of three different lengths in the rat brain were evaluated after up to one year implantation time, which corresponds to half of the animal's lifespan.

The results show that nanowire length has a significant influence on the inflammatory tissue response as well as on neuronal survival. Whereas no significant increase in glial response or loss of neurons was found for 2 μm long nanowires, the longer nanowires studied (5 and 10 μm) caused a persistent, but not escalating, glial response. Furthermore, for the 10 μm nanowires, a significant loss of neurons could be seen at one year post implantation.

2. Methods

2.1. Nanowire growth and coating

Metal organic vapour phase epitaxy (Aix 200/4, Aixtron, Germany) was used to grow gallium phosphide (GaP) nanowires from 40 nm gold aerosol particles randomly distributed on a (111)B GaP substrate (Girmet Ltd, Moscow, Russia) at an average density of $1/\mu m^2$, as previously described [22,23]. The temperature for nanowire growth was 470 °C and wire growth was initiated by supplying $Ga(CH_3)_3$ in addition to PH_3. Precursor molar fractions were 4.3×10^{-6} and 8.5×10^{-2} for $Ga(CH_3)_3$ and PH_3, respectively, in a hydrogen carrier gas flow of 6 L/min. The growth was conducted under low pressure (10 kPa). The growth duration was adjusted to produce nanowires of different lengths (2 ± 0.2 μm, 5 ± 0.2 μm and 10 μm $\pm$ 0.5 μm). The nanowire length was characterized by scanning electron microscope (SEM) imaging.

In order to obtain nanowires with a stable and inert surface chemistry, the GaP nanowires were coated with a 20 nm layer of hafnium oxide (HfO_x) using atomic layer deposition (Savannah-100 system, Cambridge NanoTech Inc., USA), resulting in a final nanowire diameter of 80 nm $\pm$ 5 nm ($\pm$10 nm for the 10 μm long nanowires) which was characterized using SEM imaging (Fig. 1). Titanium is widely used as a biomaterial; hafnium belongs to the same group (IVB) as titanium in the periodic table of elements and has been shown to display similar biocompatible traits as titanium [24,25]. In addition, hafnium oxide has been shown to be biocompatible even in a nano configuration [26]. The substrates were cleaned with in an oxygen plasma chamber (Plasma Preen, Plasmatic Systems Inc., USA) and can therefore be expected to carry hydroxyl groups at the surface [27]. The nanowires were subsequently broken off from the substrate using ultra sonication and suspended in Hank's balanced salt solution (HBSS) to a final concentration of 70,000 nanowires/ μL. For further detailed description, see Eriksson Linsmeier et al., 2009 [28].
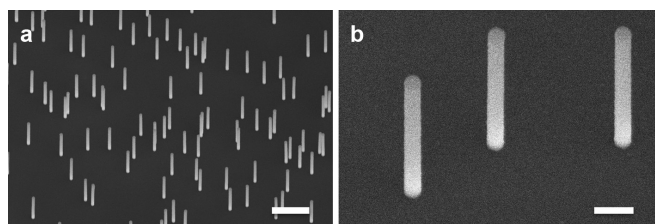
	Naïve	Stab wound	SW-control	Control	2 μm HfO$_x$	5 μm HfO$_x$	10 μm HfO$_x$
Groups at 12 weeks	**18**	**8**	**8**	**24**	**26**	**24**	**24**
12 week included	18	8	8	20	20	18	16
12 week excluded[a]	0	0	0	4	6	6	8
Groups at one year	**20**	–	–	**20**	**20**	**20**	**20**
One year included	18	–	–	16	11	15	15
One year excluded[b]	2	–	–	4	9	5	5

[a] At 12 weeks, animals were excluded for meeting predetermined histological exclusion criteria's.

[b] At one year, animals were excluded either for meeting ethical guideline exclusion criteria's (tumours) or predetermined histological exclusion criteria's.

2.2. Animals

Approval for the animal experiments described below was obtained from the Lund/Malmö local ethical committee on animal experiments. A total of 116 female Sprague–Dawley (SD) rats (Taconic, Denmark) were used in this study. All rats received food and water ad libitum and were kept in a 12-h day–night cycle. The rats weighed approximately 225 g at the beginning of the experiment. The rats followed a normal weight curve after surgery and up to the experimental end point.

For the 12 week time point, seven different experimental groups were used. Three groups received bilateral injections of 2, 5 or 10 μm long HfO$_x$-coated nanowires in HBSS. One group received bilateral control vehicle-injections (HBSS only). One group was kept naïve (no surgical procedures). An additional set of animals received stab wounds (SW) in one hemisphere and control-injections (HBSS only) in the contralateral hemisphere (SW-control). For the one-year time point, five different experimental groups were used. Three groups received bilateral injections of 2, 5 or 10 μm long HfO$_x$-coated nanowires in HBSS, and one group received bilateral control-injections (HBSS only). One group was kept naïve (no surgical procedures).

We found spontaneous tumours in eight out of 60 animals (13.33%) in the one year group (rats approximately 425 days old). Upon tumour detection, these animals were immediately terminated and excluded from the study. A summary of the animal group history is shown in Table 1. The prevalence of the tumours was distributed evenly over all groups, including the naïve group (no surgical procedures). The occurrence of spontaneous age-related tumours in SD rats has previously been well documented with a reported tumour incidence of 57–58% in female SD rats kept until day 540 or allowed to live out their lifespan [29,30]. Due to the prevalence of tumours in our naïve and control rats and the vast literature demonstrating the incidence of spontaneous tumours in aged rats, the tumours observed in our study were therefore most likely age-related, and not linked to the presence of nanowires in the brain [29–32].

2.3. Surgery

The rats were deeply anaesthetized by intraperitoneal (i.p.) injections of Fentanyl (0.3 mg/kg body weight) and Domitor vet (metedetomidin hydrochloride, 0.3 mg/kg body weight). The surgical procedures have been described in detail previously [28]. In short, the anaesthetized animals were prepared for surgery, i.e. their heads were shaved and they were placed in a stereotactic frame (KOPF instruments, USA) set under a stereomicroscope (Leica Microsystems, Germany). The scalp was disinfected using 70% ethanol solution and local anaesthetic, 0.25% Marcaine (Bupivacaine, 0.33 mg/kg body weight) in sterile water, was administered. To expose the skull a 2 cm midline incision was made. Tissue attached to the skull was

Fig. 1. SEM images of nanowires. Representative SEM images of vertical GaP nanowires coated with HfO$_x$, at low (a) and high (b) magnification. SEM images were used to determine the length and diameter of the nanowires. Stage tilt 20°. Scale bars: 1 μm (a), and 200 nm (b).

carefully removed and blood was cleansed away. Bilateral craniotomies (ø 1 mm^2) were drilled at 1.0 mm anterior and 2.5 mm lateral to bregma under stereotactic control. The dura mater was incised and deflected using fine forceps. Bilateral stereotactic injections at the above-mentioned coordinates were made using a 2 μL Hamilton syringe with a glass microcapillary (tip ø ~ 130 μm) attached. The suspension was injected into the striatum at two different depths; i) 5 mm (1 μL) and ii) 4 mm (1 μL); in total 2 μL/hemisphere over a total time of 2 × 2 min. The amount of nanowires injected corresponds to an estimation of the number of nanowires that could detach from a future nanostructured neural interface. Stab wounds were performed in an identical manner. After injections or stab wound, the skin was closed using surgical clips. The surgeries for the different groups took place in different sessions. In order to confirm that the nanowires were still individually suspended in the HBSS and had not assembled into larger aggregates, a drop of the suspension containing nanowires was ejected from the syringe onto a microscope slide and examined using a Nikon eclipse 80i microscope, before and after each injection series.

The animals received subcutaneous injections of Temgesic (buprenorphine, 50 μg/kg body weight) to reduce postoperative pain, as well as an antidote to the anaesthesia (Antisedan, atipamezole hydrochloride, 0.5 mg/kg body weight), and were awakened under supervision.

2.4. Histology

The animals were killed by an i.p. overdose of pentobarbital and transcardially perfused with 200 mL of ice-cold saline solution (sodium chloride 0.9% in distilled water) followed by 125 mL of ice-cold 4% paraformaldehyde (PFA) in 0.1 M phosphate buffer (pH 7.4). The brains were carefully removed and post-fixed in 4% PFA overnight (4 °C). In addition, lymph nodes, liver, heart and vessels from all experimental groups (12 weeks and one year) (n = 24) were dissected and post-fixed in 4% PFA.

The tissues were cryoprotected in 25% sucrose solution until equilibrated and were subsequently attached to the sectioning block using Tissue Tek O.C.T. compound (Sakura Finetek, USA). Coronal serial sections of the brains were cut (6 series) at 10 μm thickness onto Super Frost® plus slides (Menzel-Gläser, Germany) using a cryostat (Microm, Germany). The markers used to visualize activated microglia and macrophages (CD68/ED1), astrocytes (glial fibrillary acidic protein (GFAP)), and neuronal nuclei (NeuN) are summarized in Table 2. All sections were counterstained using the cell nuclei marker 4′,6-diamidino-2-phenylindole (DAPI).

The lymph nodes, liver, heart and vessels were sectioned in the same manner as mentioned above, at 10 μm thickness and labelled with ED1 and DAPI. They were subsequently screened for presence of nanowires using a Nikon eclipse 80i microscope and a laser scanning confocal microscope (Zeiss LSM 510). Nanowires scatter confocal laser light and can therefore be visualized using the laser-reflection mode.

Tissue sections were hydrated in phosphate buffered saline (PBS) and blocked with 5% normal goat serum and 0.25% Triton X-100 in PBS (blocking solution). Incubation with primary antibodies (in blocking solution) was made at room temperature (RT) overnight. Sections were subsequently rinsed in PBS followed by incubation with DAPI, goat anti-rabbit IgG Alexa 594 and goat anti-mouse IgG Alexa 488 (in blocking solution) in the dark (RT) for 2 h (Table 2). Sections were rinsed and coverslipped using PVA-DABCO (polyvinyl alcohol, Fluka/Sigma–Aldrich, Switzerland).

Prior to NeuN staining an antigen retrieval method was performed. In short, after hydration, the sections selected for NeuN staining were immersed in a 10 mM sodium citrate buffer (0.05% Tween 20, pH 6) and microwaved for 3 × 5 min at 500 W. Tris-buffer (Sigma–Aldrich, Germany) was used instead of PBS for all steps and Triton X-100 was omitted from the blocking solution, otherwise all steps were made according to the staining protocol above.

2.5. Image acquisition and analysis for quantitative assessment

In order to quantitatively evaluate the density of neurons and activation state of glial cells in defined regions of interest (ROIs) in relation to the injection site, we quantified the binding of selected markers to cell specific proteins/antigens in the tissue. In short, the sections were screened to detect the location of the scar where the ED1- and GFAP-positive area was seen at its maximum. At this location, photographs of the fluorescence of the ED1- and GFAP-positive cells and cell nuclei (DAPI) were taken at each injection site, using a DS-2MV digital camera (Nikon, Japan) mounted on a Nikon eclipse 80i microscope with a 10× objective. Image capture and analysis were performed using the NIS-Elements 3.1 software (Nikon Instruments, Japan). The adjacent brain sections were stained using NeuN, GFAP and DAPI and photographs of the injection sites were taken.

The quantification analysis was based on a previously described method [28]. In short, rectangular shaped ROIs, inner and outer ROIs (100 × 800 μm and 300 × 800 μm, respectively), were centred on the injection tract (Supplementary Fig. 1). The different cell quantifications were made by measuring the proportion of immunoreactive area (for ED1 and GFAP) and the number of cells (for NeuN and DAPI) in the total screened area for each marker and injection site for all experimental groups [28]. Due to variability in the binding specificity of ED1 and GFAP to their respective antigen, thresholds were set for each individual image at a fixed ratio of the mean background intensity for each marker. The thresholds were set to ensure that only positively stained antigens were quantified, whereas the nonspecific background staining was not. The threshold for the signal to background ratio was set to 5.5 for ED1 immunofluorescence and to 4.5 for GFAP immunofluorescence. The fraction of the area above this threshold in each ROI was quantified. Neuronal nuclei were counted manually by matching NeuN-positive cells with a co-stained DAPI-positive nucleus within the ROIs. Cell nuclei were counted manually by counting the number of DAPI-positive nuclei (above ø 3 μm to avoid counting debris/artefacts) within the ROI.

Confocal images of the scar were photographed with a laser scanning confocal microscope (Zeiss LSM 510) using a 63× oil-immersion objective (N.A. 1.4) and the ZEN software (Zeiss). Nanowires were visualized using the laser-reflection mode.

2.6. Statistical analyses

Kruskal Wallis with Dunn's multiple comparison test was used to compare the experimental groups. Wilcoxon matched-pairs signed rank test was used when paired comparisons of two experimental groups were performed (SW vs. SW-control). p-values < 0.05 (*) were considered significant. All values are presented as median values, together with 25 and 75 percentiles, as well as, minimum and maximum values. All analyses were performed using the GraphPad Prism 6.0 software (GraphPad Software Inc., USA).

3. Results

To determine the effects of the length of biostable high-aspect-ratio nanowires on the evoked inflammatory tissue response, we injected nanowires of three different lengths (2, 5 and 10 μm) into the rat striatum. The animals were killed and perfused either after 12 weeks or one year. In order to assess the degree of reactive astrocytosis and the evoked inflammatory response, brain sections from all groups were stained for ED1- (microglial cells and macrophages) and GFAP-positive cells (astrocytes). To assess the neuronal survival and the number of total cell nuclei in the scar area, NeuN (neuronal nuclei) and DAPI (cell nuclei) were used. The different markers were quantified in two regions of interest (ROIs) surrounding the injection tract (see method for detailed experimental protocol).

3.1. General observations

At both time points, areas positive for ED1 and GFAP were significantly larger for control and experimental groups, when compared to the naïve group (inner ROI) (Supplementary Table 1). The neuronal and cell nuclei density (inner ROI) in control and experimental groups was significantly lower as compared to the naïve group at both time points (Supplementary Table 1).

Excluding brain tissue, no nanowires were detected in additionally dissected and investigated tissues, i.e. in the lymph nodes, liver, heart and vessels, in any of the experimental groups.

Table 2
Summary of primary antibodies, secondary antibodies and nucleic acid stain.

Name	Characteristics	Host	Working dilution	Source
ED1 (CD68)	Activated microglia/macrophages	Mouse	1:250	Cat. Nr. MCA341R, AbD Serotec
GFAP	Glial fibrillary acidic protein	Rabbit	1:5000	Cat. Nr. Z0334, Dako
NeuN	Neuronal nuclei, neuronal marker	Mouse	1:100	Cat. Nr. MAB377, Millipore
Alexa 594	Goat anti-rabbit IgG (H + L)	Goat	1:500	Cat. Nr. A11005, Invitrogen
Alexa 488	Goat anti-mouse IgG (H + L)	Goat	1:500	Cat. Nr. A11001, Invitrogen
DAPI	Nucleic Acid Stain (4′,6-diamidino-2-phenylindole)		1:1000	Cat. Nr. D3571, Invitrogen

3.2. Effect of the suspension media

In order to investigate the effect of the control, (i.e. vehicle solution, Hank's balanced salt solution (HBSS)), we performed bilateral surgery on eight animals; stab wound (SW) and a stab wound with control injection of HBSS (SW-control) in opposing hemispheres, respectively. No significant difference in ED1-positive area, neuronal density or cell nuclei density (inner or outer ROI) could be found when comparing the responses in the two groups (SW vs. SW-control) after 12 weeks. However, GFAP-positive area was significantly higher ($p = 0.023$) in the inner ROI for the SW group (mean $17.4\% \pm 2.3\%$) as compared to SW-control (mean $10.9\% \pm 1.3\%$) (Fig. 2). These results indicate that HBSS may lower the astrocytic inflammatory response in the brain towards the stab wound caused by the injection needle.

3.3. Effect of nanowire length on the brain tissue response after 12 weeks

We injected nanowires of three different lengths (2, 5 and 10 μm) and assessed the brain tissue response and cell density 12 weeks after the injections. Representative fluorescence microscopy images of the scar tissue area after injections of control solution and nanowires of different lengths are shown in Fig. 3.

3.3.1. Microglia/macrophage response

A significant increase in ED1-positive area, in the inner ROI, was found for the group receiving 10 μm long nanowires compared to both the control group ($p = 0.0074$) and to the group receiving 2 μm long nanowires ($p = 0.018$), with a mean percentage of fluorescent area of $3.75\% \pm 0.78\%$ (for 10 μm nanowires), $1.01\% \pm 0.13\%$ (for control), and $1.11\% \pm 0.15\%$ (for 2 μm nanowires) (Fig. 4). In the outer ROI, no significant difference in ED1-positive area was found when comparing the groups (data not shown). Moreover, the overall immunoreactive area for ED1 in the outer ROI was close to zero in all groups, indicating that the microglial and macrophage activity is largely limited to the inner ROI 12 weeks after implantation.

3.3.2. Astrocytic reactivity

In the inner ROI, we observed a significant increase in GFAP-positive area in the group receiving 10 μm long nanowires compared to the control group ($p = 0.035$), with a mean percentage of fluorescent area of $18.3\% \pm 2.3\%$ and $9.34\% \pm 1.3\%$, respectively (Fig. 4). In the outer ROI, there was a significant increase in GFAP-positive area for the group receiving 5 μm long nanowires compared to the control group ($p = 0.049$), with a mean percentage of fluorescent area of $5.75\% \pm 1.1\%$ and $2.30\% \pm 0.38\%$, respectively (Fig. 4). Furthermore, a trend towards an increase in GFAP-positive area in the outer ROI was
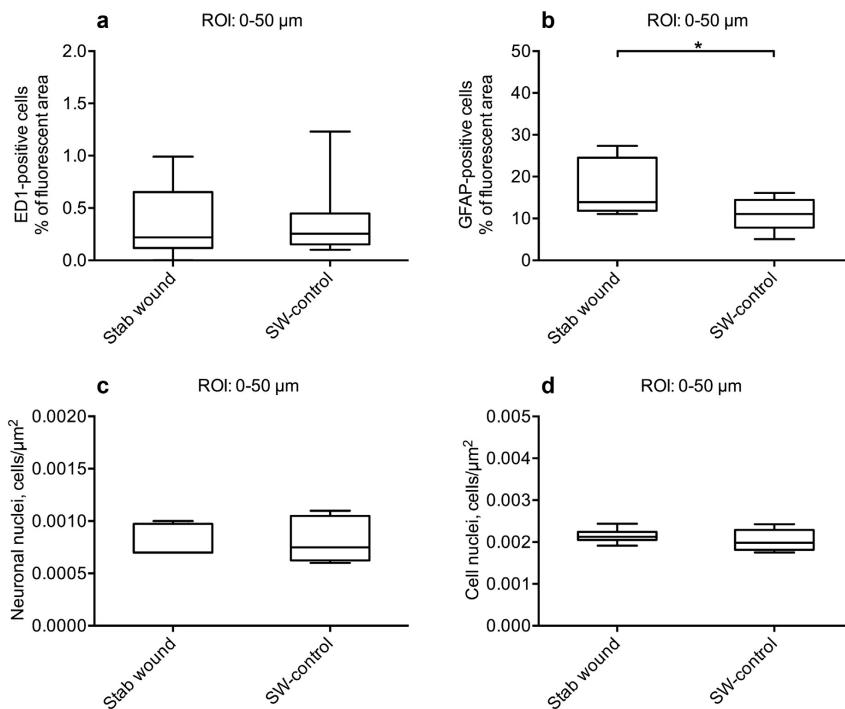

Fig. 2. Analysis of SW and SW-control after 12 weeks. (a–d) Quantification in the inner ROI (0–50 μm) of ED1-positive area (a), GFAP-positive area (b), NeuN density (c), and cell nuclei density (d) at 12 weeks for stab wound (SW) and stab wound with injection of vehicle solution, HBSS (SW-control). The boxes correspond to median values with indication of the 25 and 75 percentiles, and the whiskers show the minimum and maximum values. Wilcoxon matched-pairs signed rank test was used and the horizontal lines indicate statistical differences ($^*p < 0.05$, $^{**}p < 0.01$, $^{***}p < 0.001$).
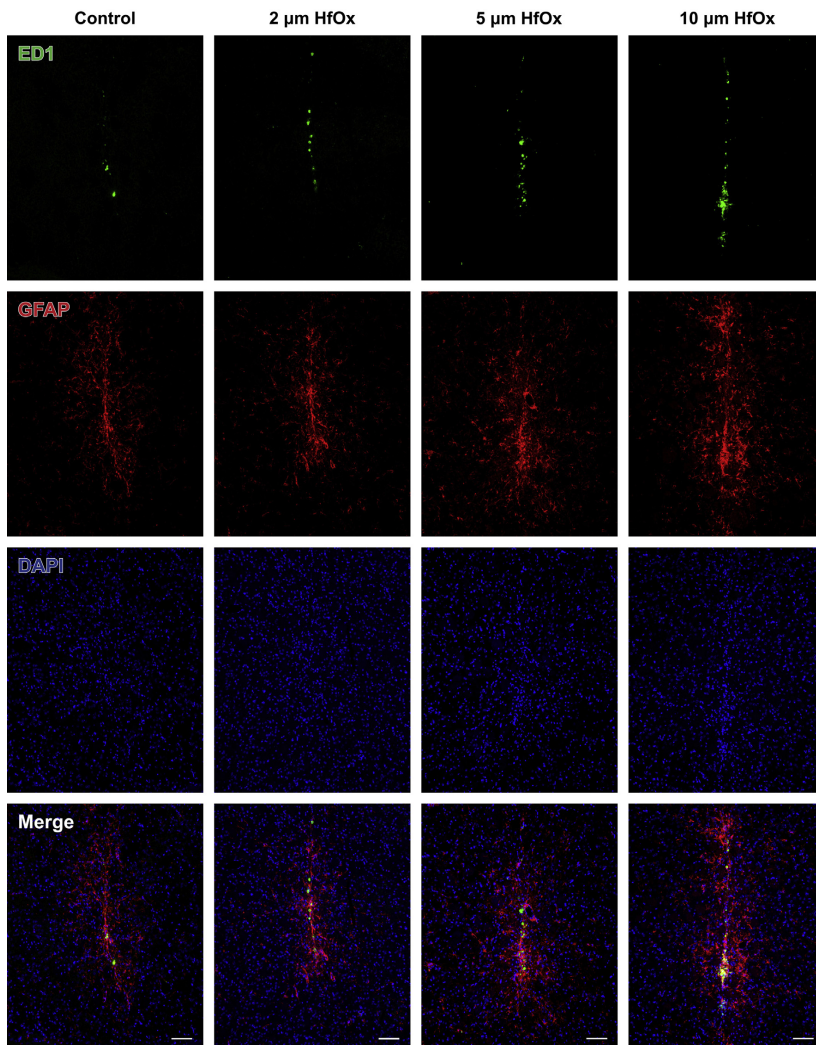
Fig. 3. *In vivo* tissue response after 12 weeks. Representative fluorescent images of the tissue response to injections of control and 2, 5 and 10 μm long HfO$_x$ (hafnium oxide) -coated nanowires at 12 weeks. ED1-positive cells (green), GFAP-positive cells (red), and cell nuclei (blue) and merge. Scale bars: 100 μm.

seen for the group receiving 10 μm long nanowires (4.45% ± 0.52%) compared to the control group ($p = 0.056$) (Fig. 4).

3.3.3. Neuronal density

There was no significant difference in the number of neuronal nuclei (NeuN), in the inner (Fig. 4) or outer ROI (data not shown) between the different groups 12 weeks after the injections. This suggests that no nanowire-induced neurotoxic effect was present at this time point.

3.3.4. Cellular density

A significant increase in the number of cell nuclei (DAPI) was found in the group receiving 10 μm long nanowires compared to the control group ($p = 0.0071$), with a mean nuclei density of 0.00265 ± 7.7e-005 μm^{-2} and 0.00227 ± 4.7e-005 μm^{-2}, respectively (Fig. 4). This corresponds to a 16.7% increase in cell nuclei in the 10 μm nanowire-injected group compared to control, which may be explained by the increase of ED1 and GFAP- positive cells in this group.
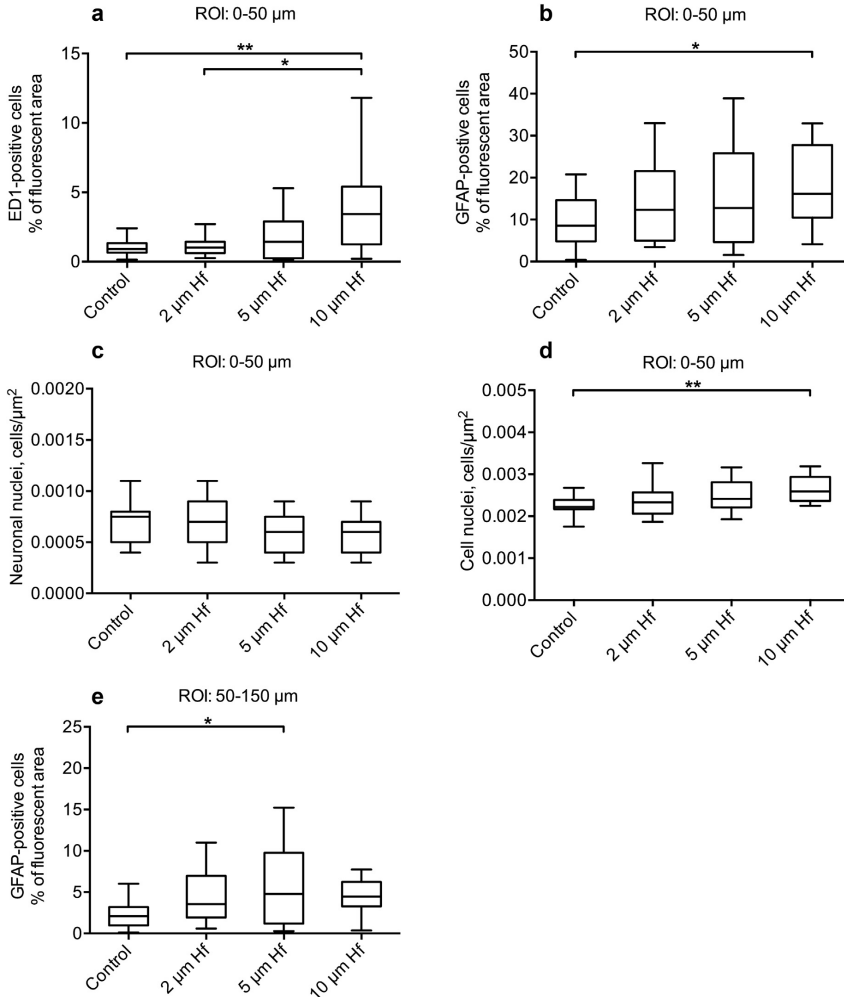
Fig. 4. Inflammatory response and neuronal density after 12 weeks. (a–d) Quantification in the inner ROI (0–50 μm) of ED1-positive area (a), GFAP-positive area (b), NeuN density (c), and cell nuclei density (d) at 12 weeks for nanowire- injected animals and control group. (e) Quantification in the outer ROI (50–150 μm) of GFAP-positive area at 12 weeks for nanowire-injected animals and control group. Hf corresponds to hafnium oxide coated nanowires. The boxes correspond to median values with indication of the 25 and 75 percentiles, and the whiskers show the minimum and maximum values. Kruskal Wallis with Dunn's multiple comparison test was used and the horizontal lines indicate statistical differences (*$p < 0.05$, **$p < 0.01$, ***$p < 0.001$).

3.4. Effect of nanowire length on the brain tissue response after one year

Representative fluorescence microscopy images of the scar tissue area after injections of control solution and nanowires of different lengths one year after surgery are shown in Fig. 5.

3.4.1. Microglia/macrophage response

In the inner ROI a significant increase in ED1-positive area was found in the group receiving 10 μm (mean area of 2.82% ± 0.59%,

$p = 0.0003$) and 5 μm long nanowires (mean area 1.65% ± 0.32%, $p = 0.029$) compared to the control group (mean area 0.690% ± 0.081%) (Fig. 6). In the outer ROI, however, there was no significant difference in ED1-positive area comparing the groups (data not shown) and the overall immunoreactive area for ED1 in this ROI was close to zero in all groups, comparable to the findings at 12 weeks.

3.4.2. Astrocytic reactivity

In the inner ROI, there was no significant difference in GFAP-positive area between any of the groups (Fig. 6). In the outer ROI,
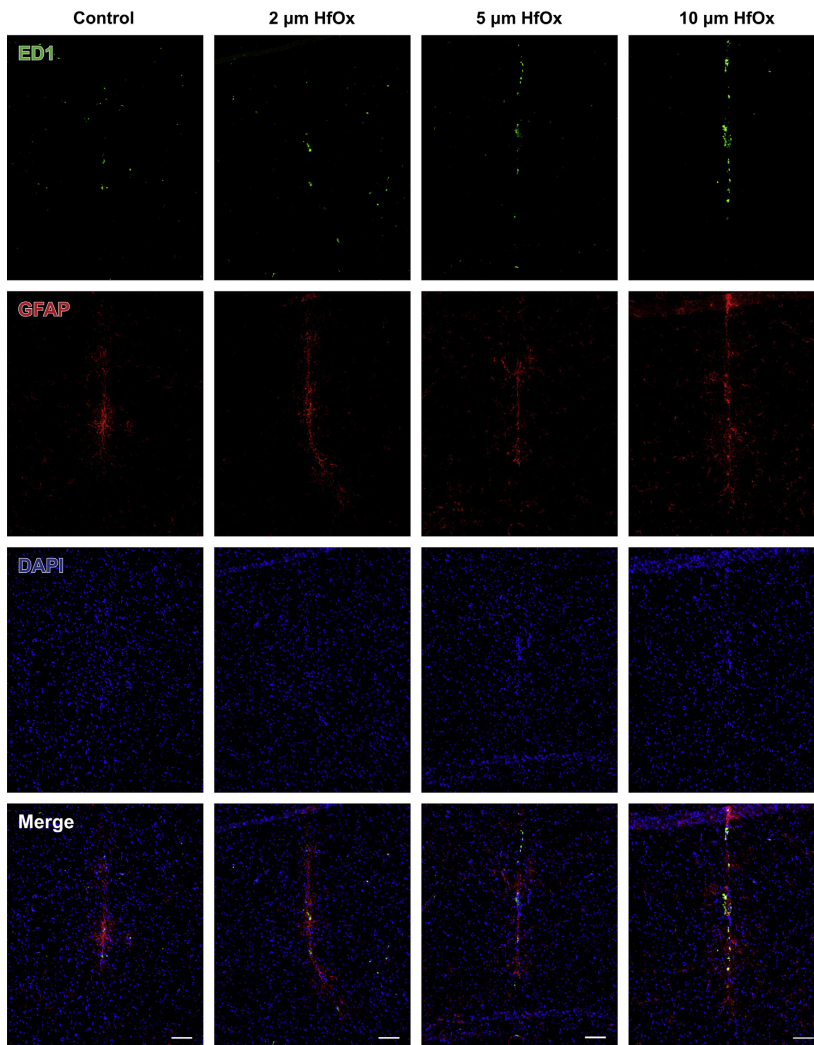
| | Control | 2 µm HfOx | 5 µm HfOx | 10 µm HfOx |

Fig. 5. *In vivo* tissue response after one year. Representative fluorescent images of the tissue response to injections of control and 2, 5 and 10 µm long HfOₓ (hafnium oxide) -coated nanowires at one year. ED1-positive cells (green), GFAP-positive cells (red), and cell nuclei (blue) and merge. Scale bars: 100 µm.

however, a significant increase of GFAP-positive area was found in the group receiving 10 µm long nanowires (7.31% ± 1.1%) compared to the group receiving 5 µm long nanowires (3.61% ± 0.46%) ($p = 0.042$) (Fig. 6).

3.4.3. Neuronal density

In the inner ROI, a significant decrease in the neuronal nuclei density was found in the group receiving 10 µm long nanowires (66.6e-005 ± 4.9e-005 µm^{-2}) compared to the control group (88.0e-005 ± 5.2e-005 µm^{-2}) ($p = 0.032$) (Fig. 6). This corresponds to a 24.2% loss of neuronal nuclei in the 10 µm nanowire group compared to control. In the outer ROI, however, no significant difference in neuronal density was found when comparing the different groups (data not shown). This finding suggests that the reduction of neurons observed in the 10 µm group in the inner ROI,
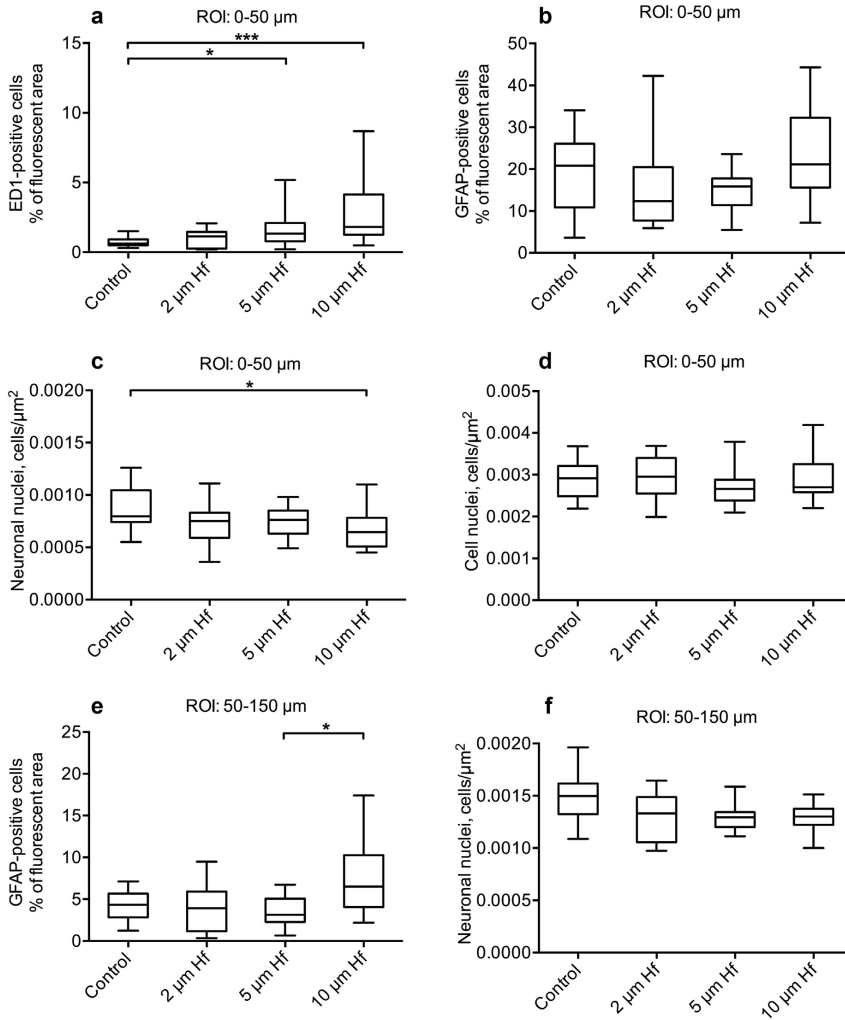
Fig. 6. Inflammatory response and neuronal density after one year. (a–d) Quantification in the inner ROI (0–50 μm) of ED1-positive area (a), GFAP-positive area (b), NeuN density (c), and cell nuclei density (d) at one year for nanowire-injected animals and control group. (e–f) Quantification in the outer ROI (50–150 μm) of GFAP-positive area (e) and NeuN density (f) at one year for nanowire-injected animals and control group. Hf corresponds to hafnium oxide coated nanowires. The boxes correspond to median values with indication of the 25 and 75 percentiles, and the whiskers show the minimum and maximum values. Kruskal Wallis with Dunn's multiple comparison test was used and the horizontal lines indicate statistical differences (*$p < 0.05$, **$p < 0.01$, ***$p < 0.001$).

was not due to a displacement of neurons from the inner ROI to the outer ROI.

3.4.4. Cellular density

There was no significant difference in the number of cell nuclei when comparing the different groups one year after the injections (Fig. 6).

3.5. Confocal analysis of the nanowire distribution

At both time points, confocal examination of the groups receiving nanowires showed that ED1-positive cells had engulfed most of the 2 μm long nanowires. However, some of the 5 μm and 10 μm long nanowires could be seen free in the tissue, i.e. not engulfed by any type of labelled cell, (Figs. 7–8). We also observed
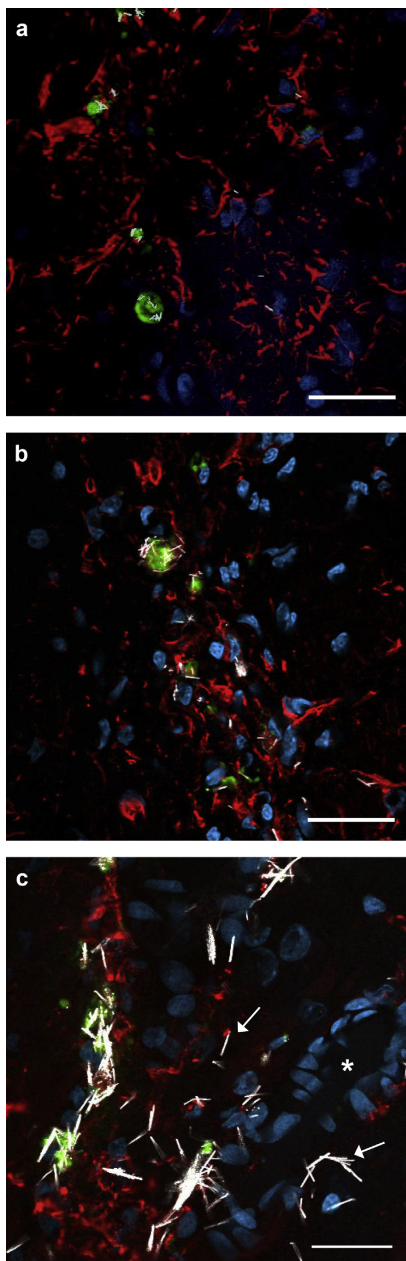
nanowires lining blood vessel walls at both time points, free or engulfed by ED1-positive cells (Figs. 7–8). Furthermore, in the centre of the injection tract, small aggregations of co-localized ED1 and GFAP staining could be observed. These aggregates resembled cell debris or cell aggregates, and the dominating majority contained nanowires, see Fig. 9. However, they were regularly devoid of DAPI-positive nuclei, suggesting that they were not viable cells. The aggregates were mostly observed in the groups with longer nanowires (5 and 10 μm) and were rarely found at the early time point, i.e. at 12 weeks.

4. Discussion

To assess possible risks involved in using future nanowire-structured neural interfaces, we analyzed the tissue response and neuronal survival after injection of non-degradable, high-aspect-ratio nanoparticles into the brain, for a period corresponding to approximately half the lifespan of a rat, i.e. one year. Importantly, while the inflammatory tissue response depends on the nanowire length, it did not escalate between 12 weeks and one year. However, for the longest nanowires, the increased microglial activation found at 12 weeks did persist for one year and the neuronal density was reduced as compared to control after one year.

At 12 weeks post implantation, ED1 and GFAP immunoreactivity was increased only in the 10 μm nanowire group as compared to control. After one year, both 5 and 10 μm nanowires groups exhibited an increase in ED1 immunoreactivity compared to the control group. The increased ED1 response observed towards longer nanowires might reflect a size dependent limit of the phagocytic capacity of macrophages and microglial cells. Indeed, the fibre pathogenicity paradigm predicts that long, thin and bio-stable fibres will lead to frustrated phagocytosis and elicit a long lasting/chronic inflammatory response. Such asbestos-like pathogenicity has been observed after implantation of long CNTs in the mice abdominal tissue [20]. More recently, the same group used silver nanowires with narrow length distributions to investigate the length threshold for asbestos-like pathogenicity in the lung and the pleura, which was determined to be around 5–10 μm [21,33]. The present results are consistent with these findings. The observed cell debris/cell aggregates, containing 5 and 10 μm long nanowires (Fig. 9), could be compared to granulomas, which supports the hypothesis that the phagocytosis of the longer nanowires cannot be completed normally. It may be speculated that longer nanowires exert a higher strain force on the membrane of the phagocytizing cells since these nanowires are close to the size of the microglial cells [34]. This strain might impede the engulfment of nanowires or lead to membrane deformation or even piercing of the cell membrane during engulfment or migration, which could lead to cell death.

In the present study, we found a higher number of 5 and 10 μm long nanowires that were free in the brain tissue (i.e. not engulfed by any type of labelled cells) compared to 2 μm long nanowires (which were almost always engulfed by ED1-positive cells). This suggests that when unable to phagocytize long nanowires, cells either undergo apoptosis without signalling to

Fig. 7. Confocal images 12 weeks after nanowire injection. Representative laser scanning confocal microscopy images of the scar after injection of 2 (a), 5 (b), and 10 μm (c) long nanowires at 12 weeks. Free nanowires, not engulfed by any labelled cell type, were observed in the scar area. ED1-positive cells (green), GFAP-positive cells (red), cell nuclei (blue), nanowires (white), free nanowires (→), and blood vessels (*). Scale bars: 30 μm.
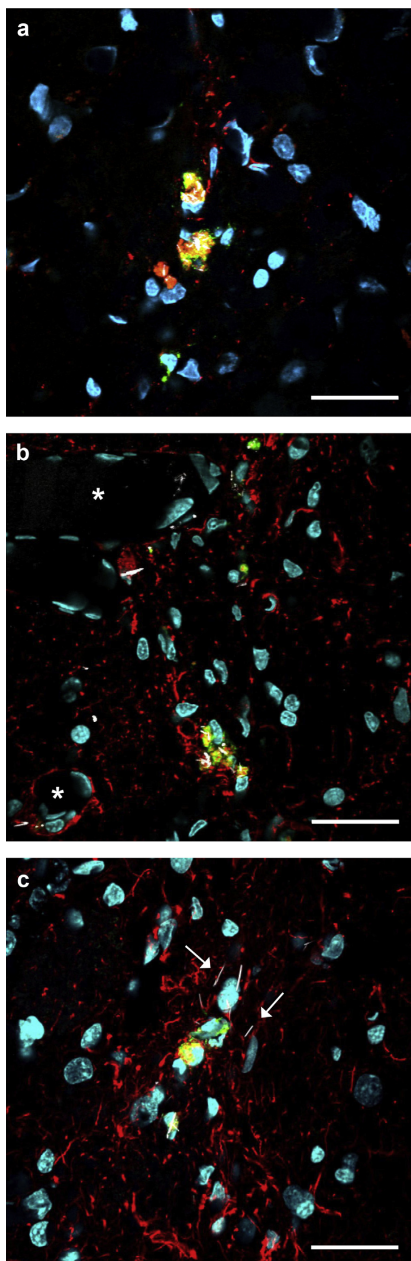
recruit new cells, or the immune cells do not detect some of the long nanowires.

Importantly, our results showed no indication of an escalation of the inflammatory tissue response over time. However, the neuronal density in the immediate vicinity of the injection tract for the 10 μm nanowire-injected group was reduced as compared to control, at the one year follow up, indicating that neurons in the 10 μm group are slowly dying over time. This might be related to the increased glial response to 10 μm nanowires as compared to shorter nanowires. It has been reported that activated glial cells may continuously secret neurotoxic substances, which could explain the neuronal cell loss one year post nanowire injection [35–37].

The nanowires used in this study are non-degradable by design and therefore cannot be cleared by phagocytic activity. However, we observed nanowires lining blood vessel walls near the injection site, both free and engulfed by ED1-positive cells (Figs. 7–8). This may suggest a clearance mechanism by translocation, where ED1-positive cells migrate and transport nanowires to blood vessels in their vicinity. Similar observations have been made several decades ago after injection of colloidal carbon into the brain [38]. Our previous study, on short and biodegradable nanowires in the brain, also suggested a nanowire clearance mechanism through the blood vessels [28]. It is known that the CNS lacks conventional lymphatic drainage. Recent studies have shown that the cerebrospinal fluid drains mainly from the subarachnoid space through the cribriform plate into nasal lymphatics and to deep cervical lymph nodes, and infiltrating monocytes are also capable of migrating via the cribriform plate [39,40]. Drainage of interstitial fluid and solutes, on the other hand, has been suggested to mainly occur through the basement membrane in the walls of capillaries, ultimately ending up in the cervical lymph nodes [39]. Hence, it is possible that the microglial cells and macrophages containing nanowires follow these routes as well. In our case, no nanowires could be detected in the dissected lymph nodes, suggesting that, either the injected nanowires could not leave the brain, or that too small amounts of nanowires were cleared out of the brain to be detected.

Vehicle injections of HBSS led to a smaller astrocytic reactivity compared to stab wound without vehicle injection. This suggests that HBSS may reduce the adverse effects caused by the stab wound. Possible explanations for this could be that the injected solution dilutes the concentration of inflammatory cytokines locally, thereby, indirectly reducing the ensuing inflammatory response at the injection site. Further studies are needed in order to determine the mechanisms behind this observation.

5. Conclusions

In conclusion, we show that the brain inflammatory response to the implantation of biostable nanorods and the loss of nearby neurons are strongly length dependent. The results indicate that, similar to the lungs and abdomen, a persistent, albeit not escalating, inflammatory response occurs in the brain when high-aspect-ratio particles, with a length equal to or greater than the size of immune cells, are present in the tissue. The obtained results

Fig. 8. Confocal images one year after nanowire injection. Representative laser scanning confocal microscopy images of the scar after injection of 2 (a), 5 (b), and 10 μm (c) long nanowires at one year. Free nanowires, not engulfed by any labelled cell type, were observed in the scar area for the longer nanowires (5 and 10 μm). ED1-positive cells (green), GFAP-positive cells (red), cell nuclei (blue), nanowires (white), free nanowires (→), and blood vessels (*). Scale bars: 30 μm.
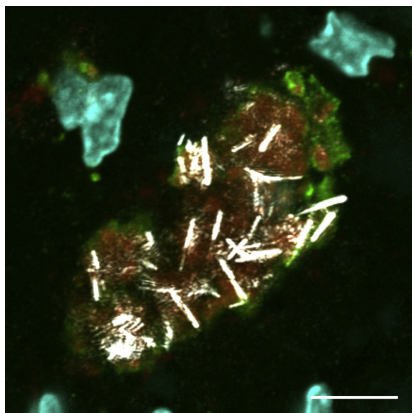
Fig. 9. Confocal image of an aggregate at one year after nanowire injection. Laser scanning confocal microscopy image of the scar area after injection of 5 μm long nanowires at one year showing the aggregates of cell debris or cells observed in the tissue at one year. ED1-positive cells (green), GFAP-positive cells (red), cell nuclei (blue), and nanowires (white). Scale bars: 10 μm.

stress the importance of using nanorods that are shorter than the size of brain immune cells, when modifying the surface of neural interfaces in order to improve their performance.

Acknowledgements

Appendix A. Supplementary data

Supplementary data related to this article can be found at http://dx.doi.org/10.1016/j.biomaterials.2014.11.051.

References

[1] Awan NR, Lozano A, Hamani C. Deep brain stimulation: current and future perspectives. Neurosurg Focus 2009;27:E2.
[2] Daly JJ, Wolpaw JR. Brain-computer interfaces in neurological rehabilitation. Lancet Neurol 2008;7:1032—43.
[3] Hochberg LR, Serruya MD, Friehs GM, Mukand JA, Saleh M, Caplan AH, et al. Neuronal ensemble control of prosthetic devices by a human with tetraplegia. Nature 2006;442:164—71.
[4] Kipke DR, Shain W, Buzsaki G, Fetz E, Henderson JM, Hetke JF, et al. Advanced neurotechnologies for chronic neural interfaces: new horizons and clinical opportunities. J Neurosci 2008;28:11830—8.
[5] Biran R, Martin DC, Tresco PA. Neuronal cell loss accompanies the brain tissue response to chronically implanted silicon microelectrode arrays. Exp Neurol 2005;195:115—26.
[6] Marin C, Fernandez E. Biocompatibility of intracortical microelectrodes: current status and future prospects. Front Neuroeng 2010;3:8.
[7] Szarowski DH, Andersen MD, Retterer S, Spence AJ, Isaacson M, Craighead HG, et al. Brain responses to micro-machined silicon devices. Brain Res 2003;983: 23—35.
[8] Williams JC, Hippensteel JA, Dilgen J, Shain W, Kipke DR. Complex impedance spectroscopy for monitoring tissue responses to inserted neural implants. J Neural Eng 2007;4:410—23.
[9] Biran R, Martin DC, Tresco PA. The brain tissue response to implanted silicon microelectrode arrays is increased when the device is tethered to the skull. J Biomed Mater Res A 2007;82:169—78.
[10] Gilletti A, Muthuswamy J. Brain micromotion around implants in the rodent somatosensory cortex. J Neural Eng 2006;3:189—95.
[11] Lind G, Eriksson Linsmeier C, Schouenborg J. The density differences between tissue and neural probes is a key factor for glial scarring. Sci Rep 2013;3:2942.
[12] Thelin J, Jorntell H, Psouni E, Garwicz M, Schouenborg J, Danielsen N, et al. Implant size and fixation mode strongly influence tissue reactions in the CNS. Plos One 2011;6:e16267.
[13] Cellot G, Cilia E, Cipollone S, Rancic V, Sucapane A, Giordani S, et al. Carbon nanotubes might improve neuronal performance by favouring electrical shortcuts. Nat Nanotechnol 2009;4:126—33.
[14] Keefer EW, Botterman BR, Romero MI, Rossi AF, Gross GW. Carbon nanotube coating improves neuronal recordings. Nat Nanotechnol 2008;3:434—9.
[15] Hallstrom W, Martensson T, Prinz C, Gustavsson P, Montelius L, Samuelson L, et al. Gallium phosphide nanowires as a substrate for cultured neurons. Nano Lett 2007;7:2960—5.
[16] Piret G, Perez M-T, Prinz CN. Neurite outgrowth and synaptophysin expression of postnatal CNS neurons on GaP nanowire arrays in long-term retinal cell culture. Biomaterials 2013;34:875—87.
[17] Prinz C, Hallstrom W, Martensson T, Samuelson L, Montelius L, Kanje M. Axonal guidance on patterned free-standing nanowire surfaces. Nanotechnology 2008;19:345101.
[18] Suyatin DB, Wallman L, Thelin J, Prinz CN, Jörntell H, Samuelson L, et al. Nanowire-based electrode for acute in vivo neural recordings in the brain. PLoS One 2013;8:e56673.
[19] Donaldson K, Murphy F, Duffin R, Poland C. Asbestos, carbon nanotubes and the pleural mesothelium: a review of the hypothesis regarding the role of long fibre retention in the parietal pleura, inflammation and mesothelioma. Part Fibre Toxicol 2010;7:5.
[20] Poland C, Duffin R, Kinloch I, Maynard A, Wallace W, Seaton A, et al. Carbon nanotubes introduced into the abdominal cavity of mice show asbestos-like pathogenicity in a pilot study. Nat Nanotechnol 2008;3:423—8.
[21] Schinwald A, Murphy FA, Prina-Mello A, Poland CA, Byrne F, Movia D, et al. The threshold length for fiber-induced acute pleural inflammation: shedding light on the early events in asbestos-induced mesothelioma. Toxicol Sci 2012;128:461—70.
[22] Suyatin DB, Hallstrom W, Samuelson L, Montelius L, Prinz CN, Kanje M. Gallium phosphide nanowire arrays and their possible application in cellular force investigations. J Vac Sci Technol B 2009;27:3092—4.
[23] Hallstrom W, Lexholm M, Suyatin DB, Hammarin G, Hessman D, Samuelson L, et al. Fifteen-piconewton force detection from neural growth cones using nanowire arrays. Nano Lett 2010;10:782—7.
[24] Mohammadi S, Esposito M, Cucu M, Ericson LE, Thomsen P. Tissue response to hafnium. J Mater Sci Mater Med 2001;12:603—11.
[25] Matsuno H, Yokoyama A, Watari F, Uo M, Kawasaki T. Biocompatibility and osteogenesis of refractory metal implants, titanium, hafnium, niobium, tantalum and rhenium. Biomaterials 2001;22:1253—62.
[26] Maggiorella L, Barouch G, Devaux C, Pottier A, Deutsch E, Bourhis J, et al. Nanoscale radiotherapy with hafnium oxide nanoparticles. Future Oncol 2012;8:1167—81.
[27] Loo Y-L, Willett RL, Baldwin KW, Rogers JA. Additive, nanoscale patterning of metal films with a stamp and a surface chemistry mediated transfer process: applications in plastic electronics. Appl Phys Lett 2002;81:562—4.
[28] Eriksson Linsmeier C, Prinz CN, Pettersson LME, Caroff P, Samuelson L, Schouenborg J, et al. Nanowire biocompatibility in the brain — looking for a needle in a 3D stack. Nano Lett 2009;9:4184—90.
[29] Davis RK, Stevenson GT, Busch KA. Tumor incidence in normal sprague-dawley female rats. Cancer Res 1956;16:194—7.
[30] Prejean JD, Peckham JC, Casey AE, Griswold DP, Weisburger EK, Weisburger JH. Spontaneous tumors in Sprague-Dawley rats and swiss mice. Cancer Res 1973;33:2768—73.
[31] Nakazawa M, Tawaratani T, Uchimoto H, Kawaminami A, Ueda M, Ueda A, et al. Spontaneous neoplastic lesions in aged Sprague-Dawley rats. Exp Anim 2001;50:99—103.
[32] Thompson SW, Huseby RA, Fox MA, Davis CL, Hunt RD. Spontaneous tumors in the Sprague-Dawley rat. J Natl Cancer Inst 1961;27:1037—57.
[33] Schinwald A, Chernova T, Donaldson K. Use of silver nanowires to determine thresholds for fibre length-dependent pulmonary inflammation and inhibition of macrophage migration in vitro. Part Fibre Toxicol 2012;9:47.
[34] Agarwal R, Singh V, Jurney P, Shi L, Sreenivasan SV, Roy K. Mammalian cells preferentially internalize hydrogel nanodiscs over nanorods and use shape-specific uptake mechanisms. Proc Natl Acad Sci U S A 2013;110: 17247—52.
[35] Hanisch UK. Microglia as a source and target of cytokines. Glia 2002;40: 140—55.

[36] Streit W, Mrak R, Griffin WS. Microglia and neuroinflammation: a pathological perspective. J Neuroinflammation 2004;1:14.

[37] Verkhratsky A, Butt A. General pathophysilogy of glia. In: Verkhratsky A, Butt A, editors. Glial neurobiology: a textbook. Chichester, UK: John Wiley & Sons, Ltd; 2007. p. 153–65.

[38] McKeever PE, Balentine JD. Macrophages migration through the brain parenchyma to the perivascular space following particle ingestion. Am J Pathol 1978;93:153–64.

[39] Weller RO, Djuanda E, Yow HY, Carare RO. Lymphatic drainage of the brain and the pathophysiology of neurological disease. Acta Neuropathol 2009;117: 1–14.

[40] Kaminski M, Bechmann I, Pohland M, Kiwit J, Nitsch R, Glumm J. Migration of monocytes after intracerebral injection at entorhinal cortex lesion site. J Leukoc Biol 2012;92:31–9.

Paper II

RESEARCH

CrossMark

Impact of degradable nanowires on long-term brain tissue responses

Lina Gällentoft[1*], Lina M. E. Pettersson[1], Nils Danielsen[1], Jens Schouenborg[1], Christelle N. Prinz[1,2*] and Cecilia Eriksson Linsmeier[1*]

Abstract

Background: A promising approach to improve the performance of neural implants consists of adding nanomaterials, such as nanowires, to the surface of the implant. Nanostructured interfaces could improve the integration and communication stability, partly through the reduction of the cell-to-electrode distance. However, the safety issues of implanted nanowires in the brain need to be evaluated and understood before nanowires can be used on the surface of implants for long periods of time. To this end we here investigate whether implanted degradable nanowires offer any advantage over non-degradable nanowires in a long-term in vivo study (1 year) with respect to brain tissue responses.

Results: The tissue response after injection of degradable silicon oxide (SiOx)-coated gallium phosphide nanowires and biostable hafnium oxide-coated GaP nanowires into the rat striatum was compared. One year after nanowire injection, no significant difference in microglial or astrocytic response, as measured by staining for ED1 and glial fibrillary acidic protein, respectively, or in neuronal density, as measured by staining for NeuN, was found between degradable and biostable nanowires. Of the cells investigated, only microglia cells had engulfed the nanowires. The SiOx-coated nanowire residues were primarily seen in aggregated hypertrophic ED1-positive cells, possibly microglial cells that have fused to create multinucleated giant cells. Occasionally, degradable nanowires with an apparently intact shape were found inside single, small ED1-positive cells. The biostable nanowires were found intact in microglia cells of both phenotypes described.

Conclusion: The present study shows that the degradable nanowires remain at least partly in the brain over long time periods, i.e. 1 year; however, no obvious bio-safety issues for this degradable nanomaterial could be detected.

Keywords: Nanowires, Biocompatibility, Neural interfaces, Brain, Biomaterial, Foreign body reaction, Tissue responses, Immunohistochemistry, Nanomedicine

Background

Micro- and nanostructured electrode surfaces have been suggested to improve recording properties and reduce tissue responses [1–7]. Thus, combining a nanostructured topography on a small, low-density and flexible interface, known to reduce glial scarring [8–10], opens up for the development of a new type of biocompatible neural interface, with potential to achieve high quality recordings from single neurons. One way of creating neural interfaces with nanostructured topography is to coat the electrode surface with nanowires [5, 11–15].

Cells have been shown to be able to grow and interact strongly with arrays of nanowires or nanopillars in vitro [13, 14, 16–20]. In particular, gallium phosphide (GaP) nanowire arrays have been shown to promote neurite outgrowth and reduce glial cell spreading [21, 22]. Previously, we have achieved successful acute in vivo recordings using neural interfaces with GaP nanowire surface modifications [15]. In order to test the biocompatibility of nanowires per se, we have recently investigated the brain tissue response to the injection of nanowires in the brain. In a first, relatively short-term nanosafety study,

*Correspondence: lina.gallentoft@med.lu.se; christelle.prinz@ftf.lth.se; cecilia.eriksson_linsmeier@med.lu.se
[1] Department of Experimental Medical Science, Medical Faculty, Neuronano Research Center (NRC), Lund University, Scheelevägen 2, 223 81 Lund, Sweden
Full list of author information is available at the end of the article

Gällentoft *et al. J Nanobiotechnol* (2016) 14:64

Page 2 of 11

we used 2 μm long GaP nanowires coated with silicon oxide (SiOx) and assessed the tissue response 1, 6 and 12 weeks after injection [23]. One important finding of this study was that many, but not all, of the injected SiOx-coated nanowires had lost their structural integrity, i.e. both the GaP core and the SiOx coating were found to be degraded into fragments in vivo, within 12 weeks. The degraded nanowire fragments were found engulfed by macrophages/microglia in the injection tract [23], indicating that the nanowire material used could be fragmented or dissolved in the brain tissue but not cleared from the brain after 12 weeks.

However, it is unknown whether degradable nanowires will be completely removed from the injection site and eventually cleared from the brain over time. Importantly, it is also not known if degradable nanowires offer any advantage over non-degradable nanowires with regard to long-term inflammatory brain tissue response and neuronal survival.

The purpose of the present study was thus to evaluate how degradable nanowires affect the long-term inflammatory brain tissue response and neuronal density and to compare with the effects of implanted non-degradable (i.e. biostable [24]) nanowires, which are known to persist in the brain for long periods of time [25]. Further aims were to investigate the possible persistence of nanowires or nanowire residues in the brain tissue after 1 year and to clarify which of the different brain cells, such as glial and neuronal cells engulf the nanowires or their residues.

To this end, we evaluated the brain tissue response to 2 μm long degradable nanowires 1 year after injection. We compared the tissue response and neuronal survival in rat striatum after injections of degradable SiOx-coated GaP nanowires (2 μm) to biostable, hafnium oxide (HfOx)-coated GaP nanowires (2 μm), dispersed in Hank's balanced salt solution (HBSS). One year post injection, the neuronal loss and the inflammatory tissue response were evaluated by quantification of microglia/macrophages, astrocytes, neuronal cell density, and total cell nuclei density, surrounding the nanowire injection site. The presence of nanowires and/or nanowire residues in cells and tissue was examined by detecting the scattered laser light in a confocal microscope.

Methods

Nanowire growth and coating

Metal organic vapor phase epitaxy (MOVPE) (Aix 200/4, Aixtron, Germany) was used to grow GaP nanowires from 40 nm gold aerosol particles on (111)B GaP substrates (Girmet Ltd, Moscow, Russia), as previously described [26]. The gold aerosol particles were randomly distributed at an average density of $1/\mu m^2$. The temperature for nanowire growth was 470 °C. The nanowire

growth was initiated by supplying trimethylgallium $(Ga(CH_3)_3)$ in addition to phosphine (PH_3). The growth time was adjusted in order to obtain a nanowire length of 2 μm. Precursor molar fractions were 4.3×10^{-6} for $Ga(CH_3)_3$ and 8.5×10^{-2} for PH_3. The hydrogen carrier gas flow was 6 L/min and the nanowire growth was conducted under low pressure (10 kPa).

The GaP nanowires were coated with a 20 nm layer of SiOx using Atomic layer deposition (Fiji, Cambridge NanoTech Inc., USA). The nanowires were subsequently broken off from the substrate using ultra sonication and suspended in HBSS as vehicle solution to a final concentration of 70,000 nanowires/μL.

The HfOx-coated nanowires were produced as described above except for the 20 nm HfOx atomic layer deposition, which was done using a Savannah-100 ALD system (Cambridge NanoTech Inc., USA), as published elsewhere [25].

Animals

Approvals for the animal experiments were obtained in advance from the Lund/Malmö local ethical committee on animal experiments (ethical permit number: M300-10). Female Sprague–Dawley (SD) rats (Taconic, Denmark) were used. The rats were kept in a 12-h day-night cycle and received food and water ad libitum. At the beginning of the experiment the rats weighed approximately 225 g and they followed a normal weight curve post surgery.

At the experimental start-point, 10 animals received striatal bilateral injections of 2 μm long degradable SiOx-coated nanowires suspended in HBSS [rats = 10, n (injections) = 20], for details see below. Two of the rats were killed before the predetermined 1 year end point of the experiment, in accordance with the ethical exclusion criterion, since they developed age-related spontaneous tumors [25]. Furthermore, one rat was excluded since it did not meet our histological inclusion criteria. The results from the remaining seven rats (n = 14) were compared to data from our previously published study [25] where rats subjected to the same injection protocol, but injected with a suspension of 2 μm biostable HfOx-coated nanowires (n = 11), were investigated. The reason to compare the results from the present study with those from an already published study was ethical, and done in order to minimize the number of animals subjected to surgery and subsequently kept for a whole year after the nanowire injections.

Surgery

The animals were anaesthetized by intraperitoneal (i.p.) injections of Fentanyl (0.3 mg/kg body weight) and Domitor vet (metedetomidin hydrochloride, 0.3 mg/

Gällentoft *et al. J Nanobiotechnol (2016) 14:64*

Page 3 of 11

kg body weight). The surgical area was shaved and the animal was positioned in a stereotactic frame (KOPF instruments, USA) under a stereomicroscope (Leica Microsystems, Germany). The scalp was disinfected using 70 % ethanol solution and local anaesthetic was administered, 0.25 % Marcaine (Bupivacaine, 0.33 mg/kg body weight) in sterile water. A 2 cm midline incision was made, connective tissue attached to the skull was carefully removed and blood was cleansed away. Under stereotactic control bilateral craniotomies (approximately ø 1 mm^2) at 1.0 mm anterior and 2.5 mm lateral to bregma were drilled. Fine forceps were used to incise and deflect the dura mater, and stereotactic injections were made bilaterally using a 2 μL Hamilton syringe with a glass microcapillary (tip ø ~130 μm) attached. The HBSS suspension with nanowires was injected into the striatum at two depths; 5 mm (1 μL) and an additional injection at 4 mm (1 μL), i.e. 2 μL/hemisphere over a total time of 2 × 2 min.

The skin was closed with surgical clips. Before and after each session of nanowire injections, a drop of the nanowire suspension was ejected from the syringe onto a microscope slide and the presence of individually suspended nanowires was confirmed using a Nikon eclipse 80i microscope (Nikon, Japan).

After surgery, the animals were awakened under supervision. Subcutaneous injections of Temgesic (buprenorphine, 50 μg/kg body weight) were administered to reduce postoperative pain, as well as an antidote to the anaesthesia (Antisedan, atipamezole hydrochloride, 0.5 mg/kg body weight).

Histology

The animals were killed by an i.p. overdose of pentobarbital 1 year post nanowire injection. The animals were transcardially perfused with ~200 mL of ice-cold saline solution (sodium chloride 0.9 % in distilled water) followed by ~125 mL of ice-cold 4 % paraformaldehyde (PFA) in 0.1 M phosphate buffered saline (PBS) (pH 7.4). The brains were gently removed and following post-fixation in 4 % PFA overnight (4 °C) they were cryo-protected in 25 % sucrose solution until equilibrated (4 °C).

Cervical lymph nodes were also dissected and prepared for histology. The brains were snap frozen using dry ice and fixed to sectioning blocks using Tissue Tek optimal cutting temperature (O.C.T.) compound (Sakura Finetek, USA). Consecutive coronal sections were cut serially (6 series) at 10 μm thickness onto Super Frost® plus slides (Menzel-Gläser, Germany) using a cryostat (Microm, Germany). The primary antibodies used to visualize activated microglia and macrophages [CD68 (ED1)], astrocytes [glial fibrillary acidic protein (GFAP)], and neuronal nuclei (NeuN) are summarized in Table 1. All stained sections were also counterstained using 4′,6-diamidino-2-phenylindole (DAPI), which labels all cell nuclei. The tissue sections were hydrated and rinsed three times using PBS and as blocking solution, 5 % normal goat serum in 0.25 % Triton X-100 (Fluka/Sigma-Aldrich, Switzerland) in PBS, was used. Following incubation with blocking solution (1 h), the first series of sections was stained with ED1 and GFAP. The second series was stained with NeuN and additionally co-stained with GFAP in order to visualize the scar. The sections were incubated with primary antibodies (in blocking solution) at room temperature (RT) overnight. The following day, sections were rinsed in PBS (three times) and incubated with DAPI, goat anti-mouse IgG Alexa 488 and goat anti-rabbit IgG Alexa 594 (in blocking solution), in light sealed chambers, for 2 h at RT (Table 1). Subsequently, sections were rinsed three times with PBS and coverslipped using PVA-DABCO (polyvinyl alcohol, Fluka/Sigma-Aldrich, Switzerland). For sections stained with NeuN (second series), an antigen retrieval protocol with a 10 mM sodium citrate buffer (0.05 % Tween 20, pH6) was performed, as previously described in Gällentoft et al. [25].

The cervical lymph nodes were sectioned and labeled with ED1 and DAPI according to the same protocol.

Image acquisition and analysis

A DS-Ri1 digital camera (Nikon, Japan) mounted on a Nikon eclipse 80i microscope (Nikon, Japan) with a 10× objective was used for image acquisition. The sections were screened for the scar using ED1- and GFAP-positive

Table 1 List of primary antibodies, secondary antibodies and nucleic acid stain used in study

Name	Characteristics	Host	Working dilution	Source
ED1 (CD68)	Activated microglia/macrophages	Mouse	1:250	Cat. Nr. MCA341R, AbD Serotec, UK
GFAP	Glial fibrillary acidic protein	Rabbit	1:5000	Cat. Nr. Z0334, Dako, Denmark
NeuN	Neuronal nuclei, neuronal marker	Mouse	1:100	Cat. Nr. MAB377, Millipore, USA
Alexa Fluor 594	Goat anti-rabbit	Goat	1:500	Cat. Nr. A11005, Invitrogen, USA
Alexa Fluor 488	Goat anti-mouse	Goat	1:500	Cat. Nr. A11001, Invitrogen, USA
DAPI	Nucleic acid stain (4′,6-diamidino-2-phenylindole)	–	1:1000	Cat. Nr. D3571, Invitrogen, USA

Gällentoft *et al. J Nanobiotechnol* (2016) 14:64

Page 4 of 11

area. Where the scar was seen at its maximum, a photograph was taken of the fluorescence of the ED1- and GFAP-positive cells and cell nuclei (DAPI). These images were used for quantification of ED1, GFAP and DAPI. The adjacent brain sections in the second series were stained with the primary antibodies against NeuN and GFAP. These images were used for quantification of NeuN. A photograph of the fluorescence of GFAP-positive cells, NeuN-positive cells and cell nuclei (DAPI), was captured in the second series. The NIS-Elements 3.1 software (Nikon, Japan) was used for image capture and analysis. The quantification analysis was performed according to a previously described method [23, 25]. In short, a rectangular shaped region of interest (ROI; total ROI area 300 × 800 μm) was centred on the injection tract to evaluate the tissue response. This area was divided into an inner ROI (100 × 800 μm) and an outer ROI (200 × 800 μm). The inner ROI was chosen to quantify the area 0–50 μm from the injection tract and the outer ROI to quantify the area 50–150 μm from the injection tract. The rationale to differentiate between these two regions is that neuronal activity can be recorded up to about 50 μm from an electrode [27]. The outer ROI measures the possible widespread tissue response radiating from the injection scar. The quantifications were carried out by measuring the proportion of immunoreactive area (for ED1 and GFAP) or by counting the number of cells (for NeuN and DAPI) within the total screened area, i.e. inner or outer ROI [23, 25]. For ED1 and GFAP, intensity thresholds were set for each individual image and for each marker at a fixed multiplier of the mean background intensity. This was done in order to ensure that no unspecific staining was included in the area assigned as ED1 or GFAP-positive. Only the fraction of the area in the ROI above this set threshold was quantified. Intensity thresholds were set at 5.5 times the background intensity for ED1 immunofluorescence and at 4.5 times for GFAP immunofluorescence. Neuronal nuclei density was quantified manually by counting the number of NeuN-positive cells (with a DAPI-positive nucleus) and cell nuclei density were quantified by counting DAPI-positive nuclei (above ø 3 μm) within the ROIs.

In order to examine the presence (or absence) of nanowires in the tissue, we used confocal imaging. Confocal images of the scar were captured using a laser scanning confocal microscope (Zeiss LSM 510, Germany) with a 63× oil-immersion objective (N.A. 1.4) and Zen software (Zeiss, Germany). Laser-reflection mode was used to visualize the nanowires within the sections. Image J was used for processing of the confocal images.

The cervical lymph nodes were scanned for presence of nanowires or residues of nanowires using confocal microscopy (scattered laser light mode).

Statistical analyses

SiOx-coated GaP nanowire injections, n = 14, were compared to HfOx-coated GaP nanowire injections, n = 11 (from a previous study [25]).

Mann–Whitney test was used for comparison of the two groups, P values <0.05 (*) were considered significant. Values within graphs are presented as median values with indication of the 25 and 75 percentiles and minimum and maximum values (boxplot). GraphPad Prism 6.0d software (GraphPad Software Inc., USA) was used to perform all analyses in the study.

The dataset supporting the conclusions of this article is included within the articles additional file (see Additional file 1).

Results

To determine the impact of degradable vs. biostable nanowire exposure on the brain tissue response, we injected 2 μm long SiOx-coated GaP nanowires into rat striatum. This was compared to the tissue response after injection of HfOx-coated 2 μm GaP nanowires. The different immunohistochemical markers were quantified in an inner and an outer ROI surrounding the injection tract, 1 year post nanowire injection.
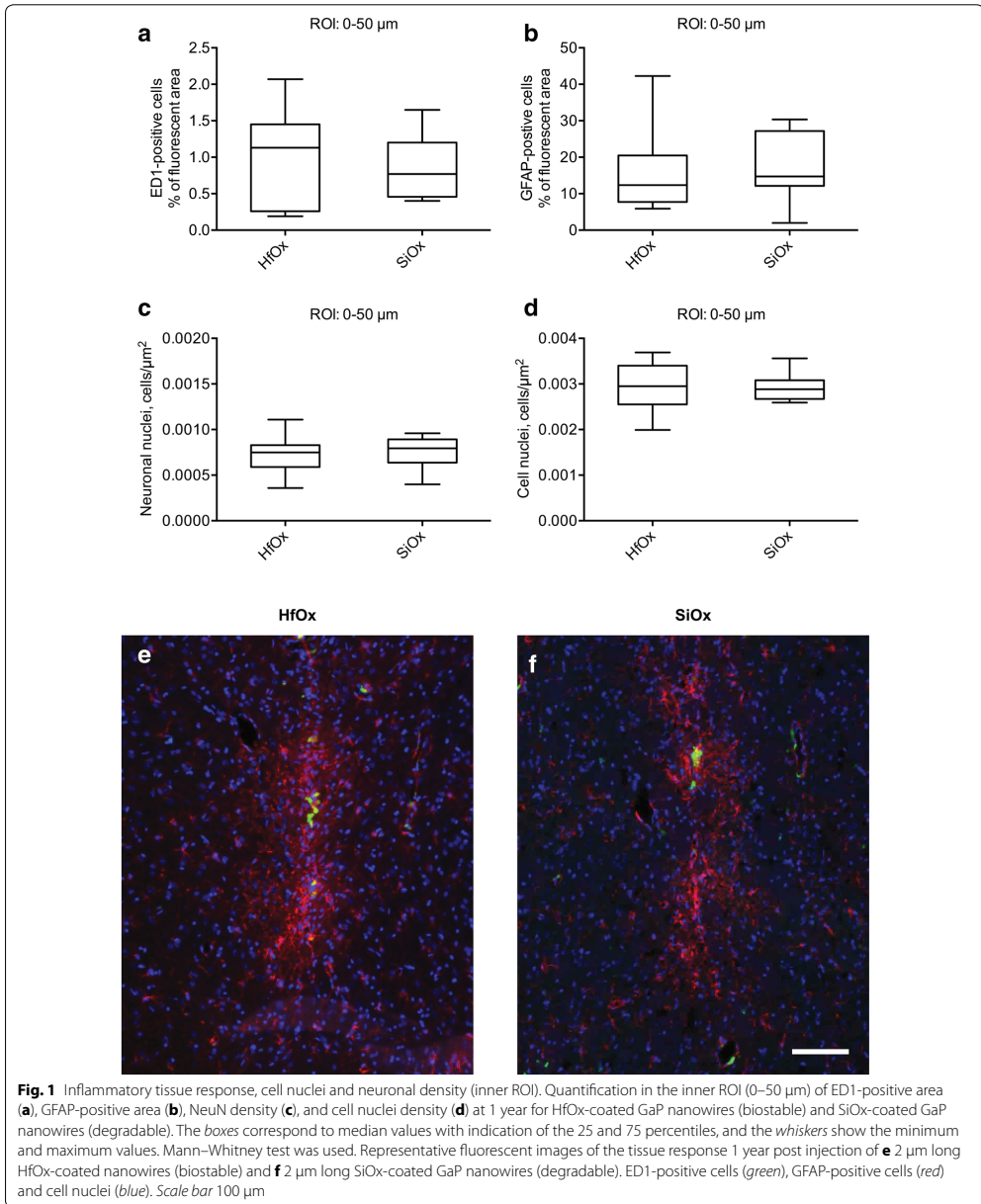
Brain tissue response towards degradable vs. biostable nanowires after 1 year (inner ROI)

One-year post injection no significant differences were found for any of the markers examined, when comparing the inner ROI (0–50 μm), in the two experimental groups. Boxplot graphs of the quantification in the inner ROI (a–d) and representative immunofluorescent images (e–f) are shown in Fig. 1.

For ED1, the median percentage of fluorescent area around the injection track of the SiOx-coated nanowires was 0.77 % (25 and 75 percentiles were 0.46 and 1.2 %, respectively), and 1.1 % (25 and 75 percentiles were 0.26 and 1.5 %, respectively) for the HfOx-coated nanowires (Fig. 1a).

The median percentage of GFAP-fluorescent brain area for animals injected with SiOx-coated nanowires was 15 % (25 and 75 percentiles were 12 and 27 %, respectively), and 12 % (25 and 75 percentiles were 7.7 and 20 %, respectively) for animals injected with HfOx-coated nanowires (Fig. 1b).

The median neuronal nuclei density, i.e. the number of neuronal nuclei (NeuN) per unit area in the inner ROI, was 8.0×10^{-4} μm^{-2} (25 and 75 percentiles were 6.4×10^{-4} and 8.9×10^{-4} μm^{-2}, respectively) for SiOx-coated nanowires and 7.5×10^{-4} μm^{-2} (25 and 75 percentiles were 5.9×10^{-4} and 8.3×10^{-4} μm^{-2}, respectively) for HfOx-coated nanowires (Fig. 1c).

Gällentoft *et al. J Nanobiotechnol* (2016) 14:64

Page 5 of 11

Fig. 1 Inflammatory tissue response, cell nuclei and neuronal density (inner ROI). Quantification in the inner ROI (0–50 µm) of ED1-positive area (**a**), GFAP-positive area (**b**), NeuN density (**c**), and cell nuclei density (**d**) at 1 year for HfOx-coated GaP nanowires (biostable) and SiOx-coated GaP nanowires (degradable). The *boxes* correspond to median values with indication of the 25 and 75 percentiles, and the *whiskers* show the minimum and maximum values. Mann–Whitney test was used. Representative fluorescent images of the tissue response 1 year post injection of **e** 2 µm long HfOx-coated nanowires (biostable) and **f** 2 µm long SiOx-coated GaP nanowires (degradable). ED1-positive cells (*green*), GFAP-positive cells (*red*) and cell nuclei (*blue*). *Scale bar* 100 µm

Gällentoft *et al. J Nanobiotechnol (2016) 14:64*

Page 6 of 11

The total cell nuclei density (DAPI), i.e. the number of cell nuclei per unit area in the inner ROI was $2.9 \times 10^{-3} \ \mu m^{-2}$ (25 and 75 percentiles were 2.7×10^{-3} and $3.1 \times 10^{-3} \ \mu m^{-2}$, respectively) for SiOx-coated nanowires and $3.0 \times 10^{-3} \ \mu m^{-2}$ (25 and 75 percentiles were 2.6×10^{-3} and 3.4×10^{-3}, respectively) for HfOx-coated nanowires (Fig. 1d).

Tissue response towards degradable vs. biostable nanowires at 1 year (outer ROI)

One year after injection no significant differences were found, for any of the markers used, when comparing the outer ROIs (50–150 μm) of the two experimental groups. Boxplot graphs of the quantification in the outer ROI (a–d) and representative immunofluorescent images (e–f) are shown in Fig. 2.

For ED1 the median percentage of fluorescent area, in the outer ROI, was 0.069 % (25 and 75 percentiles were 0.022 and 0.11 %, respectively) for SiOx-coated nanowires and 0.098 (25 and 75 percentiles were 0.058 and 0.12 %, respectively) for HfOx-coated nanowires (Fig. 2a).

The median percentage of GFAP-fluorescent area was 3.4 % (25 and 75 percentiles were 2.4 and 4.9 %, respectively) for SiOx-coated nanowires and 3.9 % (25 and 75 percentiles were 1.2 and 5.9 %, respectively) for HfOx-coated nanowires (Fig. 2b).

The median neuronal nuclei density (NeuN) in the outer ROI, i.e. the number of neuronal nuclei per unit area was $1.3 \times 10^{-3} \ \mu m^{-2}$ (25 and 75 percentiles were 1.2×10^{-3} and $1.4 \times 10^{-3} \ \mu m^{-2}$, respectively) for SiOx-coated nanowires and $1.3 \times 10^{-3} \ \mu m^{-2}$ (25 and 75 percentiles were 1.1×10^{-3} and $1.5 \times 10^{-3} \ \mu m^{-2}$, respectively) for HfOx-coated nanowires (Fig. 2c).

The median nuclei density (DAPI) in the outer ROI, i.e. the number of cell nuclei per unit area, was $2.7 \times 10^{-3} \ \mu m^{-2}$ (25 and 75 percentiles were 2.5×10^{-3} and $2.8 \times 10^{-3} \ \mu m^{-2}$, respectively) for SiOx-coated nanowires, and $2.7 \times 10^{-3} \ \mu m^{-2}$ (25 and 75 percentiles were 2.2×10^{-3} and $3.1 \times 10^{-3} \ \mu m^{-2}$, respectively) for HfOx-coated nanowires (Fig. 2d).

Confocal examination of the tissue response towards SiOx-coated (degradable) vs. HfOx-coated (biostable) nanowires at 1 year

Using confocal microscopy (scattered laser light), we found that residual nanowire material from the SiOx-coated GaP nanowires (and occasionally apparently intact nanowires) as well as intact HfOx-coated GaP nanowires engulfed by ED1-positive cells persisted in the tissue (Fig. 3). We could not detect any nanowires or nanowire residues in any other cell types investigated (neuronal cells or astrocytes).
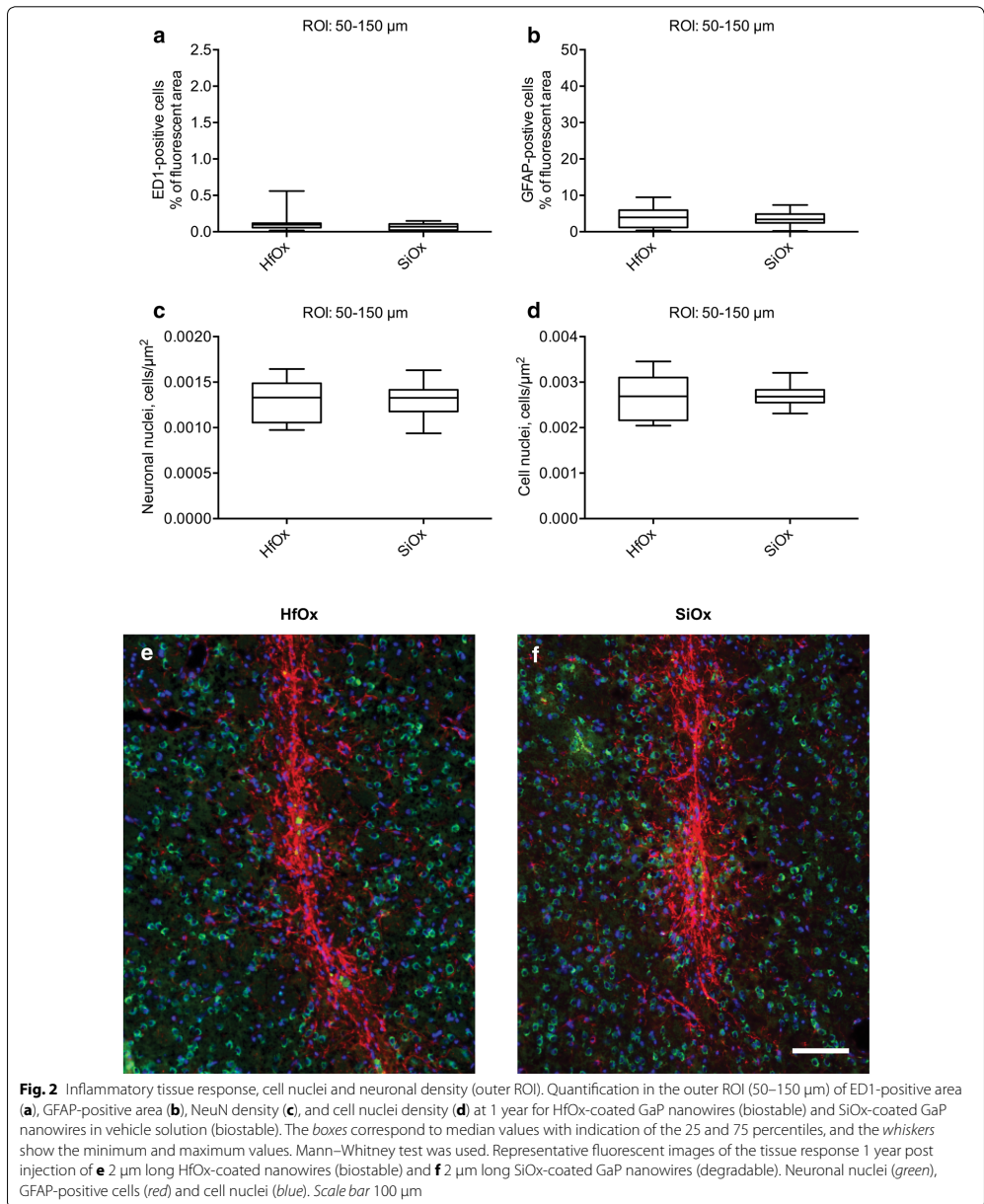
Intact HfOx-coated nanowires were found in ED1-positive cells, both in larger cell aggregates as well as in smaller ED1-positive cells (ø 5–10 μm) (Fig. 3a–e). For the degradable SiOx-coated nanowires (Fig. 3f–j), residues from nanowires were also detected inside ED1-positive cells. However, these residues were primarily seen in aggregated hypertrophic ED1-positive cells (ø approximately ≥15 μm), possibly macrophages/microglial cells that have fused to form multinucleated giant cells. SiOx-coated nanowires with an apparently intact shape were also found in the tissue, although, to a lesser extent, and primarily in single, smaller ED1-positive cells (ø 5–10 μm). These images also suggest that less material remains at or in the vicinity of the injection site for the group receiving degradable SiOx-coated GaP nanowires compared to HfOx-coated nanowires (Fig. 3a–j). Figure 4 shows merged close up laser scanning confocal microscopy images of ED1-positive cells containing intact HfOx-coated nanowires (Fig. 4a) or residues from degraded SiOx-coated nanowires (Fig. 4b). The nanowires are visualized in white inside microglia/macrophages using scattered laser light mode.

No nanowires or residues of nanowires were found in any of the cervical lymph nodes investigated.

Discussion

In this nanosafety study, we evaluated for the first time the long-term (corresponding to half the life time of the animal) impact of degradable nanowires on rat brain tissue and compared to that of non-degradable nanowires. That both the core and the coating of the SiOx-coated GaP nanowires are degraded into fragments were confirmed using confocal microscopy images (Figs. 3, 4). Despite the difference in biostability between SiOx and HfOx coated GaP nanowires, the tissue response and neuronal density were not significantly different. Moreover, both residues from degradable nanowires and intact biostable nanowires remain engulfed in the microglia/macrophages in the brain tissue 1 year post injection, indicating that clearance of nanoparticles from the brain is a very slow process.

The core material of the nanowires used in this study is GaP. GaP is a semiconductor and like many semiconductors, GaP has been shown to be susceptible to corrosion and degradation, a process that leads to a release of Ga ions [28]. We have previously evaluated the in vivo soft tissue inflammatory response after implantation of GaP discs into the abdominal wall of rats [29]. In that study an increase of ED1-positive cells after GaP disc implantation was found both in the reactive capsule and at the disc/tissue interface, possibly reflecting an increased local concentration of toxic Ga ions. In the same study, we also found elevated levels of Ga accumulated in blood,
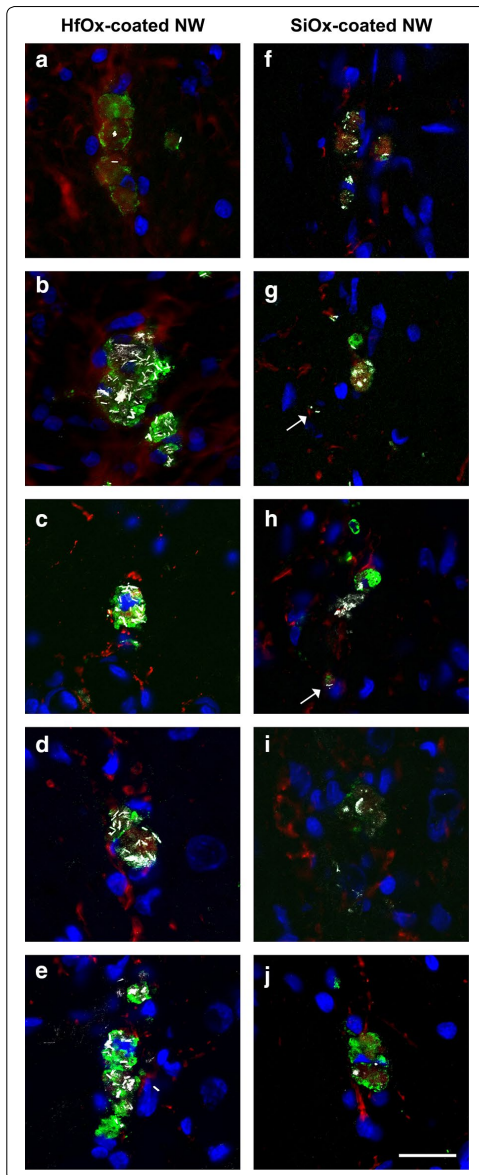
Gällentoft *et al. J Nanobiotechnol* (2016) 14:64

Page 7 of 11

Fig. 2 Inflammatory tissue response, cell nuclei and neuronal density (outer ROI). Quantification in the outer ROI (50–150 µm) of ED1-positive area (**a**), GFAP-positive area (**b**), NeuN density (**c**), and cell nuclei density (**d**) at 1 year for HfOx-coated GaP nanowires (biostable) and SiOx-coated GaP nanowires in vehicle solution (biostable). The *boxes* correspond to median values with indication of the 25 and 75 percentiles, and the *whiskers* show the minimum and maximum values. Mann–Whitney test was used. Representative fluorescent images of the tissue response 1 year post injection of **e** 2 µm long HfOx-coated nanowires (biostable) and **f** 2 µm long SiOx-coated GaP nanowires (degradable). Neuronal nuclei (*green*), GFAP-positive cells (*red*) and cell nuclei (*blue*). *Scale bar* 100 µm

Gällentoft *et al. J Nanobiotechnol (2016) 14:64*

Page 8 of 11

HfOx-coated NW   **SiOx-coated NW**

Fig. 3 Confocal images 1 year post nanowire injection. Representative laser scanning confocal microscopy images of the scar area after injection of 2 µm long HfOx-coated (**a–e**) and SiOx-coated GaP (**f–j**) nanowires 1 year post injection. The intact HfOx-coated and fragmented SiOx-coated GaP nanowires are visualized in *white* using scattered laser light mode. The images demonstrate the difference in nanowire cell load and degradability of the two types of nanowires studied. Note also the few rod-shaped SiOx-coated nanowires found in single, small ED1-positive cells (*arrows*). ED1-positive cells (*green*), GFAP-positive cells (*red*), cell nuclei (*blue*) and nanowires (*white, scattered laser light*). *Scale bar* 20 µm

the inflammatory in vivo milieu both inside and outside of activated monocytes/microglia) at 37 °C [29]. These results have been confirmed by Richards et al. [28] using GaP wafers. Taken together, these results demonstrate that the GaP core of the nanowires used in this study degrades both in vitro and in vivo.

In another study we could not detect any sub-acute or neurotoxic effect for the degradable GaP nanowires in the brain 12 weeks after nanowire injection [23]. Furthermore, no gallium was detected in other tissues investigated (blood, kidney and liver) using inductively coupled plasma sector field mass spectrometry (ICP-SFMS). This raised the question whether a possible continuous release of gallium from the nanowires locally in the brain could result in neurotoxicity when the exposure spans over a longer time period. Notably, in the present long-term study, we found no difference in the inflammatory tissue response (i.e. in ED1- or GFAP-positive cell area), in total cell nuclei density or neuronal nuclei density between the degradable and the biostable nanowire group 1 year post injection. Furthermore, we have previously shown that the brain tissue response seen 1 year after an injection of short biostable GaP nanowires is comparable to the brain tissue response seen after vehicle (HBSS only) injection [25]. Taken together, the degradable material does not result in any detectable neurotoxicity 1 year post injection. Note, however, that the amount of Ga introduced in the brain, in our degradable nanowire safety studies, are too low for measuring the amount of released Ga in the brain tissue using spectrographic methods (ICP-SFMS), as in Linsmeier et al. [29].

Feliu and colleagues [30], discuss if a biological environment may impose hostile conditions to nanoparticles, and addresses the question whether inorganic nanoparticles can be designed to be degradable in a controlled manner followed by clearance from the body via renal excretion. We have previously shown that GaP nanowires coated with 20 nm of SiOx were partially degraded after 6 and 12 weeks and that residues were found engulfed by microglia [23]. Furthermore, Hwang et al. [31], demonstrated that silicon-based electronics could be dissolved

brain, liver and kidneys 12 weeks post implantation, confirming loss of Ga from the implanted GaP discs [29]. GaP is also dissolving in pure physiological saline as well as in hydrogen peroxide (H_2O_2, 0.1, 1, 10 %) (to mimic

Gällentoft *et al. J Nanobiotechnol* (2016) 14:64
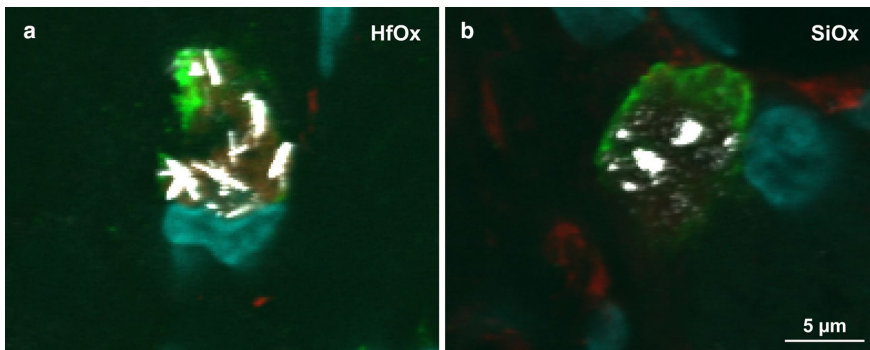
Page 9 of 11

Fig. 4 Close-up confocal images. Merged close-up of laser scanning confocal microscopy images showing ED1-positive cells in the scar area after injection of 2 μm long HfOx-coated (**a**) and SiOx-coated GaP (**b**) nanowires 1 year post injection. The images show internalization of intact HfOx-coated and degraded SiOx-coated GaP nanowires in microglia/macrophages. ED1-positive cells (*green*), GFAP-positive cells (*red*), cell nuclei (*blue*) and nanowires (*white, scattered laser light*). *Scale bar* 5 μm

under physiological conditions. These material dissolving properties are further demonstrated by Peled et al. [32], who reported a dissolution rate of ca. 2.15 nm/day for bare SiOx nanowires (20 nm in diameter) when exposed to PBS (37 °C) leading to non-continuous, segmented, nanowire structures after approximately 7–10 days of exposure. Similar dissolution rates was presented by Zhou et al. [33], who showed that the SiOx nanowires (30 nm in diameter) exhibited dissolution after about 10 days when exposed to PBS or Neurobasal neuron cell culture media (ThermoFisher Scientific, USA) which is a closer analog (than PBS) to an in vivo milieu. These studies further confirm that the GaP nanowire core as well as the SiOx-coating degrades and fragmentizes over time, thus, it might be expected that the SiOx-coated GaP nanowires would be completely dissolved in vivo after 1 year. We therefore hypothesized that the nanowire residues would be fully dissolved and cleared from the brain tissue after 1 year. However, the present data shows that nanowire residues and occasionally intact nanowires persist in the brain, even after 1 year, suggesting that nanoparticle clearance from the brain, if it is taking place, is a very slow process. Indeed, we were not able to detect any nanowires or nanowire residue in the cervical lymph nodes, which is a known destination for emigrating monocytes [34]. This suggests that there is a very small or non-existing migration of microglia/monocytes loaded with degraded and intact nanowires to these lymph nodes, supporting the idea that nanoparticles in the brain might be eliminated in an extremely slow manner.

Our results could be compared to previous reports showing that nanoparticles can accumulate in the brain. For instance, Lee et al. [35], found that small colloidal silver (10 and 25 nm) nanoparticles remain in the brain tissue 4 months after oral delivery. Furthermore, van der Zande et al. [36], found that polyvinylpyrrolidone-coated silver nanoparticles were not cleared from the brain, 84 days post-oral delivery. Kreyling et al. [37], injected radiolabeled polymer-coated gold nanoparticles in the tail vein of rats and were able to measure radioactivity from both the core and shell in the brain already after 1 h. This might suggest that certain nanoparticles can pass the blood brain barrier into the brain and accumulate in the brain since the elimination of the nanoparticles appears to be a more complex process.

When using confocal microscopy to compare activated microglial cells in the injection tract, we found a clear difference in microglial cell load comparing the two nanowire groups (Fig. 3). This suggests that some of the SiOx-coated material have indeed been cleared from the injection tract or that the residue from the nanowires are degraded into very fine fragments, which might not be visualized using confocal microscopy, since smaller debris scatter the light to a lesser degree. While there is an apparent difference in microglia load, there is as mentioned above, no significant difference in the proportion of ED1-positive cell area when comparing the degradable and biostable nanowire groups. It may be speculated that degraded fragments or particles, due to their larger surface area as compared to biostable nanowires, provided an about equal effective stimulus to the microglia cells as that of biostable nanowires.

Gällentoft *et al. J Nanobiotechnol* (2016) 14:64

Page 10 of 11

The degradable nanowires or residues from the degradable nanowires were found only engulfed by ED1-positive cells and were not found inside neurons or astrocytes. Interestingly, we found two phenotypes of activated ED1-positive microglia cells. One phenotype was the hypertrophic ED1-positive cells (ø approximately ≥15 μm) that contained a load of residues from the degradable nanowires or of intact biostable nanowires. These hypertrophic cells were most often found in cell aggregations, possibly multinucleated giant cells. Occasionally, intact biodegradable nanowires were detected in activated single, smaller sized ED1-positive cells (ø 5–10 μm). It is possible, that the presence of nanowires in the brain tissue can give rise to formation of multinucleated giant cells. These are highly activated cells, which produce large amounts of reactive oxygen species [38]. It might then be hypothesized that some of the ED1-positive cells, which engulf nanowires, fuse to become giant cells, which then might accelerate the breakdown of the degradable nanowires into fragments/residues. Hence, the finding that the SiOx-coated nanowires in the single, smaller ED1-positive cells appear to contain more intact nanowires as compared to the large ED1-positive cells or the aggregates of ED1-positive cells is consistent with this hypothesis.

In conclusion, we found engulfed intact nanowires and nanowire residues inside ED1-positive cells only. No obvious bio-safety issues or neurotoxicity were observed after injection of degradable 2 μm long GaP nanowires into rat striatum. Degradable nanowires with apparently intact shape were rarely found in the brain. When degraded, both the coating and the core of the degradable nanowires were fragmented and the remnants were not cleared from the brain even 1 year post nanowire injection. We observed no advantage or disadvantage of using degradable nanowires as compared to biostable nanowires in this long-term nanosafety study. It is important to mention that we can not exclude that other types of degradable materials could offer an advantage over biostable nanobiomaterials in other experimental setups. However, we found that dissolution and removal of inorganic material from the brain are very slow processes; these are very interesting findings which prompt for further studies.

Additional file

Additional file 1. Excel-file with raw data.

Authors' contributions
All authors (LG, LMEP, ND, JS, CNP, CEL) made substantial contributions to conception, planning and design, interpretation of data and revising the manuscript critically for important intellectual content. LG and CEL carried out all experiments, analyzed all data and wrote the manuscript. CNP manufactured the nanowires and carried out the confocal microscopy. All authors read and approved the final manuscript.

Author details
[1] Department of Experimental Medical Science, Medical Faculty, Neuronano Research Center (NRC), Lund University, Scheelevägen 2, 223 81 Lund, Sweden. [2] Division of Solid State Physics/NanoLund, Lund University, P.O. Box 118, 221 00 Lund, Sweden.

References
1. Cellot G, Cilia E, Cipollone S, Rancic V, Sucapane A, Giordani S, et al. Carbon nanotubes might improve neuronal performance by favouring electrical shortcuts. Nat Nanotechnol. 2009;4(2):126–33. doi:10.1038/nnano.2008.374.
2. Hallstrom W, Martensson T, Prinz C, Gustavsson P, Montelius L, Samuelson L, et al. Gallium phosphide nanowires as a substrate for cultured neurons. Nano Lett. 2007;7(10):2960–5. doi:10.1021/nl070728e.
3. Keefer EW, Botterman BR, Romero MI, Rossi AF, Gross GW. Carbon nanotube coating improves neuronal recordings. Nat Nanotechnol. 2008;3(7):434–9. doi:10.1038/nnano.2008.174.
4. Persson J, Danielsen N, Wallman L. Porous silicon as a neural electrode material. J Biomater Sci Polymer Edn. 2007;18(10):1301–8. doi:10.1163/156856207782177846.
5. Rosengren A, Wallman L, Danielsen N, Laurell T, Bjursten LM. Tissue reactions evoked by porous and plane surfaces made out of silicon and titanium. IEEE Trans Biomed Eng. 2002;49(4):392–9. doi:10.1109/10.991167.
6. Robinson JT, Jorgolli M, Shalek AK, Yoon M-H, Gertner RS, Park H. Vertical nanowire electrode arrays as a scalable platform for intracellular interfacing to neuronal circuits. Nat Nanotechnol. 2012;7(3):180–4. doi:10.1038/nnano.2011.249.
7. Timko BP, Cohen-Karni T, Qing Q, Tian B, Lieber CM. Design and implementation of functional nanoelectronic interfaces with biomolecules, cells, and tissue using nanowire device arrays. IEEE Trans Nanotechnol. 2010;9(3):269–80. doi:10.1109/TNANO.2009.2031807.
8. Kohler P, Wolff A, Ejserholm F, Wallman L, Schouenborg J, Linsmeier CE. Influence of probe flexibility and gelatin embedding on neuronal density and glial responses to brain implants. PLoS ONE. 2015;10(3):e0119340. doi:10.1371/journal.pone.0119340.
9. Lind G, Linsmeier CE, Schouenborg J. The density differences between tissue and neural probes is a key factor for glial scarring. Sci Rep. 2013;3:2942. doi:10.1038/srep02942.
10. Thelin J, Jorntell H, Psouni E, Garwicz M, Schouenborg J, Danielsen N, et al. Implant size and fixation mode strongly influence tissue reactions in the CNS. PLoS ONE. 2011;6(1):e16267. doi:10.1371/journal.pone.0016267.
11. Elnathan R, Kwiat M, Patolsky F, Voelcker NH. Engineering vertically aligned semiconductor nanowire arrays for applications in the life sciences. Nano Today. 2014;9(2):172–96. doi:10.1016/j.nanotod.2014.04.004.
12. Hochbaum AI, Fan R, He R, Yang P. Controlled growth of Si nanowire arrays for device integration. Nano Lett. 2005;5(3):457–60. doi:10.1021/nl047990x.

Gällentoft *et al. J Nanobiotechnol (2016) 14:64*

Page 11 of 11

13. Kim W, Ng JK, Kunitake ME, Conklin BR, Yang P. Interfacing silicon nanowires with mammalian cells. J Am Chem Soc. 2007;129(23):7228–9. doi:10.1021/ja071456k.

14. Patolsky F, Timko BP, Yu G, Fang Y, Greytak AB, Zheng G, et al. Detection, stimulation, and inhibition of neuronal signals with high-density nanowire transistor arrays. Science. 2006;313(5790):1100–4. doi:10.1126/science.1128640.

15. Suyatin DB, Wallman L, Thelin J, Prinz CN, Jörntell H, Samuelson L, et al. Nanowire-based electrode for acute in vivo neural recordings in the brain. PLoS ONE. 2013;8(2):e56673. doi:10.1371/journal.pone.0056673.

16. Prinz CN. Interactions between semiconductor nanowires and living cells. J Phys Condens Matter. 2015;27(23):233103. doi:10.1088/0953-8984/27/23/233103.

17. Shalek AK, Robinson JT, Karp ES, Lee JS, Ahn D-R, Yoon M-H, et al. Vertical silicon nanowires as a universal platform for delivering biomolecules into living cells. PNAS. 2010;107(5):1870–5. doi:10.1073/pnas.0909350107.

18. Xie C, Hanson L, Cui Y, Cui B. Vertical nanopillars for highly localized fluorescence imaging. PNAS. 2011;108(10):3894–9. doi:10.1073/pnas.1015589108.

19. Xie C, Hanson L, Xie W, Lin Z, Cui B, Cui Y. Noninvasive neuron pinning with nanopillar arrays. Nano Lett. 2010;10(10):4020–4. doi:10.1021/nl101950x.

20. Xie C, Lin Z, Hanson L, Cui Y, Cui B. Intracellular recording of action potentials by nanopillar electroporation. Nat Nanotechnol. 2012;7(3):185–90. doi:10.1038/nnano.2012.8.

21. Piret G, Perez M-T, Prinz CN. Neurite outgrowth and synaptophysin expression of postnatal CNS neurons on GaP nanowire arrays in long-term retinal cell culture. Biomaterials. 2013;34(4):875–87. doi:10.1016/j.biomaterials.2012.10.042.

22. Piret G, Perez MT, Prinz CN. Support of neuronal growth over glial growth and guidance of optic nerve axons by vertical nanowire arrays. ACS Appl Mater Interfaces. 2015;7(34):18944–8. doi:10.1021/acsami.5b03798.

23. Linsmeier CE, Prinz CN, Pettersson LME, Caroff P, Samuelson L, Schouenborg J, et al. Nanowire biocompatibility in the brain—looking for a needle in a 3D stack. Nano Lett. 2009;9(12):4184–90. doi:10.1021/nl902413x.

24. Helmus MN, Gibbons DF, Cebon D. Biocompatibility: meeting a key functional requirement of next-generation medical devices. Toxicol Pathol. 2008;36(1):70–80. doi:10.1177/0192623307310949.

25. Gällentoft L, Pettersson LME, Danielsen N, Schouenborg J, Prinz CN, Linsmeier CE. Size-dependent long-term tissue response to biostable nanowires in the brain. Biomaterials. 2015;42:172–83. doi:10.1016/j.biomaterials.2014.11.051.

26. Suyatin DB, Hallstram W, Samuelson L, Montelius L, Prinz CN, Kanje M. Gallium phosphide nanowire arrays and their possible application in cellular force investigations. J Vac Sci Technol B. 2009;27(6):3092–4. doi:10.1116/1.3264665.

27. Buzsaki G. Large-scale recording of neuronal ensembles. Nat Neurosci. 2004;7(5):446–51. doi:10.1038/nn1233.

28. Richards D, Luce P, Zemlyanov D, Ivanisevic A. Quantitative analysis of the functionalization of gallium phosphide with organic azides. Scanning. 2012;34(5):332–40. doi:10.1002/sca.21012.

29. Linsmeier CE, Wallman L, Faxius L, Schouenborg J, Bjursten LM, Danielsen N. Soft tissue reactions evoked by implanted gallium phosphide. Biomaterials. 2008;29(35):4598–604. doi:10.1016/j.biomaterials.2008.08.028.

30. Feliu N, Docter D, Heine M, del Pino P, Ashraf S, Kolosnjaj-Tabi J, et al. In vivo degeneration and the fate of inorganic nanoparticles. Chem Soc Rev. 2016;. doi:10.1039/c5cs00699f.

31. Hwang S-W, Tao H, Kim D-H, Cheng H, Song J-K, Rill E, et al. A physically transient form of silicon electronics. Science. 2012;337(6102):1640–4. doi:10.1126/science.1226325.

32. Peled A, Pevzner A, Peretz Soroka H, Patolsky F. Morphological and chemical stability of silicon nanostructures and their molecular overlayers under physiological conditions: towards long-term implantable nanoelectronic biosensors. J Nanobiotechnology. 2014;12:7. doi:10.1186/1477-3155-12-7.

33. Zhou W, Dai X, Fu TM, Xie C, Liu J, Lieber CM. Long term stability of nanowire nanoelectronics in physiological environments. Nano Lett. 2014;14(3):1614–9. doi:10.1021/nl500070h.

34. Kaminski M, Bechmann I, Pohland M, Kiwit J, Nitsch R, Glumm J. Migration of monocytes after intracerebral injection at entorhinal cortex lesion site. J Leukoc Biol. 2012;92(1):31–9. doi:10.1189/jlb.0511241.

35. Lee JH, Kim YS, Song KS, Ryu HR, Sung JH, Park JD, et al. Biopersistence of silver nanoparticles in tissues from Sprague–Dawley rats. Part Fibre Toxicol. 2013;10:36. doi:10.1186/1743-8977-10-36.

36. van der Zande M, Vandebriel RJ, Van Doren E, Kramer E, Rivera ZH, Serrano-Rojero CS, et al. Distribution, elimination, and toxicity of silver nanoparticles and silver ions in rats after 28-day oral exposure. ACS Nano. 2012;6(8):7427–42. doi:10.1021/nn302649p.

37. Kreyling WG, Abdelmonem AM, Ali Z, Alves F, Geiser M, Haberl N, et al. In vivo integrity of polymer-coated gold nanoparticles. Nat Nano. 2015;10(7):619–23. doi:10.1038/nnano.2015.111.

38. Tambuyzer BR, Ponsaerts P, Nouwen EJ. Microglia: gatekeepers of central nervous system immunology. J Leukoc Biol. 2009;85(3):352–70. doi:10.1189/jlb.0608385.

Paper III

Gelatin/glycerol coating to preserve mechanically compliant nanowire electrodes from damage during brain implantation

Jolanda A. Witteveen
Neuronano Research Center, Lund University, S-22100 Lund, Sweden

Dmitry B. Suyatin
Neuronano Research Center and Division of Solid State Physics, Lund University, S-22100 Lund, Sweden

Lina Gällentoft, Jens Schouenborg, and Nils Danielsen
Neuronano Research Center, Lund University, S-22100 Lund, Sweden

Christelle N. Prinz[a)]
Neuronano Research Center and Division of Solid State Physics, Lund University, S-22100 Lund, Sweden

Chronically implanted neural implants are of clinical importance. However, currently used electrodes have several drawbacks. Some weeks after implantation in the brain, a glial scar forms around the electrode, causing decreased electrode functionality. Nanostructures, and in particular nanowires, are good candidates to overcome these drawbacks and reduce glial scar formation. Using a mechanically compliant substrate with protruding nanowires could further decrease the glial scar formation by reducing the mechanical mismatch between the tissue and the electrode. However, flexible substrates require strengthening upon brain implantation. One solution consists of embedding the implant in a gelatin-based matrix, which is resorbable. In the case where nanostructures are present at the surface of the implant, it is crucial that the embedding matrix also preserves the nanostructures, which can be challenging considering the forces involved during the drying phase of gelatin. Here, the authors show that freestanding gallium phosphide nanowires coated with hafnium oxide (HfO_2), titanium (Ti), and gold (Au) were preserved in a gelatin-glycerol embedding matrix with subsequent implantation in 1% agar, which is a model for brain implantation. © *2010 American Vacuum Society.* [DOI: 10.1116/1.3498764]

I. INTRODUCTION

Chronically implanted neural electrodes are used as therapy for various neurological and neuropsychiatric disorders.[1–3] However, some of the currently used electrodes have several drawbacks, such as low spatial resolution, large dimensions, high rigidity, and poor biocompatibility. The latter three contribute to a foreign body response, which results in the activation and hypertrophy of microglia and astrocytes and in decreased neuron viability, eventually creating a glial scar around the electrodes. The glial scar "encapsulates" the implant and may thereby increase the distance between the electrode and the neurons, resulting in increased impedance, which contributes to the decreased functionality that most electrodes show over time.[4,5] The use of nanoscaled electrodes holds promise for overcoming most of these drawbacks. Nanostructures improve the electrode properties by increasing the surface/volume ratio. Their small size opens up the possibility to stimulate or record from a specific site of interest. Nanostructures are also believed to mimic the extracellular matrix in a more efficient way than flat surfaces, thereby reducing scar tissue formation.[6] This results in improved electrode electrical properties and spatial resolution as well as decreased tissue response.[5,7,8] Nanowires have been successfully interfaced with biological cells and tissue in recent years.[9–14] In previous works, we showed that neurons could thrive on gallium phosphide (GaP) nanowire substrates, even when penetrated by the nanowires.[10] We showed that neurons formed focal adhesions at the nanowire site.[15] We also showed that nanowires in suspension, implanted in the brain, show no subacute or chronic toxicity.[16] Our previous results show that nanowires are an excellent candidate for designing electrodes for brain implantation. The nanowire based electrodes under development in our laboratory will consist of freestanding GaP nanowires coated with HfO_2, Ti, and Au and will be standing on a very thin substrate (<30 μm). While fabricating such thin electrode shaft remains a challenge, we can already foresee that we will not be able to directly implant the electrodes due to their small buckling force. Indeed, upon implantation in the brain, the electrodes need to be unbendable to enable precise positioning in the brain. Several solutions to insert flexible electrodes have been reported; however, most are complicated and require either some special equipment, an incision in the brain prior to implantation, or some special electrodes.[4,17,18] Recently, we found that needles made of pure gelatin can be inserted into the brain and proposed that such gelatin needles can be used as a conduit for implanting highly flexible structures into soft tissue.[19–21] Gelatin is a mixture of proteins derived from collagen by means of hydrolysis.[22,23] It has a widespread usage, from the food industry and pharmaceutical industry to vascular and nerve regeneration grafts.[22,24–26]

Gelatin dissolves in aqueous solutions and forms a gel at temperatures below 34 °C[27] in a reversible process. Moreover, gelatin embedding has been shown to reduce tissue reactions to the implant, possibly due to the hemostatic properties of gelatin and also due to the fact that the surface of gelatin becomes very slippery when wetted, thus reducing the injury of the tissue during the implantation procedure.[19] Here, we propose a simple solution for embedding nanoelectrodes in a stiff, resorbable gelatin-based material to provide mechanical support during implantation and compliance once implanted. We show that using only gelatin destroyed the nanowires, while adding glycerol to the gelatin solution preserved most nanowires. The embedded nanowire substrates could sustain implantation in agar.

II. MATERIALS AND METHODS

A. Epitaxial growth of nanowires

Nanowires were grown using metal organic vapor phase epitaxy (AIX200/4, Aixtron AG) from gold nanoparticle seeds on (111)B GaP substrates, as described earlier.[10,28] The nanowires were 4–5 μm long and had a diameter of 60–80 nm, which was determined by the size of the gold seeds. The density of nanowire on the surface was $1/\mu m^2$. After the nanowire growth, the substrates were coated with a 50 nm layer of HfO_2 using atomic layer deposition (Savannah-100, Cambridge NanoTech) and were subsequently coated with 15 nm Ti and 75 nm Au in a magnetron sputtering system (Orion 5, AJA International), which resulted in additional 3–5 nm Ti and 20–25 nm Au layers on the nanowire walls. The final nanowire diameter was estimated to be between 200 and 240 nm.

B. Nanowire substrate embedment

Gelatin from porcine skin type A ($\sim$300 Bloom) (Sigma Aldrich) was dissolved in de-ionized water at a concentration of 50 mg/ml (5%) or 100 mg/ml (10%), heated up to 70 °C, and subsequently cooled down to 50 °C. When needed, glycerol was added to the 100 mg/ml gelatin solution at a concentration of 100/40 gelatin/glycerol (w/w) or 100/60 gelatin/glycerol (w/w) and left for 20 min at 50 °C. The electrodes were dip-coated in the gelatin or gelatin/glycerol solution and dried horizontally at room temperature overnight. When needed, the embedding matrix was removed from the nanowire substrates by soaking the substrates in water at 50 °C for 90 min.

C. Brain model insertion

A 1% agar solution was made and heated up to 80–90 °C for 15 min and was allowed to cool down at room temperature. The embedded nanowire substrates were inserted in the agar gel and immediately retracted using a micromanipulator (Kopf Instruments) at 25 μm/s. Agar gels are widely used models for mimicking the mechanical properties of the brain.
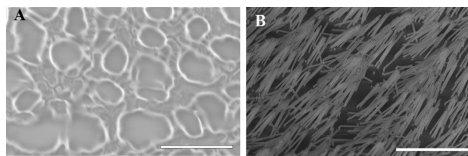

FIG. 1. SEM images of a nanowire substrate embedded in a 5% gelatin solution (A) before and (B) after gelatin removal. The nanowires are bent, broken, or agglomerated due to the forces generated during the gelatin drying step. Scale bars: 10 μm.

D. Analysis

Analysis was done using scanning electron microscopy (SEM) (microscope JSM 6400F, SEM Leo 1560, or FEI Nova NanoLab 600) at 10 or 20 kV, with stage tilted at 20° unless otherwise noted. Combined focused ion beam and SEM (FIB-SEM) (FEI Nova Nanolab 600) was used to mill and image cross-sections of the samples. Images were taken using the electron beam. Milling through the samples was performed, using the ion beam at a typical current of 7 nA on the gelatin surface onto which tungsten was deposited using the gas injection system.

The percentage of broken/bent nanowires was estimated by counting the number of nanowires, which had a horizontal projection of 1.5 μm or more on SEM images taken with no stage tilt. On a non-tilted stage, the nanowires that are not affected by the embedding/insertion process remain vertical and are pointlike on the images, while a 1.5 μm length corresponds to a bending of 20°. For each sample, a total area of 6645 μm^2 was imaged in the middle of the sample and the broken/bent nanowires were quantified using a cell counter plugin in the IMAGE J software.

III. RESULTS AND DISCUSSION

Figure 1 shows a nanowire substrate embedded in 5% gelatin (A) before and (B) after washing the gelatin away. The texture of the gelatin shows a spongy aspect. Figure 1(B) shows the nanowires after the gelatin removal. The nanowires are either bent, broken, or agglomerated with the same spongy pattern that was present in the gelatin layer. This is due to the internal forces during the drying process, caused by stress in the cross-links. A nanowire substrate was washed according to the gelatin removal process and the nanowires remained vertical, showing that the gelatin is responsible for the nanowire damage and not the washing step. Therefore, the internal forces in the gelatin need to be reduced in order to preserve the nanowires after embedding. There are various ways of altering the physical properties of gelatin, though a reproducible way is to add a plasticizer. Plasticizing the gelatin could reduce the internal forces, since it affects the amount of water present in the gel upon drying. One of the most used biocompatible plasticizers is glycerol.[29] Glycerol is thought to reduce interactions between the collagen chains, thereby increasing the gel flexibility and increasing the water content in the gel.[30] It is there-
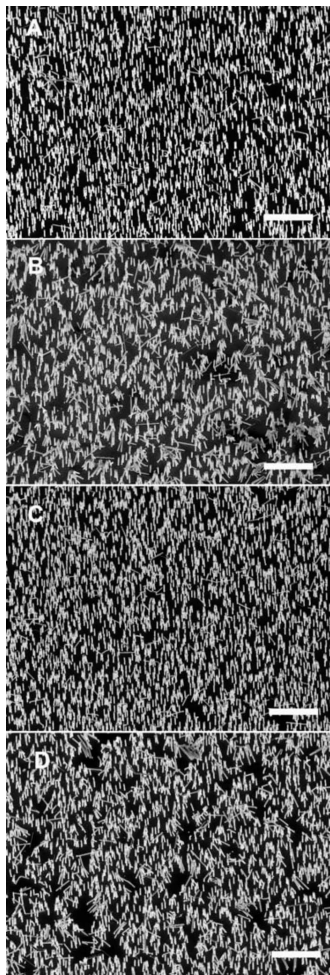
FIG. 2. SEM images of nanowires after gelatin/glycerol matrix removal: (A) control: nanowire substrate rinsed in water at 50 °C and dried, (B) nanowires embedded in a 100/40 gelatin/glycerol (w/w) gel, (C) nanowires embedded in 100/60 gelatin/glycerol, and (D) nanowires embedded in 100/60 gelatin/glycerol and inserted in 1% agar. Scale bars: 10 μm.

fore a matter of finding the correct proportion of gelatin/glycerol in order to have an embedding material soft enough to preserve the nanowires and stiff enough to be implanted in the brain. Figure 2 shows SEM images of nanowire substrates after the embedding matrix removal: (A) control (washed), (B) nanowire substrate embedded in 100/40 gelatin/glycerol, (C) nanowire substrate embedded in 100/60 gelatin/glycerol, and (D) nanowire substrate embedded in 100/60 gelatin/glycerol and inserted in agar. After embed-
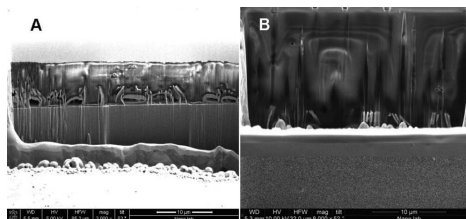
FIG. 3. SEM image of a cross-section of a nanowire substrate embedded in (A) 10% gelatin and (B) 100/60 gelatin/glycerol (w/w). The milling was done using FIB. The stage was tilted at 52°.

ding the nanowire electrodes in a 100/40 gelatin/glycerol (w/w) solution, 18% of the nanowires were bent or broken. Control surfaces showed 5% of broken/bent nanowires. Further increasing the concentration of glycerol to 100/60 gelatin/glycerol led to only 8.5% of the nanowire being broken/bent, which is acceptable. A 100/60 gelatin/glycerol embedded nanowire substrate was dipped in agar and showed 13% of broken/bent nanowires after gelatin/glycerol removal. Therefore, a 100/60 gelatin/glycerol solution seems to be appropriate for brain insertion, since the embedding process preserved 96% of the nanowires and 95% of the remaining nanowires were subsequently protected during the implantation in agar. This shows that the plasticized gelatin is flexible enough to preserve the nanowires and strong enough to protect them upon implantation.

Figure 3 shows a cross-section view of the nanowires embedded (A) in 10% gelatin and (B) in 100/60 gelatin/glycerol (w/w). Nanowires can be seen standing on the substrates. The layer of gelatin on top of the nanowires in (A) is 8 μm thick, while the layer of gelatin/glycerol in (B) is 20 μm thick. In Fig. 3(A), air bubbles can be seen trapped in the 10% gelatin layer, which is not the case for the gelatin/glycerol coated sample. Trapped air bubbles in the high viscosity 10% gelatin matrix could be an additional possible explanation for the higher rate of bent nanowires in 10% gelatin compared to 100/60 gelatin/glycerol.

IV. CONCLUSION

We showed that implanting mechanically compliant nanowire substrates embedded in a temporary protective and stiffening layer of gelatin/glycerol is feasible and would leave the nanowires intact. Ninety six percent of the nanowires could withstand coating with 100/60 gelatin/glycerol and 95% of those 96% survived subsequent insertion in agar, which models the mechanical properties of brain tissue. This method proved to protect the nanowire structures and provided sufficient strength for brain implantation. The fact that the matrix is resorbable will make it possible to have very flexible electrodes once implanted in the brain, and, if combined with the presence of nanowires on the implant, this could lead to future electrodes with unprecedented biocompatibility and endurance. This method can also be implemented in a wide range of applications, whenever a stiffen-

ing and protective matrix is required for inserting a nanofabricated structure in a biological body.

[1]K. L. Collins, E. M. Lehmann, and P. G. Patil, Neurobiol. Dis. **38**, 338 (2010).

[2]H. E. Ward, N. Hwynn, and M. S. Okun, Neurobiol. Dis. **38**, 346 (2010).

[3]L. R. Hochberg *et al.*, Nature (London) **442**, 164 (2006).

[4]D. B. Jaroch, M. P. Ward, E. Y. Chow, J. L. Rickus, and P. P. Irazoqui, J. Neurosci. Methods **183**, 213 (2009).

[5]V. S. Polikov, P. A. Tresco, and W. M. Reichert, J. Neurosci. Methods **148**, 1 (2005).

[6]J. L. McKenzie, M. C. Waid, R. Shi, and T. J. Webster, Biomaterials **25**, 1309 (2004).

[7]E. W. Keefer, B. R. Botterman, M. I. Romero, A. F. Rossi, and G. W. Gross, Nat. Nanotechnol. **3**, 434 (2008).

[8]N. A. Kotov *et al.*, Adv. Mater. **21**, 3970 (2009).

[9]W. Kim, J. K. Ng, M. E. Kunitake, B. R. Conklin, and P. Yang, J. Am. Chem. Soc. **129**, 7228 (2007).

[10]W. Hällström, T. Mårtensson, C. Prinz, P. Gustavsson, L. Montelius, L. Samuelson, and M. Kanje, Nano Lett. **7**, 2960 (2007).

[11]A. K. R. Shalek *et al.*, Proc. Natl. Acad. Sci. U.S.A. **107**, 1870 (2010).

[12]Q. Qing, S. K. Pal, B. Tian, X. Duan, B. P. Timko, T. Cohen-Karni, V. N. Murthy, and C. M. Lieber, Proc. Natl. Acad. Sci. U.S.A. **107**, 1882 (2010).

[13]W. Hällström, M. Lexholm, D. B. Suyatin, G. Hammarin, D. Hessman, L. Samuelson, L. Monteliust, M. Kanje, and C. N. Prinz, Nano Lett. **10**, 782 (2010).

[14]W. Hällström, C. N. Prinz, D. Suyatin, L. Samuelson, L. Montelius, and M. Kanje, Langmuir **25**, 4343 (2009).

[15]C. Prinz, W. Hällström, T. Mårtensson, L. Samuelson, L. Montelius, and M. Kanje, Nanotechnology **19**, 345101 (2008).

[16]C. E. Linsmeier, C. N. Prinz, L. M. E. Pettersson, P. Caroff, L. Samuelson, J. Schouenborg, L. Montelius, and N. Danielsen, Nano Lett. **9**, 4184 (2009).

[17]R. Das, D. Gandhi, S. Krishnan, L. Saggere, and P. J. Rousche, IEEE Trans. Biomed. Eng. **54**, 1089 (2007).

[18]P. J. Rousche, D. S. Pellinen, D. P. Pivin, Jr., J. C. Williams, R. J. Vetter, and D. R. Kirke, IEEE Trans. Biomed. Eng. **48**, 361 (2001).

[19]G. Lind, C. E. Linsmeier, J. Thelin, and J. Schouenborg, J. Neural Eng. 7, 046005 (2010).

[20]J. Schouenborg, Electrode array, WO2008091197.

[21]J. Schouenborg, Medical electrode, electrode bundle and electrode bundle array, WO2009075625.

[22]S. R. R. Singh, K. V. Venugopal, and R. Manikandan, Pharm. Technol. 36 (2002).

[23]I. Yakimets, N. Wellner, A. C. Smith, R. H. Wilson, I. Farhat, and J. Mitchell, Polymer **46**, 12577 (2005).

[24]I. Arvanitoyannis, E. Psomiadou, A. Nakayama, S. Aiba, and N. Yamamoto, Food Chem. Toxicol. **60**, 593 (1997).

[25]J. Y. Chang, T.-Y. Ho, H.-C. Lee, Y.-L. Lai, M.-C. Lu, C.-H. Yao, and Y.-S. Chen, Artif. Organs **33**, 1075 (2009).

[26]C. Lekakou, D. Lamprou, U. Vidyarthi, E. Karopoulou, and P. Zhdan, J. Biomed. Mater. Res., Part B: Appl. Biomater. **85B**, 461 (2008).

[27]J. A. Payne, A. V. McCormick, and L. F. Francis, J. Appl. Polym. Sci. **73**, 553 (1999).

[28]D. B. Suyatin, W. Hällström, L. Samuelson, L. Montelius, C. N. Prinz, and M. Kanje, J. Vac. Sci. Technol. B **27**, 3092 (2009).

[29]S. Rivero, M. A. García, and A. Pinotti, Innovative Food Sci. Emerging Technol. **11**, 369 (2010).

[30]P. Bergo and P. J. A. Sobral, Food Hydrocolloids **21**, 1285 (2007).

Paper IV

Multiple Implants Do Not Aggravate the Tissue Reaction in Rat Brain

Gustav Lind*, Lina Gällentoft, Nils Danielsen, Jens Schouenborg, Lina M. E. Pettersson

Department of Experimental Medical Sciences, Neuronano Research Center, Medical Faculty, Lund University, Lund, Sweden

Abstract

Chronically implanted microelectrodes are an invaluable tool for neuroscientific research, allowing long term recordings in awake and behaving animals. It is known that all such electrodes will evoke a tissue reaction affected by its' size, shape, surface structure, fixation mode and implantation method. However, the possible correlation between tissue reactions and the number of implanted electrodes is not clear. We implanted multiple wire bundles into the brain of rats and studied the correlation between the astrocytic and microglial reaction and the positioning of the electrode in relation to surrounding electrodes. We found that an electrode implanted in the middle of a row of implants is surrounded by a significantly smaller astrocytic scar than single ones. This possible interaction was only seen between implants within the same hemisphere, no interaction with the contralateral hemisphere was found. More importantly, we found no aggravation of tissue reactions as a result of a larger number of implants. These results highlight the possibility of implanting multiple electrodes without aggravating the glial scar surrounding each implant.

Introduction

Multielectrode arrays, such as chronically implanted electrodes for stimulation or recording within the central nervous system (CNS), show great promise as research tools and diagnostic and therapeutic devices in years to come [1,2,3]. To achieve this, multiple multielectrode arrays have to be functional inside the CNS for years or decades without causing significant damage to the surrounding tissue. However, all types of electrodes available today show deteriorating recording capabilities over time [4,5,6]. This is suggested to be, at least partly, due to the tissue reactions surrounding the electrodes that over time will increase the impedance of the electrodes. This may ultimately insulate the recording surfaces and thus prevent recording of electrical signals or forcing stimulation parameters to be altered [7,8,9,10,11]. The tissue reactions surrounding different types of neural implants have been extensively studied with regards to size [12,13], shape [10,14,15,16], surface structure and material [17,18,19,20], fixation mode [13,21] and implantation method [14,22]. However, to the best of our knowledge, interactions between the tissue reactions to multiple electrodes implanted in the brain have not been studied. This is a key question to be answered since the potential additive effect of multiple glial scars could affect both the quality of recordings from implanted electrodes and the validity of the neural signals recorded.

The aim of this study was to evaluate the effect of the number of implants on the glial scar, defined in this study as the accumulation of reactive astrocytes and activated microglia, surrounding each single implant. Two different aspects of this problem were investigated. First, we examined whether the tissue reaction to an electrode was affected by implantation of other electrodes in its close vicinity, i.e. if glial scars interact within a hemisphere. Second, we examined whether the tissue reactions to an electrode is affected by the presence of contralateral implants, i.e. if glial scars interact between hemispheres. We chose to focus on the astrocytic and microglial reactions, which are main components of the glial scar, and the most commonly investigated [4,10,12,13,15,20,21,23,24,25]. The astrocytic reaction is monitored by measuring immunoreactivity to GFAP, an intermediate filament protein expressed in all astrocytes but highly up regulated in reactive astrocytes in response to an injury. The astrocytes are also the constituent of the *glia limitans* layer surrounding implanted materials which delimit the normal neural tissue from the damaged tissue and implanted materials. To monitor the microglial reaction we measure immunoreactivity to ED1, a cellular surface protein expressed exclusively on cells of monocytic lineage, in the brain primarily microglial cells, when activated by an injury. These cells are mainly responsible for phagocytosis of damaged tissue and foreign material and are thus a good measure of the damage caused by an implant. In addition, activation of these glial components has been claimed to correlate with alterations in impedance of implanted electrodes [9,11].

After six weeks, the astrocytic scar surrounding the middle out of five implants was significantly smaller compared to the single contralateral implant, suggesting that an intrahemispheric interaction might be taking place, reducing the astrocytic response around the central implant. However, we did not find any evidence of interactions between hemispheres. Furthermore, we did not find any difference between microglial reactions in the different groups. Most importantly however, the large number of implants did not seem to aggravate the reaction to any of the

implants, indicating a possibility of implanting multiple electrodes at diverse locations in the brain.

Methods

Animals, Anaesthesia and Ethics Statement

All procedures in this study were approved in advance by the Malmö/Lund Animal Ethics Committee on Animal Experiments. Implantations were made in female Sprague-Dawley rats (n = 23) (Taconic, Denmark), weighing 200–250 g. Animal handling and anaesthetic procedures are described elsewhere [26]. In brief, animals were anaesthetized with intraperitoneal injections of fentanyl (0.3 mg/kg body weight) and Domitor vet (medetomidin hydrochloride, 0.3 mg/kg body weight). After surgery, the animals received subcutaneous injections of an antidote to the anaesthesia (Antisedan, atipamezole hydrochloride, 0.5 mg/kg body weight) as well as Temgesic (buprenorphine, 50 µg/kg body weight) to reduce postoperative pain.

Implants

The implants in this study were identical to the gelatine embedded wire bundles used in a previous study in our laboratory [25]. Implants consist of a wire bundle of 32 tungsten wires with a diameter of 7.5 µm and an insulation layer of 3 µm polyimide,moulded into a gelatine needle (gelatine type B, VWR BDH, Sweden) resulting in a final diameter of 300 µm. The gelatine is intended to give stability to the highly flexible wires while penetrating the meninges. It dissolves during, or soon after, implantation leaving only the wire bundle in place in the cortex. The wire bundle have an approximate diameter of 180 µm. Animals were kept for one or six weeks and were divided into the following experimental groups; 1) killed after one week, implanted with five wire bundles in the left hemisphere with 1 mm between each bundle, and one wire bundle in the right hemisphere (n = 6); 2) killed after one week, implanted with one wire bundle in the left hemisphere, and no implant in the right hemisphere (n = 6); 3) killed after six weeks, implanted with five wire bundles in the left hemisphere, with 1 mm between each bundle, and one wire bundle in the right hemisphere (n = 6); 4) killed after six weeks, implanted with one wire bundle in the left hemisphere, and no

Figure 1. Schematic overview of implant locations in the different study groups. Dorsal view of the cerebral cortex with implant locations indicated by black dots. The implant in the left hemisphere of Group 1 & 3 is referred to as the contralateral implant; the implants in the right hemisphere in group 1 & 3 are referred to as middle and outer implants respectively; the implant in the right hemisphere of group 2 & 4 is referred to as the solitary implant and has no contralateral counterpart. Distances between implants in the right hemisphere of group 1 & 3 are 1 mm. Unnamed implants are not analyzed.
doi:10.1371/journal.pone.0047509.g001

implants in the right hemisphere (n = 5). A schematic overview of the groups is presented in Figure 1.

Surgery and Implantation Procedure

The animal was attached to a stereotactic frame (KOPF instruments, USA) under anaesthesia prior to surgical procedures. Small craniotomies (1 mm^2) were made at the single bundle implantation site while one large craniotomy (6×1 mm) was made at the five bundle implantation site. The dura mater was incised and deflected. Implants were attached to a hydraulic micromanipulator (KOPF instruments, USA) using gelatine. Implantations were made one bundle at a time at a speed of 10 µm/s, to a depth of 2 mm. Once the target depth was reached, the gelatine attaching the implant to the micromanipulator was flushed with saline solution until dissolved, releasing the implant. This method is designed to be able to release the implants without moving them while inside the brain. The implants were left untethered without any attachment to the skull or each other. This ensures that the electrodes move along with the brain, and do not translate movements between the brain and the skull which is thought to be one of the major causes of chronic reactions to neural implants. The skin was closed using surgical clips and the animals were monitored during awakening.

Histology

The animals were killed by an i.p. overdose of pentobarbital and were transcardially perfused with 200 ml of ice-cold 0.1 M phosphate buffered saline (PBS) followed by 150 ml of ice-cold 4% paraformaldehyde in 0.1 M phosphate buffer, pH 7.4. The brains were dissected and immersed in 4% paraformaldehyde overnight. The brains were then cryoprotected in 25% sucrose until they were no longer able to float and were cryosectioned horizontally using a cryostat (Microm, Germany) in increments of 10 µm onto Super Frost ® plus slides (Menzel-Gläser, Germany). After blocking in goat serum to prevent unspecific binding, the sections were incubated with primary antibodies; rabbit anti-glial fibrillary acidic protein (GFAP, an astrocytic cytoskeleton protein; 1:5000, Cat. Nr. Z0334, Dako, Denmark) and mouse anti-CD68 (ED1, a marker for activated microglial cells, 1:250, Cat. Nr. MCA341R, AbD Serotec, UK) at room temperature overnight. The specificities of the antibodies have been tested elsewhere (GFAP by the manufacturer and ED1 by Bao et al. [27]) by Western Blot (two-dimensional quantitative immunoelectrophoresis or SDS-PAGE respectively). Both antibodies show a single precipitate with roughly the appropriate molecular weight when tested on brain or spinal cord extract, indicating good specificity for the targeted antigen. Thereafter, sections were rinsed three times in PBS followed by incubation in secondary antibodies; goat anti-rabbit Alexa594 (1:500, Invitrogen, USA) and goat anti-mouse Alexa488 (1:500, Invitrogen, USA) for 2 hours in the dark at room temperature. Sections were rinsed three times in PBS and coverslipped using PVA/DABCO (Fluka/Sigma-Aldrich, Switzerland).

Image Acquisition & Analysis

All histological images were obtained using a DS-2MV Digital camera (Nikon, Japan) mounted on a Nikon eclipse 80i microscope with a 10x objective. Image capture and analysis were performed using the NIS-Elements 3.1 software (Nikon Instruments). Images from the middle of the shaft of each bundle track, at an approximate depth of 1 mm below brain surface, were captured from the middle and outer bundles, their contralateral counterpart, as well as the solitary bundles (see Figure 1 for explanation). Regions of interest (ROIs) were set at 0–50 µm and
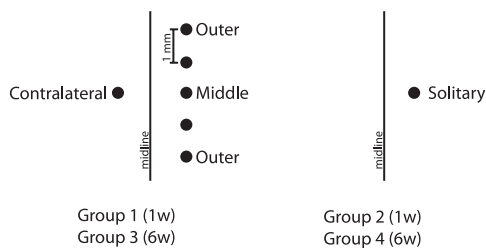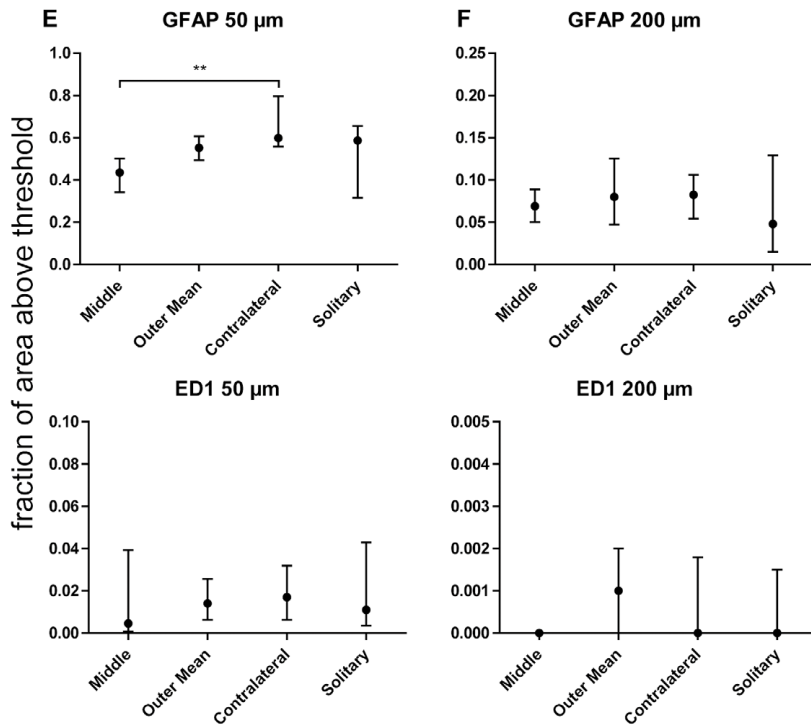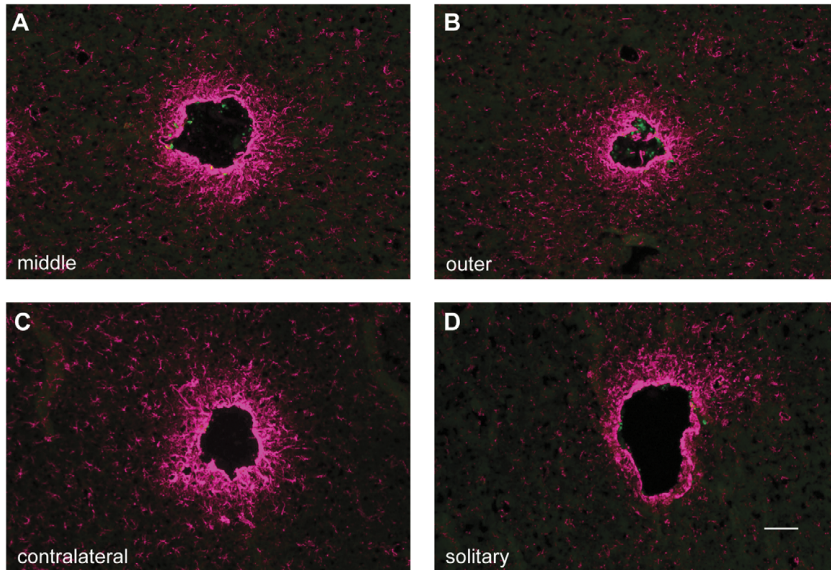
Figure showing panels A (middle), B (outer), C (contralateral), D (solitary), and graphs E (GFAP 50 μm), F (GFAP 200 μm), ED1 50 μm, and ED1 200 μm plotting fraction of area above threshold for Middle, Outer Mean, Contralateral, and Solitary.

50–200 μm distance from the rim of the artefact left by the wire bundles. The histological quantification method has previously been described in detail [13,25]. In brief, thresholds were set for each individual image and for each marker at a fixed multiplier of the mean background intensity. The fraction of the area in each ROI above this threshold was calculated. Intensity thresholds were set at six times the background intensity for GFAP immunofluorescence and at five times for ED1 immunofluorescence.

Statistical Analyses

Non-parametric statistics, the Kruskal-Wallis and the Dunn's post hoc test for selected pairs were used in this study. Comparisons were made between i) the middle implant and a mean of the two outer implants; ii) the middle implant and the contralateral implant; and iii) between the contralateral implant and the solitary implant (see figure 1 for explanation), for each ROI and time point. All values are presented as median values with indication of the interquartile range and p-values of <0.05 were considered significant. All analyses were performed using the GraphPad Prism 5.03 software (GraphPad Software Inc., USA).

Results

Interactions within a Hemisphere

To evaluate whether any interactions within a hemisphere were present we compared the tissue reactions towards the middle implant to that towards the contralateral implant and the outer implants (Figure 1). We found significantly less immunofluorescence for GFAP at the middle implant in the innermost ROI (0–50 μm) after six weeks when compared to the contralateral implant (Figure 2). This suggests that a large number of implants in one hemisphere do not aggravate the tissue reactions to each implant. Notably, the middle scar exhibited less GFAP staining than both the contralateral scar and the outer scars in every animal (in the inner ROI at the six week time point), even if the difference between the middle and outer scars was not statistically significant. Furthermore, there was a similar tendency after one week, where the contralateral implant exhibited higher GFAP levels than the middle implant in the inner ROI in all animals except one, and the outer implant exhibited higher levels than the middle implant in all animals (Figure 3). These differences were not statistically significant. No differences or tendencies to differences were seen between any of the groups when analysed with regards to ED1-staining (Figures 2, 3).

Interactions between Hemispheres

Potential interactions between hemispheres were examined by comparing tissue reactions to the contralateral implant to those of the solitary implant (Figure 1). No statistically significant differences were found between these groups, neither for astrocytic nor microglial reactions, and the median values were similar in all groups (Figures 2, 3). This indicates that the five implants in one hemisphere do not affect the astrocytic reactions to the contralateral implant.

Discussion

Concerns, regarding an adverse additive effect on tissue reactions after implantation of multiple electrodes into the brain, have been raised. This question is central to chronic electrophysiology since an escalating additive reaction could preclude the possibility of recording valid physiological signals from diverse brain areas. We wanted to address this issue and also investigate possible contralateral effects in response to implantation. Interestingly, our results indicate that glial reactions to chronic neural electrodes implanted in close vicinity of each other are not more severe than those to single electrodes. The significant difference seen between middle and contralateral implant in the six week group might even suggest that a larger number of implants slightly reduce the tissue reactions to each implant, but further studies would be needed to provide a definite answer to this. Most importantly, our findings indicate that it is possible to implant multiple electrode bundles without aggravating the glial scar surrounding each implant. This enables implantation of functional neural interfaces consisting of a number of electrodes implanted at different sites in the brain, which gives the opportunity to study how different remote brain areas interact with each other without the potential confounding factor of an increased glial scar.

The mechanism behind the decreased astrocytic scar formation around the central implant is not directly explored in this study, and can thus only be speculated on. It seems, however, that we have discovered an interesting feature of the development of reactive astrocytosis. The most intuitive reason for a difference in glial scar formation between two implants would be that there is a difference in the damage caused by these implants. In this study, the implants are identical, and the implantation procedures are identical, the only difference is the positioning of the electrodes. The only way we can envision that this would affect the damage caused by the electrodes is if the movements of the outer electrodes in relation to the brain are larger than of the middle ones, i.e. if there were to be a stabilizing effect. However, the electrodes in this study are free-floating, with no attachment to the skull or each other. Thus, the movements between the electrodes and the tissue should be minimal, and not likely to cause any significant differences between the different implants. Furthermore, the fact that no differences were seen between the groups after staining for ED1 also indicates that there is no difference in the actual damage caused by the different implants.

It should be pointed out that the implanted free-floating wire bundles are not identical to any functioning electrodes available today which require a solid connection to a connector on the skull. Our wire bundles are not attached to anything except the brain, which means that they are not affected by the movements of the skull in relation to the brain. Hence, if we had used electrodes tethered to the skull, the hemisphere implanted with a large number of electrodes would have been more stabilized in relation to the skull than the hemisphere with only one implant. Thus the movements between the electrodes and the brain would differ, as well as the resulting tissue damage caused by the relative movements. By using free-floating electrodes we hope to eliminate such movements, isolating the effect of the number of implant on
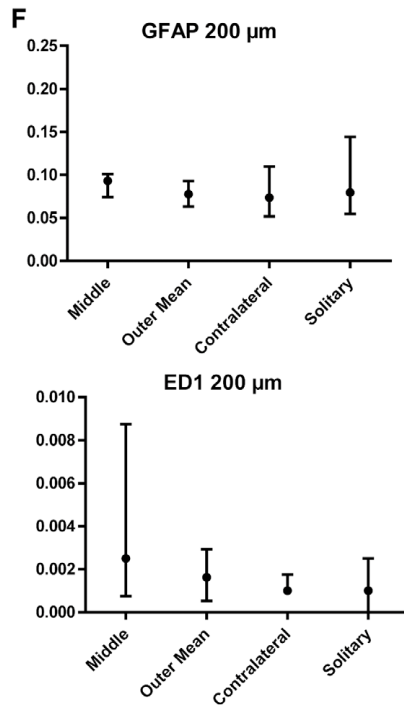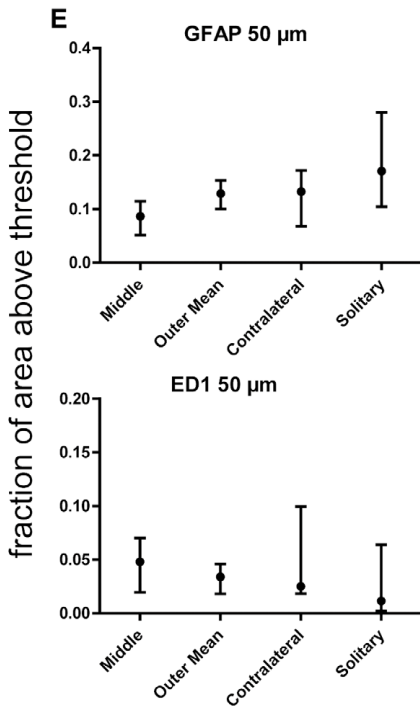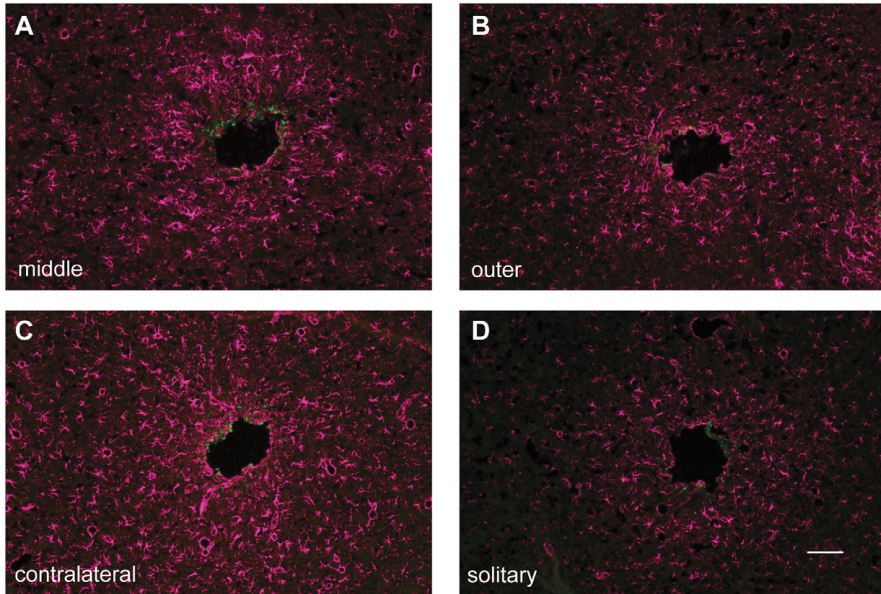
Figure showing panels A (middle), B (outer), C (contralateral), D (solitary), and graphs E (GFAP 50 µm, GFAP 200 µm, ED1 50 µm, ED1 200 µm) with fraction of area above threshold plotted for Middle, Outer Mean, Contralateral, and Solitary.

Figure 3. Glial reactions surrounding implants after one week. Example pictures of GFAP (magenta) & ED1 (green) staining from middle (A), outer (B), contralateral (C) & solitary (D) implant locations after one week. Scale bar 100 μm. Quantifications of GFAP & ED1 staining after one week in 0–50 μm ROI (E) & 50–200 μm ROI (F). Circles & error bars signify median values & interquartile ranges. X-axes show different implant locations. Y-axes show the fraction of area in each ROI that is above the set threshold. No statistically significant differences between the tissue reactions at the different implant locations was found in any of these groups, n = 6 for all groups.
doi:10.1371/journal.pone.0047509.g003

the tissue reaction, which is the focal point of this study. Furthermore, even if a solid lead to the skull is a requisite for intracortical electrodes today, the development of implantable light weight telemetry units can be foreseen to provide means for using completely free-floating electrodes in electrophysiology in the near future [28].

If the damage caused by each implant is virtually identical, the difference in astrocytic scarring that we still see is most likely explained by some innate property of the astrocytes being recruited to the scar. Two main theories regarding how reactive astrocytes are recruited to an injury have been described [29,30,31]. Astrocytes may be recruited from local resident quiescent astrocytes that differentiate into reactive astrocytes and proliferate [30,32,33], or from distal precursor cells, for instance from the subventricular zone [34,35].

If cells are being recruited from a distal source this might be mediated via chemotaxis as astrocytes are known to express chemokine receptors [36]. The presence of a larger chemotactical gradient in the middle of a group of implants, where all the implants may additively contribute to the gradient, than at the edges, is likely. In this case the middle implant would be able to recruit a larger proportion of astrocytes than the outer ones. However, if the astrocytes are competitively recruited from a local pool of quiescent astrocytes, the outer implants would have access to a larger pool of astrocytes compared to the middle ones who will have to compete with neighboring implants. In this scenario, the middle implant would exhibit a smaller scar than the outer ones, consistent with what we found in the present study. It should be pointed out that the proliferation of astrocytes is likely to contribute more to the amount of scarring than the initial number of recruited cells. Still, a difference in the initial number of astrocytes recruited could lead to a difference in the scar formation.

The point should also be raised that even if research regarding biocompatibility of multielectrode arrays today aim at reducing the reaction to implantation, the fact remains that reactive gliosis also has a very important defensive function. Indeed, numerous studies have shown detrimental effects of deletion of genes central to the process of reactive gliosis, such as absence of a normal glial

scar, increased edema surrounding the injury, more extensive damage to the blood brain barrier and a significantly increased area of inflammation after injury [37,38,39,40]. Thus, while reactive gliosis has detrimental effects on neuronal regeneration in the chronic phase, it is essential to limit the extent of a brain injury in the acute phase [37,40,41,42]. The reduction of reactive gliosis should perhaps only be seen as positive when correlated with a reduced damage to the tissue, and therefore a reduced need for defensive and repair mechanisms. In our study, the inflicted tissue damage is the same at all implantation sites, and therefore also the need for protective mechanisms. Thus, if the tissue response is not able to keep up with the tissue damage, a reduced tissue reaction should perhaps even be considered to be negative, actually increasing the vulnerability of the neural tissue. Further long term studies are needed to investigate a possible cut off when the number of implants might be too large for the tissue response to handle.

In conclusion, our results suggest that it is possible to implant electrodes in multiple brain sites without aggravating the tissue response, thus providing validity to large-scale electrophysiological recordings from multiple chronically implanted electrodes. Our finding that the middle implant exhibits the least amount of reactive astrocytosis might suggest that the astrocytes are recruited to the injury site in a competitive manner from a local pool rather than an additive manner from distal migrating cells, but this mechanism is not investigated in this study and further studies would be required to shed light on the subject.

Acknowledgments

Author Contributions

Conceived and designed the experiments: GL LG ND JS LMEP. Performed the experiments: GL LG. Analyzed the data: GL LG. Contributed reagents/materials/analysis tools: GL LG. Wrote the paper: GL LG ND JS LMEP.

References

1. Awan NR, Lozano A, Hamani C (2009) Deep brain stimulation: current and future perspectives. Neurosurgical focus 27: E2.
2. Daly JJ, Wolpaw JR (2008) Brain-computer interfaces in neurological rehabilitation. Lancet Neurol 7: 1032–1043.
3. Kipke DR, Shain W, Buzsaki G, Fetz E, Henderson JM, et al. (2008) Advanced neurotechnologies for chronic neural interfaces: new horizons and clinical opportunities. J Neurosci 28: 11830–11838.
4. Polikov VS, Tresco PA, Reichert WM (2005) Response of brain tissue to chronically implanted neural electrodes. J Neurosci Methods 148: 1–18.
5. Rousche PJ, Normann RA (1998) Chronic recording capability of the Utah Intracortical Electrode Array in cat sensory cortex. J Neurosci Methods 82: 1–15.
6. Williams JC, Rennaker RL, Kipke DR (1999) Long-term neural recording characteristics of wire microelectrode arrays implanted in cerebral cortex. Brain Res Brain Res Protoc 4: 303–313.
7. Biran R, Martin DC, Tresco PA (2005) Neuronal cell loss accompanies the brain tissue response to chronically implanted silicon microelectrode arrays. Exp Neurol 195: 115–126.
8. Krack P, Fraix V, Mendes A, Benabid AL, Pollak P (2002) Postoperative management of subthalamic nucleus stimulation for Parkinson's disease.

Movement disorders : official journal of the Movement Disorder Society 17 Suppl 3: S188–197.
9. McConnell GC, Butera RJ, Bellamkonda RV (2009) Bioimpedance modeling to monitor astrocytic response to chronically implanted electrodes. J Neural Eng 6: 055005.
10. Szarowski DH, Andersen MD, Retterer S, Spence AJ, Isaacson M, et al. (2003) Brain responses to micro-machined silicon devices. Brain Res 983: 23–35.
11. Williams JC, Hippensteel JA, Dilgen J, Shain W, Kipke DR (2007) Complex impedance spectroscopy for monitoring tissue responses to inserted neural implants. Journal of Neural Engineering 4: 410–423.
12. Stice P, Gilletti A, Panitch A, Muthuswamy J (2007) Thin microelectrodes reduce GFAP expression in the implant site in rodent somatosensory cortex. Journal of Neural Engineering 4: 42–53.
13. Thelin J, Jorntell H, Psouni E, Garwicz M, Schouenborg J, et al. (2011) Implant size and fixation mode strongly influence tissue reactions in the CNS. PLoS One 6: e16267.
14. Edell DJ, Toi VV, McNeil VM, Clark LD (1992) Factors influencing the biocompatibility of insertable silicon microshafts in cerebral cortex. IEEE transactions on bio-medical engineering 39: 635–643.
15. Seymour JP, Kipke DR (2007) Neural probe design for reduced tissue encapsulation in CNS. Biomaterials 28: 3594–3607.

16. Skousen JL, Merriam SM, Srivannavit O, Perlin G, Wise KD, et al. (2011) Reducing surface area while maintaining implant penetrating profile lowers the brain foreign body response to chronically implanted planar silicon microelectrode arrays. Progress in brain research 194: 167–180.

17. He W, Bellamkonda RV (2005) Nanoscale neuro-integrative coatings for neural implants. Biomaterials 26: 2983–2990.

18. Johansson F, Wallman L, Danielsen N, Schouenborg J, Kanje M (2009) Porous silicon as a potential electrode material in a nerve repair setting: Tissue reactions. Acta biomaterialia 5: 2230–2237.

19. Lu Y, Wang D, Li T, Zhao X, Cao Y, et al. (2009) Poly(vinyl alcohol)/poly(acrylic acid) hydrogel coatings for improving electrode-neural tissue interface. Biomaterials 30: 4143–4151.

20. Winslow BD, Christensen MB, Yang WK, Solzbacher F, Tresco PA (2010) A comparison of the tissue response to chronically implanted Parylene-C-coated and uncoated planar silicon microelectrode arrays in rat cortex. Biomaterials 31: 9163–9172.

21. Biran R, Martin DC, Tresco PA (2007) The brain tissue response to implanted silicon microelectrode arrays is increased when the device is tethered to the skull. J Biomed Mater Res A 82: 169–178.

22. Kozai TD, Marzullo TC, Hooi F, Langhals NB, Majewska AK, et al. (2010) Reduction of neurovascular damage resulting from microelectrode insertion into the cerebral cortex using in vivo two-photon mapping. Journal of Neural Engineering 7: 046011.

23. Eriksson Linsmeier C, Prinz CN, Pettersson LM, Caroff P, Samuelson L, et al. (2009) Nanowire biocompatibility in the brain–looking for a needle in a 3D stack. Nano Lett 9: 4184–4190.

24. He W, McConnell GC, Bellamkonda RV (2006) Nanoscale laminin coating modulates cortical scarring response around implanted silicon microelectrode arrays. Journal of Neural Engineering 3: 316–326.

25. Lind G, Linsmeier CE, Thelin J, Schouenborg J (2010) Gelatine-embedded electrodes–a novel biocompatible vehicle allowing implantation of highly flexible microelectrodes. Journal of Neural Engineering 7: 046005.

26. Linsmeier CE, Wallman L, Faxius L, Schouenborg J, Bjursten LM, et al. (2008) Soft tissue reactions evoked by implanted gallium phosphide. Biomaterials 29: 4598–4604.

27. Bao F, Chen Y, Dekaban GA, Weaver LC (2004) Early anti-inflammatory treatment reduces lipid peroxidation and protein nitration after spinal cord injury in rats. Journal of neurochemistry 88: 1335–1344.

28. Kim S, Bhandari R, Klein M, Negi S, Rieth L, et al. (2009) Integrated wireless neural interface based on the Utah electrode array. Biomedical microdevices 11: 453–466.

29. Alonso G (2005) NG2 proteoglycan-expressing cells of the adult rat brain: possible involvement in the formation of glial scar astrocytes following stab wound. Glia 49: 318–338.

30. Buffo A, Rite I, Tripathi P, Lepier A, Colak D, et al. (2008) Origin and progeny of reactive gliosis: A source of multipotent cells in the injured brain. Proceedings of the National Academy of Sciences of the United States of America 105: 3581–3586.

31. Komitova M, Serwanski DR, Lu QR, Nishiyama A (2011) NG2 cells are not a major source of reactive astrocytes after neocortical stab wound injury. Glia 59: 800–809.

32. Cavanagh JB (1970) The proliferation of astrocytes around a needle wound in the rat brain. Journal of anatomy 106: 471–487.

33. Latov N, Nilaver G, Zimmerman EA, Johnson WG, Silverman AJ, et al. (1979) Fibrillary astrocytes proliferate in response to brain injury: a study combining immunoperoxidase technique for glial fibrillary acidic protein and radioautography of tritiated thymidine. Developmental biology 72: 381–384.

34. Chojnacki AK, Mak GK, Weiss S (2009) Identity crisis for adult periventricular neural stem cells: subventricular zone astrocytes, ependymal cells or both? Nature reviews Neuroscience 10: 153–163.

35. Levison SW, Goldman JE (1993) Both oligodendrocytes and astrocytes develop from progenitors in the subventricular zone of postnatal rat forebrain. Neuron 10: 201–212.

36. Andjelkovic AV, Kerkovich D, Shanley J, Pulliam L, Pachter JS (1999) Expression of binding sites for beta chemokines on human astrocytes. Glia 28: 225–235.

37. Bush TG, Puvanachandra N, Horner CH, Polito A, Ostenfeld T, et al. (1999) Leukocyte infiltration, neuronal degeneration, and neurite outgrowth after ablation of scar-forming, reactive astrocytes in adult transgenic mice. Neuron 23: 297–308.

38. Faulkner JR, Herrmann JE, Woo MJ, Tansey KE, Doan NB, et al. (2004) Reactive astrocytes protect tissue and preserve function after spinal cord injury. The Journal of neuroscience : the official journal of the Society for Neuroscience 24: 2143–2155.

39. Pekny M, Johansson CB, Eliasson C, Stakeberg J, Wallen A, et al. (1999) Abnormal reaction to central nervous system injury in mice lacking glial fibrillary acidic protein and vimentin. The Journal of cell biology 145: 503–514.

40. Pekny M, Nilsson M (2005) Astrocyte activation and reactive gliosis. Glia 50: 427–434.

41. McKeon RJ, Schreiber RC, Rudge JS, Silver J (1991) Reduction of neurite outgrowth in a model of glial scarring following CNS injury is correlated with the expression of inhibitory molecules on reactive astrocytes. The Journal of neuroscience : the official journal of the Society for Neuroscience 11: 3398–3411.

42. Wilhelmsson U, Li L, Pekna M, Berthold CH, Blom S, et al. (2004) Absence of glial fibrillary acidic protein and vimentin prevents hypertrophy of astrocytic processes and improves post-traumatic regeneration. The Journal of neuroscience : the official journal of the Society for Neuroscience 24: 5016–5021.

LUND UNIVERSITY
Faculty of Medicine